INFORMATION TO USERS

This manuscript has been reproduced from the microfilm master. UMI films the text directly from the original or copy submitted. Thus, some thesis and dissertation copies are in typewriter face, while others may be from any type of computer printer.

The quality of this reproduction is dependent upon the quality of the copy submitted. Broken or indistinct print, colored or poor quality illustrations and photographs, print bleedthrough, substandard margins, and improper alignment can adversely affect reproduction.

In the unlikely event that the author did not send UMI a complete manuscript and there are missing pages, these will be noted. Also, if unauthorized copyright material had to be removed, a note will indicate the deletion.

Oversize materials (e.g., maps, drawings, charts) are reproduced by sectioning the original, beginning at the upper left-hand corner and continuing from left to right in equal sections with small overlaps.

UMI®

Molecular Gas in Barred Galaxy Nuclei

By

Glen Raymond Petitpas, B.Sc., M.Sc.

A Thesis

Submitted to the School of Graduate Studies

in Partial Fulfilment of the Requirements

for the Degree

Doctor of Philosophy

McMaster University

Molecular Gas in Barred Galaxy Nuclei

DOCTOR OF PHILOSOPHY (2001)　　　　　　　McMaster University

(Physics and Astronomy)　　　　　　　　　　Hamilton. Ontario

TITLE:　Molecular Gas in Barred Galaxy Nuclei

AUTHOR:　Glen Petitpas. B.Sc.. M.Sc.

SUPERVISOR:　Dr. Christine D. Wilson

NUMBER OF PAGES:　xviii. 199

Abstract

Double bars have been proposed as a means of transporting molecular gas past inner Lindblad resonances into the nuclear regions. where it can fuel active or starburst nuclei. Thus far. the existence of double bars has been determined by isophote twists seen in the near infrared. which could probe the bulge properties of these galaxies rather than the disk properties. We have observed two double bar galaxy candidates (NGC 2273 and NGC 5728) in ^{12}CO $J=1-0$ with the Caltech Millimeter Array. Despite the similar near infrared images of the two galaxies. we see rather different nuclear morphologies in the CO maps. NGC 2273 shows evidence of a nuclear bar misaligned from the main stellar bar by $\sim 90°$. and aligned with the near infrared isophote twists. NGC 5728 shows an arc of CO clumps that peaks just to the south-west of the dynamical center and curves to the south-east where it follows the dust lane to the south. The lack of a nuclear bar in the CO maps of NGC 5728 may be evidence that it is in a later stage of evolution. Bar dissolution may have just begun. and the gas has responded first. which may explain why we see a nuclear bar in the near infrared images of NGC 5728. but not in the CO maps.

Models of these double barred galaxies show that the nuclear molecular morphology depends on the assumed gas properties. We have performed a multi-transition CO study of the nuclei of seven double barred galaxies that exhibit a variety of molecular gas morphologies in order to determine if the molecular gas properties are correlated with the nuclear structure and activity. We find that the ^{12}CO $J=3-2/J=2-1$ line ratio is lower in galaxies with

molecular bars in the nucleus and higher in galaxies with CO emission dispersed around the galactic center. This suggests that the molecular gas may be cooler (and perhaps more viscous) enhancing the gas's ability to clump together and flow inwards. The galaxies without central concentration show signs of past star formation which may have exhausted, heated, and dispersed the molecular gas in the nucleus, resulting in the observed distributions and high CO line ratios. The multiline CO data corroborates our hypothesis that the galaxies with nuclear molecular bars are at an earlier stage of double barred galaxy evolution. The star formation that is currently taking place may eventually exhaust and/or disperse the molecular gas in the nucleus, resulting in a non-nuclear barred morphology, such as we see in NGC 5728.

In an attempt to detect other double barred galaxies that are bright enough in CO emission to be mapped at high resolution, we have undertaken a CO survey with the JCMT and NRAO 12-m of all double barred galaxies that are observable from the northern hemisphere. We do not detect any new candidates, which suggests for some of these galaxies that they are rather gas deficient, which is in conflict with the models of double barred galaxies which require large amounts of molecular gas to prevent the kinematically hot population of stars from destroying the nuclear bars.

As a cautionary tale, we include a detailed set of CO observations of the nearby starburst galaxy M82. Its close proximity (compared to the other galaxies in this thesis) allow us to observe the molecular gas properties at a much higher spatial resolution. We find temperature and density gradients across the nucleus of M82, that would otherwise be undetectable in the more

distant galaxies. I point out that in the more distant galaxies, we are simply measuring the average gas properties across the nucleus, and will require a larger, more sensitive a submillimetre array before we are capable of such detailed studies of these double barred galaxies.

For my mother...

Co-Authorship

The original work contained in Chapters 3 through 5 are preprints of articles that will be, or already are, submitted to the Astrophysical Journal. Chapter 6 is a reprint of a paper already published in the Astrophysical Journal. For all of these papers, I am first author, with Christine Wilson as co-author.

The ideas developed in these Chapters are the result of a collaborative effort between myself and my supervisor, Christine Wilson. I wrote all of the telescope applications myself, and I wrote each Chapter in its entirety. Revisions made during the preparation of articles for submission to journals and the subsequent peer review process (for Chapter 6) were a collaborative mental effort, with me preparing the final written materials.

Acknowledgement

There are naturally many people to thank. so I'll start with the most obvious. my supervisor. Christine Wilson. Despite being on perhaps every single radio astronomy committee in Canada. she has still found more than enough time to aid and assist my progress over the last 4 years (+2 if you count my Masters Degree). Her patience seems curiously unlimited. Due in part to my poor organizational skills and bad memory. I am certain that she has had to tell me similar things a variety of times. and never flinched. Nor did she flinch when I decided to start a new topic for my thesis *nearly two years in!*. Amazing.

I thank Christine for teaching me to be a careful researcher. with attention paid to details often overlooked by others. I also thank her for encouraging me to become a much better speaker. writer. and presenter. These skills are crucial for success. but are often not emphasized. The research positions I have been offered are a testament her training me as a scientist: the awards I have won are a testament to her training me as a communicator of science.

I must also thank all the people who have put up with me in that crowded office over the last four years. namely. Brenda Matthews. Dave Lepischak. Tracy Webb. Marcel Vandalfsen. and. Waldemar Okon. I have always enjoyed the humorous and insightful conversations that have erupted. in spite of the break in work rhythm.

Extra special thanks to the office staff. Wendy Malarek. Cheryl Johnson. Daphne Kilgour. and Rosemary McNeice. for helping me with nearly every aspect of bureaucratic things. Without them. I almost certainly would have been killed very early on by complicated forms and paperwork. Their kindness and friendship will be very much missed.

Table of Contents

List of Tables

List of Figures

List of Appendices

Chapter 1

Introduction

"Galaxies are the island universes within which reside most stars, much of the gas, and a little of the mass in the cosmos"

E.S. Phinney

Galaxies are large ensembles of stars, gas, and dark matter that are bound together by gravity. They come in a variety of sizes and shapes, but the majority are in the form of disk galaxies. These galaxies contain a disk of stars and gas, which can take on a variety of morphologies, such as spiral arms and bars. This disk is partially surrounded by a spherical halo, as well as a more centrally concentrated 'bulge' of purely stars, that can be either spherical or triaxial in shape. All of these are believed to reside inside a deep gravitational potential caused by a currently unobservable halo of dark matter.

1.1 Overview of this Thesis

It is known that the nuclei of many galaxies are too bright to be the result of ordinary star formation. The luminosity of some of these nuclei would require star formation rates of up to 300 $M_\odot$/year. If this is the case, these galaxies will need some form of refueling mechanism in order to sustain these rates long enough to be as common as they are observed to be.

More than half of all galaxies are observed to contain large elongated structures (called bars) passing through their centers (see Figure 1.1). These large scale perturbations can steal angular momentum from the gas in the disk, allowing it to flow inward toward the nucleus. At the centres of many barred galaxies are inner Lindblad resonances (ILRs), which play an important role in the evolution of barred galaxies. They may be responsible for trapping infalling material into a circumnuclear ring, stopping the inflow of molecular gas into the nuclear regions where it would otherwise be used to feed black holes and power starburst activity. Shlosman, Frank, & Begelman (1989) proposed that material in a nuclear ring may become unstable and form a nuclear bar that may be able to transport the molecular material interior to the ring, where it can repeat this process through a series of nested bars until it reaches the black hole or nuclear starburst.

Studies of barred galaxies have revealed the presence of isophote twists in the nuclear regions, often interior to inner Lindblad resonances. These twists are thought to be the signature of a nuclear bar, but there are other mechanisms that could cause twisted isophotes (Elmegreen et al. 1996):

1. *The twisted inner regions of the main bar:* Shaw et al. (1993) proposed that the isophote twists are the result of molecular gas getting trapped in the x_2 orbits of the barred galaxy potential. Because of the torques on the molecular gas by the large scale bar, the gas in the x_2 orbits[1] begins to drift back towards the large scale bar. The nuclear gas 'bar' has enough mass to drag the stellar component of the main bar out of phase, resulting in a twisted region of the main bar that resembles a nuclear bar, but the whole system (large scale +

---

[1]The x_1 orbits run parallel to the large scale bar and x_2 orbits run perpendicular to the x_1 orbits and have major axes less than the minor axes of the x_1 orbits. See §2.7.1 for details.

Figure 1.1: The Prototypical Barred Galaxy NGC 1300

This figure shows the prototype barred galaxy NGC 1300. Note the prominent dust lanes (shown lighter in this negative image) along opposite edges of the bar (nearly horizontal in this image). These dust lanes are thought to occur in the shocked regions alone the leading edge of the bar. (Photo taken at Kitt Peak MDM 1.3 m telescope by Eric Schulman).

nuclear bar) rotate at the same pattern speed. The nuclear 'bar' will always lead the large scale bar.

2. *A kinematically distinct nuclear bar:* Friedli & Martinet (1993) proposed that the isophote twists are the result of inflowing gas collecting at the ILR. and gaining enough mass to become kinematically separate from the large scale bar. In this model. the nuclear bar can be at any angle with respect to the large scale bar. This model is favoured by studies of many isophote twist galaxies where a wide variety of nuclear bar offset angles is observed.

3. *A triaxial stellar bulge:* The original explanation for the isophote twists is by Kormendy (1979) who proposed that they are the result of a triaxial stellar bulge seen in projection.

All of these theories can be tested using high resolution observations of the molecular gas in the galaxies containing isophote twists. The first two models require large amounts of molecular gas. so I can (at the simplest level) check to make sure that these galaxies contain at least 4 to 10% molecular gas. At a higher level. the first two models predict similar gas morphologies. but different gas dynamics. So in theory. I can use the rotation curves derived from the molecular gas observations to search for a kinematically distinct bar (as predicted by Friedli & Martinet 1993) in a sample of galaxies with isophote twists.

The last model predicts that the isophote twists are the result of a triaxial stellar bulge. Molecular gas observations are also capable of testing this theory. Since the bulges are generally devoid of molecular gas. I should expect to see no trace of a nuclear bar in the CO maps of these galaxies.

The dominant molecule in the interstellar medium is hydrogen (H_2). Molecular hydrogen emits in the ultraviolet. but does not have any transitions that emit

strongly at wavelengths that can penetrate the Earth's protective atmosphere. In order to trace the molecular gas. I must use carbon monoxide. which is known empirically to be an excellent tracer of hydrogen (Scoville & Sanders 1987). Theoretically. it is believed to be rotationally excited by collisions with the more abundant (by a factor of 10^4) molecular hydrogen. Another benefit of CO over H_2 is that there are a variety of different rotational transitions (the so called J transitions) that are readily excitable by various gas temperature and densities that exist in the interstellar medium. Warmer. denser gas will more readily excite the CO into higher J transitions. When the CO drops back down to a lower rotational level. it emits a photon of known wavelength (typically in the millimetre or sub-millimetre wavelength range) that can be observed from Earth. For example. a CO molecule excited into the $J=2$ level. will decay back to the $J=1$ level and emit a photon at 230 GHz ($\lambda \sim 1$ mm). This is called the $J=2-1$ emission line of CO. The Doppler shift of this photon away from the rest frequency for that J transitions allows us to probe the dynamics of the molecular gas.

In this thesis I will use many of the different rotational transitions of CO to probe the gas distributions and dynamics in a sample of barred galaxies. The first science chapter uses only the CO $J=1-0$ transition to probe the dynamics and distribution of the cooler gas in the nuclei of double barred galaxies. The later chapters will use many different transitions of CO and its isotopomers to probe the physical conditions of the warmer. denser gas at the centres of these galaxies.

1.2 Outline of this Thesis

In **Chapter 2**. I summarize some of the relevant studies of all barred galaxies (not necessarily those with nuclear bars). I discuss the details of the important

resonances that occur in barred galaxies, and I also describe the different types of nuclear activity that are observed to exist in the nuclei of galaxies.

In **Chapter 3**, I use high resolution maps of the $J=1-0$ transition of ^{12}CO (115 GHz) to determine the morphology and mass of the molecular gas in galaxies thought to contain nuclear bars. I see a wide variety of gas distributions, which leads me to wonder how can the molecular gas in galaxies with similar gravitational potentials behave so differently from galaxy to galaxy? Perhaps the molecular gas is cooler and more visous in one galaxy compared to another.

In **Chapter 4**, I observe a variety of different transitions of ^{12}CO and ^{13}CO in an effort to place constraints on the physical conditions of the molecular gas in these galaxies. By observing a variety of transitions and isotopomers of CO (e.g. ^{13}CO, $C^{18}O$) I can compare the relative line strength and use statistical mechanics to determine the densities and temperatures of the gas. I was only able to compile enough data to study six galaxies in detail in Chapter 4. In order to confirm the findings of this chapter, I will need to observe a larger sample of galaxies using a variety of CO observations.

In **Chapter 5** I present the results of a CO survey of the centers of double bar galaxies candidates. I wish to find bright targets for future high resolution mapping (as in Chapter 3) as well as multi-transition CO studies to determine the molecular gas physical conditions (as in Chapter 4). The failure to detect any new candidates places strong constraints on the molecular gas masses in these galaxies and casts some doubt into the models of Shaw et al. (1993) and Friedli & Martinet (1993) which require large amounts of molecular gas.

The current generation of sub-millimetre telescopes do not have sufficient angular resolution or sensitivity to study the higher rotational transitions of CO on the scales needed to determine the details of the gas properties in the nucleus. For

all of the galaxies in this thesis (except NGC 4736). the 21″ beam of the James Clerk Maxwell Telescope covers the entire region of the galaxy interior to the inner Lindblad resonance. Therefore. in Chapter 4. I am only measuring the average molecular gas properties. In order to demonstrate the variety of gas properties that can exist in the nuclear regions of barred galaxies. **Chapter 6** presents a detailed study of the molecular gas properties of the nearby barred starburst galaxy M82. Its close proximity allow us to resolve the individual peaks of emission associated with the inner Lindblad resonance as well as the central peak at the nucleus. Detailed studies similar to those demonstrated for M82 for the more distant galaxies in our sample will greatly improve our understanding of the fueling of starbursts and AGN through barred galaxies. All this will be possible with the arrival of the Atacama Large Millimeter Array in the next decade.

"Heh. ho! Let's go!"

Joey Ramone

Bibliography

Elmegreen. D. M.. Elmegreen. B. G.. Chromey. F. R.. Hasselbacher. D. A.. &
Bissell. B. A.. 1996. *AJ* **111**. 1880.

Friedli. D. & Martinet. L.. 1993. *A&A* **277**. 27.

Kormendy. J.. 1979. *ApJ* **227**. 714.

Scoville. N. Z. & Sanders. D. B.. 1987. H2 in the galaxy. In *ASSL Vol. 134:
Interstellar Processes.* pp. 21.

Shaw. M. A.. Combes. F.. Axon. D. J.. & Wright. G. S.. 1993. *A&A* **273**. 31.

Shlosman. I.. Frank. J.. & Begelman. M. C.. 1989. *Nature* **338**. 45.

Chapter 2

Background on Single and Double Barred Galaxies

2.1 Why Study Barred Galaxies?

Galaxies are the largest structures that are visible with the naked eye. yet they are the smallest features resolvable in the current generation of cosmological simulations of the early universe. Thus. galaxies are the building blocks of the universe. and understanding how they evolve will be of great benefit to future simulations of the universe. Future simulations of the Big Bang and beyond will be able to follow the evolution of galaxies from their very formation through to the galaxies similar to those we see today. The ability of these models to correctly predict galaxy evolution within their models will be a very strict test of the computer code's accuracy. It is up to us observers to have galaxy evolution understood by the time the computers and codes are powerful enough to accomplish these simulations.

Approximately 77% of all visible galaxies contain disks (the other 20% are elliptical and 3% irregular). Of the disk galaxies. 79% of them are barred galaxies (classified as SAB or SB galaxies in RC3: de Vaucouleurs et al. 1991). and thus more than half of all galaxies contain bars. In addition to being the most abundant. barred galaxies are also known to be very rich in interesting dynamics. which are believed to be responsible for the rapid evolution of these systems compared to unbarred

galaxies. In the following sections. I will summarize the results of many studies of barred galaxies. I hope to show that barred galaxies are a 'dynamicist's playground' (Benedict et al. 2000). and that the fascinating dynamics can lead to a variety of interesting phenomena that influence the evolution and ultimate self-disruption of these systems.

2.2 Historical Studies of Galaxies

Galaxies appear as smudges of light to the naked eye and small telescopes. apparently much fainter than most of the stars we see in the night-time sky. In reality these galaxies are composed of billions of stars much brighter than the Sun. but the great distances to these objects render them apparently fainter. This was not immediately obvious to early astronomers. In the late 1800s. Charles Messier. while hunting for comets (also faint smudges of light. but contained within our Solar System). encountered 104 smudges that did not move through the sky the way comets do. As a result. the Messier Catalogue of non-comets contains a variety of spectacular objects such as new stars. dying stars. clusters of stars. and 40 galaxies.

These smudges of light (that were not comets) were originally called nebulae. Galaxies (or 'spiral nebulae'. as they were called in the early 1900s) are so distant that the individual stars could not be resolved with their current generation of telescopes. All nebular objects were originally thought to be nearby objects. similar to the bright nebulae of star forming regions and the planetary nebula of dying stars. In the mid-1920s. Edwin Hubble. using the largest telescope in the world (at that time: the 100 inch Hooker Telescope at Mt. Wilson) was able to resolve individual Cepheid variable stars in the 'spiral nebula' M31 (Messier 31). By measuring the period of brightness oscillations of these stars. and using the well known Period-Luminousity relation for these Cepheids. Hubble was able to determine the true

brightness of these stars. By comparing the apparent brightness of these stars to the true brightness (and the fact that brightness falls off as distance^{-2}), he was able to determine that M31 was outside of the Milky Way. and thus a galaxy unto itself.

Many years later. we now know that there are more galaxies beyond the Milky Way than is easily imaginable. They come in a wide variety of sizes. shapes. colours. and brightnesses. The galaxies that are of particular interest to this thesis are the flattened disk shaped galaxies that contain extremely bright nuclei. Figure 2.1 shows sketches of the different types of galaxies that are discussed in this thesis. Of particular interest are the barred galaxies (SB-SAB: the bottom galaxies in Figure 2.1). which show a large rectangular or oval distortion passing through the centre. The SB galaxies contain strong. easily recognizable bars. while the SAB galaxies contain weaker bars that are often difficult to identify. These galaxies can be sub-classified again depending on the relative size of the bulge (the bright spherical section in the middle). with early types having larger. brighter bulges and usually tagged with the letters "a" or "b". Later type galaxies have smaller bulges and are designated "b" or "c". For example. consider the SB(s) galaxy in the lower left of Figure 2.1. As it is drawn. it is actually a late type galaxy SB(s)c. while its early type counterpart [an SB(s)a] would have a much more extended bulge. so that only the very ends of the bar would be visible.

2.3 Star Formation and Black Holes in Galaxy Nuclei

The nuclei of barred galaxies are often the setting for a variety of spectacular phenomena. In this section I will briefly summarize some of the different forms of nuclear activity that occur in the centers of all galaxies.
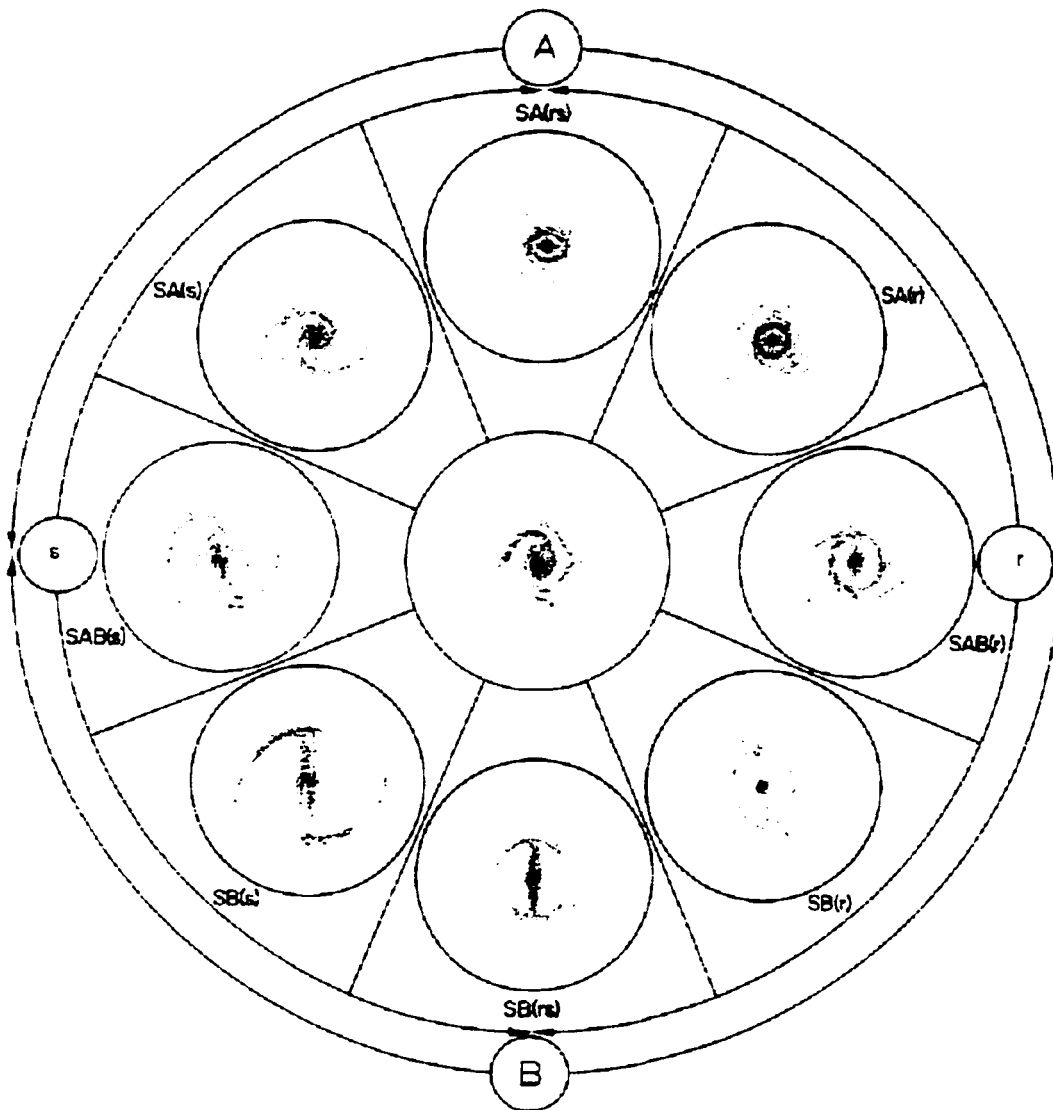
Figure 2.1: de Vaucouleurs' Wheel of Galaxies

This Figure shows the inner cover of the Second Reference Catalogue of Bright Galaxies (RC2) by de Vaucouleurs, de Vaucouleurs, & Corwin (1976). It shows galaxies as they are catagorized by bar strengths and spiral arms. It does not show the additional late and early type classifications based on bulge strength.

The basic form of activity is a starburst. It is simply a galaxy that is undergoing a very high rate of star formation: approximately 100 $M_\odot$/year, compared to a more normal rate of 2 - 3 $M_\odot$/year in the Milky Way. These galaxies release up to 98% of their energy in the infrared (the Milky Way releases only 30% in the IR). Typical galaxy centres contain 10^9 $M_\odot$ of molecular gas (the fuel for this star formation) so there should only be enough material to feed these starbursts for 10^7 years. For galaxy ages of 10 Gyrs, we should expect to see 0.1% of galaxies containing starbursts. Observationally, the occurence of nuclear star formation ranges from 8% in S0 galaxies, to 80% in Sc galaxies (Ho et al. 1997b). Thus, if this activity is as common as it is observed to be, there must be some form of refueling mechanism. Since the hot young stars formed in starbursts ionize the surrounding regions of leftover hydrogen gas, causing what are called H II (ionized H) regions, the nuclei of starburst galaxies are often called H II nuclei.

Another form of activity in galaxies is a Seyfert nucleus. It appears as an extremely bright point source at the very centres of some galaxies. These nuclei are so bright, that the only known mechanism that can convert mass into energy efficiently enough to be responsible for these luminosities is the accretion of material onto a black hole (Kormendy & Richstone 1995 and references therein). While spectra of most galaxies exhibit an absorption spectra resulting from the absorption lines in the stars that make up the galaxy, the spectra of Seyfert galaxies show bright emission lines. Seyfert 1 galaxies are those which exhibit broad allowed emission lines (such as H I, He I, H II) and narrow forbidden lines (such as [O III]). Seyfert 2 galaxies show only narrow emission for both allowed and forbidden lines. In the Unified Model of active galactic nuclei, a black hole is surrounded by a dusty torus, and Seyfert 1s are those for which we are viewing straight down into the torus, while

Seyfert 2s are those in which the emission from the black hole must pass through the torus (broadening the allowed lines) before it reaches us (Antonucci 1993).

Many forms of galaxies have spectra that resemble Seyfert 2 spectra. except that their forbidden lines tend to arise in less highly ionized atoms. These less active AGNs are known as Low Ionization Nuclear Emission Region (LINER) galaxies. They were originally thought to be associated with starburst activity. but now are attributed to the low luminousity tail of the Seyfert family (Binney & Merrifield 1998).

2.4 Observations of Nuclear Activity in Barred Galaxies

Galaxies are made of mostly stars (90% by mass) and some gas (10% by mass: mostly molecular). Although this gas is out-weighed by the stars. it is a crucial component of almost all galaxies. It supplies a method of dissipating energy that cannot otherwise be dissipated by the collisionless stars. In addition to adding interesting physics into galaxy dynamics. molecular gas has many other important roles in the evolution of barred galaxies. It is believed that the gas is responsible for fueling the wide variety of activity seen in the centres of galaxies. From Seyfert galaxies (thought to be a black hole accreting the material surrounding it) to starbursts (which show very high rates of star formation activity). molecular gas must be getting transported into the nucleus where it fuels these activities. Most active galactic nuclei (AGNs) are so luminous. that if they were converting molecular gas into energy via accretion on to a black hole or through vigorous star formation. they would still exhaust all their fuel in the local area in a very short time (Combes 1994 and references therein). Shlosman. Frank, & Begelman (1989) showed that viscous drag is not efficient enough to transport enough gas into the nucleus to feed the

AGN. Thus. there must be some other mechanism responsible for the transportation of gas into the inner 10 pc of a galaxy.

All models and simulations agree that galactic bars are an excellent mechanism for transporting material from the disk of a galaxy inwards towards the nucleus. The gravitational potential of the slower rotating bar can steal angular momentum from disk material. causing it to fall inwards towards the nucleus. If this theory is correct. then we should see a higher incidence of nuclear activity in barred galaxies compared to spiral galaxies. This topic has been under investigation for quite a while. In the following sections. I summarize some of the more recent results from comparisons of nuclear activity in barred and spiral galaxies.

2.4.1 Bars in Active Galaxies at Optical Wavelengths

One of the original studies comparing nuclear activity with large scale galaxy morphology was performed by Hawarden et al. (1986) in which they compare the galaxy type (as determined by RC2: de Vaucouleurs. de Vaucouleurs. & Corwin 1976: see Figure 2.1) with nuclear starburst activity (as indicated by a high infrared luminousity observed by IRAS). They neglected galaxies that contained Seyfert or LINER activity. Their sample contained a variety of disk galaxy types with the ratio SA:SAB:SB = 74:55:53. Within this sample. they find that more than one third of the barred galaxies have infrared luminosities greater than twice that of unbarred galaxies. This result suggests that these galaxies contain vigorous star formation activity in their nuclei. perhaps as a result of inflow along the bars. They find that much of the star formation in these barred galaxies occurs in a circumnuclear ring located near the inner Lindblad resonances (see §2.6).

Since they ignored Seyfert and LINERs. Hawarden et al. (1986) can not address the possibility that bars are responsible for the fueling of AGN. If most of the star formation in their sample occured in a circumnuclear ring. is it possible for bars to feed AGN where the gas much reach all the way into the nucleus? Moles. Marquez. & Perez (1995) compiled a list of active (Seyfert or LINER) galaxies from the catalog of Veron-Cetty & Veron (1991) and cross referenced it against the RC3 catalogue (de Vaucouleurs et al. 1991) to obtain a sample of 308 active galaxies with known morphological type. Of these. only 16 (5%) are elliptical galaxies. 279 (91%) are disk (barred or spiral) galaxies. and the remaining 13 (4%) are irregulars or 'other'. Thus. from this alone. it is clear that the majority of active galaxies occur in galaxies with disks.

Of the 279 active disk galaxies. only 186 of them have reliable information regarding the presence or absence of bars. Of these 186. 136 (73%) of them contain bars. We now believe that 79% of all disk galaxies are barred. so the value determined by Moles. Marquez. & Perez (1995) suggests that there is no over-abundance of bars in active galaxies. They do note that in the galaxies without bars. there is usually a companion galaxy nearby or the galaxies have some sort of distortion such as a ring.

Ho et al. (1997a) studied the occurence of bars in a sample of low luminosity active galactic nuclei. Again. in order to determine the morphological classifications for the galaxies in their sample. they turned to the RC3 catalogue (de Vaucouleurs et al. 1991). In their sample of over 300 disk galaxies. they detect a marginal over-abundance of bars in galaxies containing H II nuclei (which suggests enhanced star formation). as well as a very slight decrease in the incidence of bars in galaxies with AGN (either Seyfert or LINER). The differences are statistically insignificant though. possibly the result of selection effects. They do see a tendency for galaxies

with bars to show higher star formation rates. but overall. the presence of of bars does not seem to enhance a galaxy's chance of undergoing some form of nuclear activity. Ho et al. (1997a) speculate that the reason for this lack of AGN activity may be in the existence of inner Lindblad resonances in barred galaxies preventing the inflowing material from reaching the nucleus.

The studies discussed so far in this section have based the existence of a bar on observations made at optical wavelengths. It is known that dust in these galaxies can obscure light at these wavelengths and perhaps mask bar structures. It has recently been found that near infrared images are a much more reliable method of tracing the mass distribution of a galaxy. Mulchaey & Regan (1997) used near infrared (NIR) images of a sample of barred and non-barred spiral galaxies (as classified by optical catalogues) to study the light distributions of the older population of stars. Since the NIR images are less prone to extinction. these should give a better representation of the underlying gravitational potential. They find that all of the barred galaxies in their sample. also appeared barred in the NIR. but surprisingly. 55% of the 'non-barred' galaxies show elongated barred structures. Seigar & James (1998) also found that galaxies that were previously classified as un-barred in optical images showed signatures of barred structures in the NIR. In addition. they noted that bars that have low axial ratios (weak bars) appears as stronger bars in the NIR images. In this new light (pun intended) a variety of groups began to re-investigate the abundance of bars in AGN.

2.4.2 Bars in Active Galaxies in the Near Infrared

One of the original NIR studies of barred and spiral structure in AGN galaxies was by McLeod & Rieke (1995). They studied the NIR morphology of a spectro-scopically determined sample of AGN. While they did find that some of the galaxies

that were previously classified as un-barred showed bar structures in the NIR, there were not enough to modify the findings of the optical studies discussed in the previous section. They too concluded that there was no over-abundance of bars in AGN galaxies. One note to this study is that since the sample was derived from the spectroscopically limited CfA survey of Huchra & Burg (1992), there is a wide range of distances to these galaxies. Recession velocities of $> 10\ 000$ km s^{-1} are not uncommon in this sample (the highest is $> 45\ 000$ km s^{-1}!) and thus, they have distances of > 100 Mpc (for a generous H_0 of 100 km s^{-1} kpc^{-1}). Thus, in these more distant galaxies, the barred morphologies may be difficult to resolve. In addition, this sample also includes some highly inclined galaxies that would tend also to make bar identification difficult.

To alleviate some of these complications, Mulchaey & Regan (1997) studied the NIR morphology of a sample of galaxies that are limited to recession velocities less than 5000 km s^{-1} (distances of 50 Mpc) and also restricted their sample to galaxies with lower inclinations. These restrictions left them with 30 Seyfert galaxies and 25 normal galaxies. Their sample included 29 galaxies that were previously classified as un-barred but, as before, 16 of these showed bars in the NIR images. The final tally is that 70% of their galaxies show bar structures. When comparing the Seyfert and normal galaxies, they find a nearly identical occurence of bars in the Seyfert galaxies and normal galaxies, again, suggesting that bars are not a universal fueling mechanism for AGN. They do suggest that it is possible that perhaps bars were once present in the Seyfert galaxies, but they were destroyed by the creation of a central back hole which helped 'sphericalize' the gravitational potential (see §2.10). They did note a slight increase in the occurence of double bars in the Seyfert galaxies compared to normals, but nothing statistically significant.

In an attempt to reduce the effects of poor resolution on the determination of bars in the previous studies. Peletier et al. (1999) undertook a 0.7″ resolution NIR survey of the CfA galaxies used in McLeod & Rieke (1995). In this paper they also discuss a less subjective method for determining the existence of bars. which searches for an increase in ellipticity with increasing radius. followed by a range of radius where the position angle for the ellipses remains constant. These features would not be aparent in isophote twists that are the result of a triaxial stellar bulge. In the subsequent papers resulting from this survey. Knapen. Shlosman. & Peletier (2000) find that the Seyfert galaxies are barred more often (79% ± 7.5%) than the non-active galaxies (59% ± 9%). The fraction of 'non-axisymmetric' hosts increases when interacting systems are included. They conclude by stating that this 2.5σ result could be improved upon by re-observing these galaxies at even higher resolutions.

2.4.3 Molecular Gas in Active Barred Galaxies

The best way to observe the interstellar medium (ISM) would be to observe the molecular hydrogen gas directly. Since H_2 is a homonuclear. diatomic molecule. there are not many rotational transitions allowed. Those that do occur tend to lie at ultraviolet frequencies that are blocked by our atmosphere. The next best thing is to observe the second most abundant molecule. carbon monoxide (CO). It is believed to trace molecular gas through collisions with molecular hydrogen. and it has many rotational transition that lie in regions of the electromagnetic spectrum that are can pass through our atmosphere.

Many galaxies have been studied in CO on a case-by-case basis. but one of the first large scale surveys of galaxies at high resolution was performed by Sakamoto et al. (1999). They mapped 20 nearby galaxies in CO and find no clear correlation

between the type of nuclear activity (Seyfert. LINER. H II) and the amount of molecular gas in the centers of these galaxies. They do see a correlation between the gas mass fraction and the occurence of H II nuclei. in that galaxies with high gas mass fractions tend to preferentially undergo strong nuclear star formation. They propose that this is caused by an increase in gravitational instability of the nuclear gaseous disk of galaxies with high gas mass fractions.

In addition to an increase in starburst activity in galaxies with high gas mass fractions. Sakamoto et al. (1999) also find an increase (by roughly a factor of 2) in the molecular gas concentration in barred galaxies compared to unbarred galaxies (concentration = surface density of gas at R < 500 pc divided by the surface density of gas in the entire galaxy). This is the first statistical evidence for an increase in gas concentration at the centers of barred galaxies.

In a similar high resolution study of CO in a larger sample of 45 nearby galaxies. Sheth (2000) noticed that in addition to having increased gas concentrations. the gas surface density of the nuclei of barred galaxies is three times higher than the nuclear gas surface density of unbarred galaxies. This may also explain the increased star formation activity that has been observed by many authors (e.g.. Hawarden et al. 1986). So it seems clear from these two studies (Sakamoto et al. 1999: Sheth 2000) that bars play an important role in transportation of molecular gas inwards and the subsequent nuclear activity and evolution of the nuclei of galaxies.

So. what I hope the reader has learned thus far is that a) optical images are not necessarily a good way to determine the morphological type for galaxies. b) higher resolution NIR imaging is needed in order to study a large sample of galaxies out and beyond 100 Mpc. and c) direct observations of molecular gas in the centres of barred galaxies gives us a direct probe of the ISM and its role in feeding AGN and starburst activity. Given the results of the most recent high resolution NIR and CO

studies of activity in barred galaxies, it appears that bars are good at transporting molecular gas inwards. With this observational background out of the way, I shall now discuss the simulations of barred galaxies and the evolution of these models over the last couple of decades.

2.5 The Formation Mechanisms of Barred Galaxies

Early simulations of rotationally supported disk galaxies comprised entirely of stars had great success in reproducing bars. In fact, it was feared that the bar instability may be too dominant. Nearly any axially symmetric disk of stars that is rotating is prone to this bar instability. Hohl (1971) modeled a galaxy as an axially symmetric rotating disk made of 10^5 stars and found that it rapidly developed a bar structure with trailing spiral arms. Without any means of disspating energy, the velocity dispersion of the stars compared to their orbital energy rapidly increased and the spiral arms were destroyed. The elongated bar structure remained, but was greatly decreased in strength.

Observationally, it seems that one third of all disk galaxies are not barred. Numerically, the bar instability is so dominant that Ostriker & Peebles (1973) noted that there seems to be quite a few galaxies that appear to be rotationally supported yet are immune to the bar instability. They studied a series of flattened galaxy models with a variety of energy inputs and found that the only thing that could keep a bar instability from forming very rapidly is the presence of an unusually massive spherically symmetric halo surrounding the disk. They find that the only way to create disks that resist the bar instability is to have a halo to disk mass ratio of 1 to 2.5 and a ratio of kinetic to potential energy of 0.14 ± 0.02. Later models confirmed the early findings that bars are ubiquitous, robust, and can exist for at

least a Hubble time (e.g. Sellwood 1981). In fact. Sellwood (1981) notes "exceptions to the stability criteria postulated by Ostriker and Peebles remain distressingly difficult to find".

One of the first detailed studies of the dynamics of barred galaxies was undertaken by Contopoulos & Papayannopoulos (1980). They studied the stable orbits in a series of barred galaxy potentials (ranging from strongly barred to weakly barred potentials). They modeled the test galaxy potential as the sum of a spherically symmetric component (the halo) and an elongated bar potential. To simulate a weak. intermediate. and strongly barred galaxy. they set the bar potential to 1%. 10%. and 100% of the total gravitational potential respectively. In addition to this. they also varied the speed at which the bar perturbation rotated (called the pattern speed) with respect to the circular velocity. By adjusting the pattern speed of the bar. they can vary the number. strength. and location of the different resonances. These resonances are important enough to the models and to observations of barred galaxies that I pause to give a brief description of the more common resonances.

2.6 Resonances in Barred Galaxies

Stars and molecular clouds orbiting the centre of a galaxy oscillate radially in addition to their tangential orbits around the galactic nucleus. The frequencies of these radial oscillations are called epicycle frequencies (κ). The objects' orbital frequencies about the galactic nucleus are called their circular frequencies (Ω). In a barred spiral galaxy. the bar will rotate at a (usually) different frequency called the pattern speed (Ω_b). Resonances occur when an object (star or cloud) encounters successive crests of the bar potential at a frequency that coincides with its epicycle frequency. namely

$$m(\Omega - \Omega_b) = \pm\kappa$$

(Binney & Tremaine 1987) where m is equal to 2 for Lindblad resonances, and 4 for the ultraharmonic resonances. The inner Lindblad resonance refers to the condition $\Omega_b = \Omega - \kappa/2$ while the outer Lindblad resonance occurs at $\Omega_b = \Omega + \kappa/2$. Most 'real' rotation curves allow for two ILRs (see Figure 2.2) and the one nearest the nucleus is called the inner inner Lindblad resonance (IILR) while the second ILR is often called the outer inner Lindblad resonance (OILR).

Calculations of the locations of ILRs require knowledge of the rotation curve of the galaxy as well as the bar pattern speed. The value of κ can be calculated from the rotation curve using

$$\kappa = \sqrt{R\frac{d\Omega^2}{dR} + 4\Omega^2}$$

(Binney & Tremaine 1987) but since $\Omega = V_{rot}/R$ this reduces to

$$\kappa = \sqrt{4\Omega^2 + 2\Omega\frac{dV_{rot}}{dR}}.$$

The bar pattern speed (Ω_b) is usually estimated by assuming that the corotation resonance ($\Omega = \Omega_b$) occurs just past the end of the bar (simulations suggest $1.2\times$ the bar radius to be precise). These parameters are shown in detail in Figure 2.2. In this figure the bar pattern speed (Ω_b) is shown by the horizontal line at 35 km s^{-1}/kpc. Since this line intersects the $\Omega - \kappa/2$ curve in two places ($R = 1$ and 3 kpc), these are the locations of the Inner ILR and Outer ILR respectively. Notice that if the bar pattern speed were raised to 80 km s^{-1}/kpc, then it would not intersect the $\Omega - \kappa/2$ curve, and thus there would be no inner Lindblad resonance.

2.7 Barred Galaxy Models

All the models to be discussed in this section have not necessarily been attempting to model the nuclei of barred galaxies, but all of them make predictions regarding the nuclear structure. In the following section, I will emphasize primarily the models
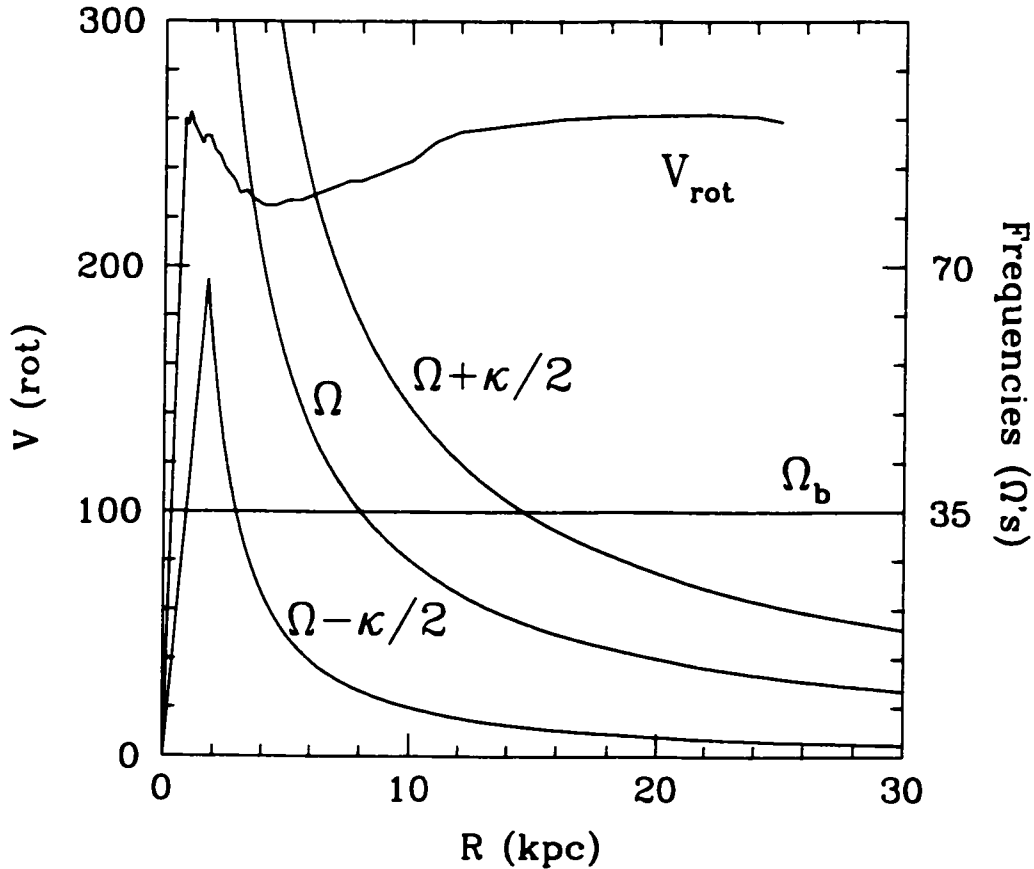
Figure 2.2: Typical Rotation Parameters for Barred Galaxies

This figure (adapted from Shaw et al. 1993) shows the parameters discussed in the text for a typical barred galaxy. The inner Inner Lindblad Resonance occurs where the bar pattern speed (Ω_b, the horizontal line) crosses the $\Omega - \kappa/2$ curve nearest the galactic centre ($R \approx 1$ kpc). The outer ILR occurs where the bar pattern speed crosses the $\Omega - \kappa/2$ curve further from the nucleus ($R \approx 3$ kpc). Corotation occurs where the bar pattern speed crosses the angular frequency curve Ω ($=V_{rot}/R$). Outer Lindblad Resonance occur where $\Omega_b = \Omega + \kappa/2$. Note that in this particular example, if the bar pattern speed is increased from 35 to a (unrealistic) value of >75 km s^{-1}/kpc, there will be no ILR in this galaxy.

predictions for the gas distributions in the nuclei of barred galaxies, even if it was not the focus of the paper or discussed in detail in the text.

2.7.1 Bars and Spiral Arms

In addition to determining the location of resonances, Contopoulos & Papayannopoulos (1980) also derived the families of stable orbits for varying bars strengths. For weak bars, there are two basic families of stable, periodic orbits: the so called x_1 and x_2 families. The x_1 orbits run along the length of the bar (inside the corotation resonance: see §2.6) and are likely responsible for the barred appearance of galaxies. The x_2 orbits are the dominant orbits between the inner Lindblad resonances (ILRs). They also note that if the bar is stronger or is rotating such that there are no ILRs, the x_2 family of orbits that run perpendicular to the bar cannot exist, and the x_1 orbits dominate (see Figure 2.3 for example).

The shortcoming of this, and similar models is the absence of a dissipative material (such as the molecular gas) that we know permeates the interstellar regions of galaxies. These purely stellar calculations do not include any method of loosing energy through viscous molecular cloud collisions, nor did they include any feedback mechanisms such as energy injection due to supernovae. More recent models discussed below incorporate these features.

Early studies of molecular gas in galaxies treated the gas as a continuous fluid (e.g. Roberts 1969). As such, density waves (Lin & Shu 1964) in galaxies are capable of compressing this fluid in the spiral arms of a galaxy, which was though to be the cause of the enhanced star formation in these regions. Later studies of the interstellar material in our own Galaxy showed that the interstellar medium was not a uniform fluid, but consisted of very distinct phases. The phase that contains the most mass

was the cold dense clumpy phase, mostly in the form of Giant Molecular Clouds (e.g. Solomon, Sanders, & Scoville 1979). In this context, the gas in the galaxy can not be simply modeled as a continuous fluid, and the generalizations made from this fluid theory likely did not apply to the interstellar medium of real galaxies.

One of the first simulations to incorporate the effects of molecular gas dissipation is by Combes & Gerin (1985). They point out that purely stellar N-body simulation of barred galaxies can only produce short-lived bars, mostly because of the increase of velocity dispersion relative to the orbital velocities (Hohl 1971). The addition of a dissipative component may be able to prevent this disk "heating", allowing longer-lived spiral arms. Combes & Gerin (1985) assume that the gravitational potential is dominated by stars, and that the stars do not interact with molecular clouds, except through the gravitational potential. The clouds, on the other hand, can exchange mass through collisions and can grow through coalescence. In the event of a cloud collision, clouds can merge together or fragment into two or three pieces depending on the impact parameter of the collision. The largest clouds have finite lifetimes and after 40 Myr, cloudlets are reinjected back into the ISM assuming a power-law mass distribution with each cloudlet given a random velocity to simulate the effects of supernovae.

The first cases studied by Combes & Gerin (1985) was for strong and weak bars where the bar is rotating fast enough that there are no ILRs. In this case, there is no shock on the leading edge of the bar enhancement as seen in the purely fluid models, but there is an increase in cloud collisions in this region. They also note an increase in molecular gas cloud collisions near the bar ends, which may account for the increased star formation activity seen at the bar ends of some galaxies. The long term evolution of these systems results in the gradual formation of a ring at approximately the radius at which the bar ends. This is the result of the rapidly

rotating bar transferring angular momentum to the particles. causing the spiral pattern to wind to a ring in approximately 10 rotations (a few Gyr).

The more interesting case (and the one more relevant to the galaxies studied in this thesis) is the case of a weak bar that is rotating slowly enough so that there are two. one. or just barely one ILR present[1]. In the slow bar cases. there are clear signs that the gaseous bar actually leads the stellar bar by $\sim 20°$. This slowly rotating bar (unlike the fast bar) steals angular momentum from the gas clouds. causing them to flow towards the nucleus. At the radius of the ILRs. the clouds tend to gather in elliptical orbits aligned with the bar and there is observational evidence for nuclear rings of clouds at approximately this radius in many barred galaxies (e.g. Gerin. Combes. & Nakai 1988). The ellipticity of this ring increases as the bar speed is decreased. i.e. circular rings are formed for faster bars. while elongated rings with major axes approaching the ILR radius form for slower bars[2]. Thus according to these models. the nuclear gas morphology for weak. slowly rotating bars is almost entirely determined by the rotation speed of the bar perturbation. Their models did not. however. predict the wide variety of dust lanes that are observed on the leading edges of galaxy bars.

2.7.2 Shocks and Dust Lanes

The prominent feature of many barred galaxies are the dark dust lanes that run along the leading edge of the bar. These are often thought to be associated with

---

[1] It should be pointed out that just because the bar is rotating slowly. it does not guarantee the existence of an ILR because κ and Ω are calculated under the assumption that the potential is axisymmetric. This is clearly not strictly true for barred galaxies. See §2.6 for details.

[2] This phenomenon is also seen in the models of Athanassoula (1992); see Figure 2.3.

shocks caused by the abrupt change in direction of the gas streams as it crossed the bar perturbation. Confirmation of this theory is found in direct measurements of the velocity jumps that occur across these dust lanes. Despite the difficulty in resolving such features, evidence for such velocity jumps is found in Fabry-Perot Hα maps of the SB galaxy NGC 1365 by Teuben et al. (1986). Velocity jumps of ∼150 km s^{-1} were seen at the positions of the dust lanes in the SB galaxy NGC 6221 by Pence & Blackman (1984). Additional support that the dust lanes occur at shocks in the gas flow is seen in radio continuum maps of barred galaxies. Since shocks mark regions of compressed gas, dust, magnetic fields, and high energy particles, they should be bright in radio emission. Observations of the SB galaxies NGC 1097 (Ondrechen & van der Hulst 1983) and M83 (Ondrechen 1985) show that the dust lanes are very prominent in the continuum maps.

In an attempt to explain the variety of dust lanes observed along the leading edge of galactic bars, Athanassoula (1992) used a hydrodynamical code to model the gas flows in and around the bar of galaxies. Particle codes such as the one used in Combes & Gerin (1985) may be more realistic, but it is more difficult to accurately model shocks in a particle based code. The model consisted of two axisymmetric components: a bulge and a disk. The third component was the bar, which is modeled as an ellipsoid. The gas disk is ideal, isothermal, non-viscous, non-self-gravitating and infinitely thin. By varying many of the bar parameters, Athanassoula was able to create a catalogue of dust lane morphologies for different bar strengths, pattern speeds, masses, and central concentrations (which determine the rotation curve).

For the case of a galaxy with a weak bar (axial ratio of 2.5) rotating slowly enough to allow the existence of inner Lindblad resonances, the gas shocks (hence dust lanes) occur along the leading edge of the bar, and are slightly curved to reflect the lenticular shape of the weak bar. For the faster of the bar speeds (still allowing

two ILRs) these regions of enhanced density curve in towards the nucleus where they wrap around the ILR. forming a circumnuclear ring (see upper right panel of Figure 2.3). When the same model is re-run. but with the bar speed is decreased. the gas density is enhanced down the very centre of the bar. and there is no longer a circumnuclear ring (left-most panels: Figure 2.3). The gas seems to just cross the nucleus and reconnect with the dust lane on the other side of the bar. For the case of a very slow rotating bar. the x_2 orbits are either absent or negligible. so the x_1 orbits dominate. and the gas shocks occur along the centre of the bar. For the faster bar. the x_2 orbits dominate near the nucleus. forcing the x_1 orbits to be widened to at least the major axis diameter of the x_2 orbits (see lower panel of Figure 2.3). Thus. for bars with similar axial ratios. masses. and central concentration. the location of the dust lanes sets limits on the pattern speed of a galactic bar.

Athanassoula (1992) proceeded to vary different model parameters. while holding the others constant. She showed that increasing the strength of the bar has a similar effect on the dust lanes as decreasing the bar pattern speed. For weak bars (low axial ratios). the dust lanes were curved along the leading edge of the bar. then circled the nucleus at the ILR radius. The difference in this models is that for very strong bars. the x_2 orbits actually extend wider than the x_1 orbits. and thus cannot survive. Even without x_2 orbits for the stronger bars. all trials with different axial ratios succeeded in producing circumnuclear rings. but they were elongated perpendicular to the bar for strong bars.

It was also shown that increasing the bar mass and decreasing the central concentration has similar effects on the dust lanes and nuclear gas morphology as decreasing the bar pattern speed (as shown in Figure 2.3). High mass bars and low central concentrations result in dust lanes that cross the center of the galaxy and reconnect on the other side. The nuclear molecular gas resembles very elongated
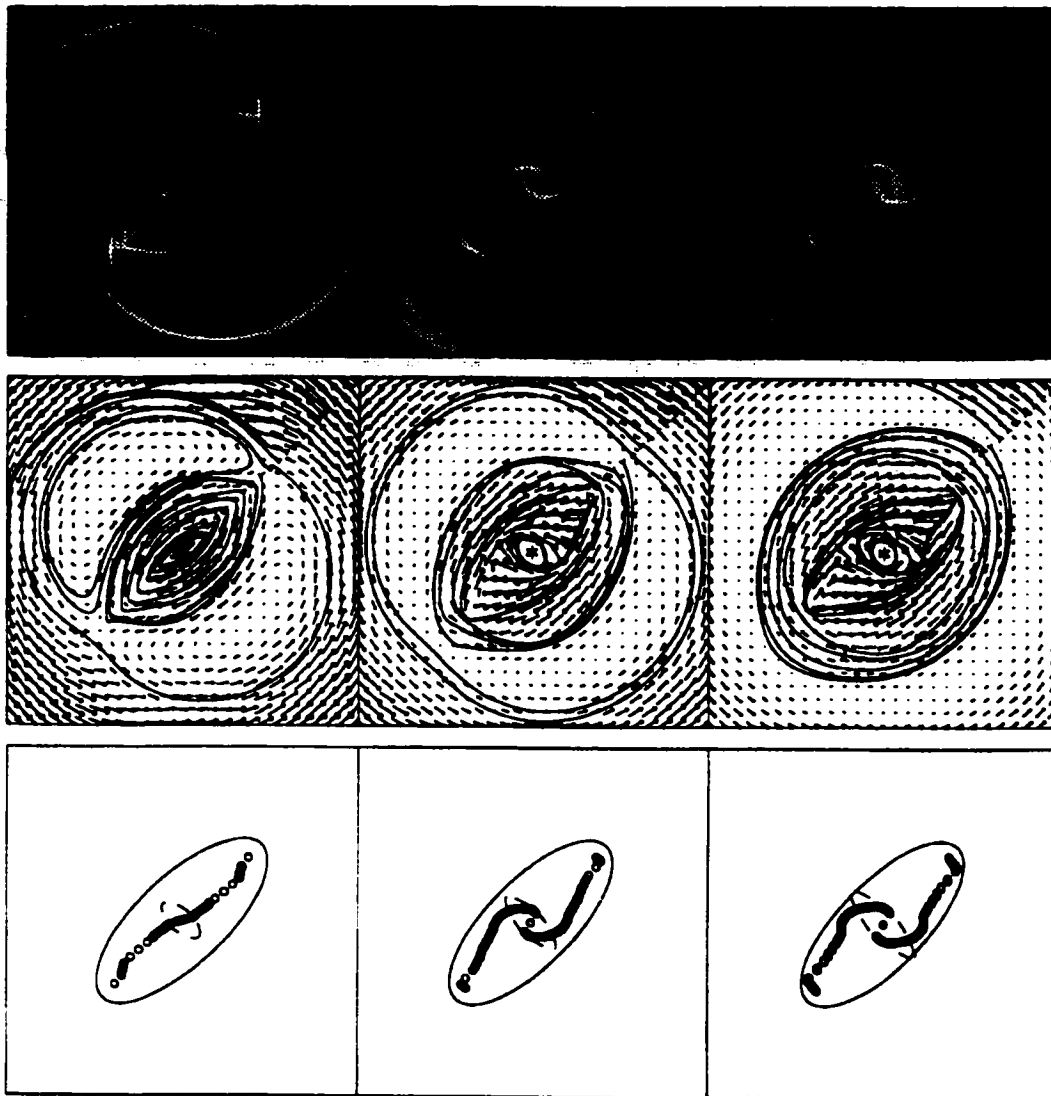
Figure 2.3: Galactic Gas Morphology for Different Bar Pattern Speeds Allowing ILRs

This figure (taken from Athanassoula 1992) shows the variation in the behavior of the molecular gas in a barred galaxy with Inner Lindblad Resonances. The bar pattern speed increases to the right. The top panel is the gas density (white is high), the middle panel are the gas velocities, and the lower panel marks the regions of highest density where the velocity jumps and gas densities are the highest. The dust lanes should occur along these lines. The solid line in the bottom panels marks the x_1 orbit, the dashed line marks the x_2 orbits.

rings that are tipped with respect to the galactic bar. Low mass bars and high central concentrations result in curved dust lanes and very circular nuclear rings of gas.

The final conclusion of all models of Athanassoula (1992) is that in order for dust lanes to appear offset along the leading edge of the bar. barred galaxies must have ILRs and stable x_2 orbits. Otherwise the dust lanes pass straight through the centre. In all models. the dust lanes are regions of high shear. which may explain the lack of star formation near the leading edge of the bar. despite the high gas density. Form the point of view of this thesis. the major conclusions drawn from Athanassoula (1992) is that a variety of bar parameters may be responsible for the nuclear gas morphologies in barred galaxies.

2.7.3 Inflow

Bars and open spiral arms have long been believed to be a good way to transport gas into the nuclei of galaxies. Despite the paucity of strong observational evidence. this inflow is generally thought to be responsible for the feeding of starburst and active galactic nuclei. bar dissolution. and bulge growth (Combes & Gerin 1985: Pfenniger & Norman 1990). It is clear from Figure 2.3 that the gas flow in and around bars has a very complicated structure. There are signs of both inflow and outflow within the bar. If the gas does not encounter a shock. it will simply follow stable orbits with very little net inflow. For the gas that encounters a shock though. the inflow velocities may exceed 100 km s^{-1}. This is not the inflow rate. it is the maximum. The average inflow velocity (including the outflow regions) for the entire galaxy is more on the order of 1 km s^{-1} (Athanassoula 1992).

There is indirect observational evidence for inflow in barred galaxies. One example is the shallower metallicity gradients in barred galaxies which suggests a mixing effect (Vila-Costas & Edmunds 1992: Dutil & Roy 1999). Another indirect piece of evidence for inflow in barred galaxies is that Hα luminosities are higher in the nuclei of barred galaxies compared unbarred galaxies. This suggests more vigorous star formation is taking place in the barred galaxies. perhaps fueled by inflow of molecular material from the outer disk (Ho. Filippenko. & Sargent 1997a).

Until recently there have been very few direct measurements of the rate of inflow in barred galaxies. Quillen et al. (1995) have estimated the inflow rates for the barred galaxy NGC 7479. They modeled the galactic potential based on near infrared images which trace the older stellar population. thought to dominate the mass of a galaxy. From this they were able to derive a theoretical deprojected rotation curve which allowed them to estimated the bar pattern speed (assuming the bar ends at the corotation radius). Assuming that the gas velocities along the leading edge of the bar were purely radial (Figure 2.3 show this may be a good approximation) the angular momentum of the gas is given by $l \approx r^2 \Omega_b$. so the torque on the gas is $\tau = d\Phi/d\theta = dl/dt \approx (dr/dt)2r\Omega_b$. where Φ is the gravitational potential and r and θ are the usual polar coordinates. Thus. the inflow speed is

$$\frac{dr}{dt} \approx \frac{d\Phi/d\theta}{2r\Omega_b}.$$

So by knowing the potential Φ for all r and θ from the modeling of the NIR images. and the bar pattern speed (Ω_b) they were able sum all the torques along their CO maps to estimate an inflow speed of 10-20 km s^{-1}.

Benedict. Smith. & Kenney (1996) compare the observed rotation curve of the barred galaxy NGC 4314 derived from high resolution CO maps to theoretical circular velocity rotation curves for mass models derived from near infrared images of this galaxy. The deviations of the CO velocities from circular suggest that inflow

speeds of 20 to 90 km s^{-1} are present near the dust lanes. Using a rather simplified argument (they assume that all the molecular gas in the inner 7″ flows inward at 30 km s^{-1}), this corresponds to mass inflow rates of 7 $M_\odot$/year.

Using a more complicated method to determine the mass inflow rate. Regan. Vogel. & Teuben (1997) compared a variety of observations with a hydrodynamical models and estimated the gas inflow speed for NGC 1530 to be 85-200 km s^{-1}. Assuming that all mass in the dust lanes reaches the nucleus. they obtain an upper limit of mass inflow rate. The mass flux $\dot{M}$ along the dust lane at a distance d from the nucleus can be written

$$\dot{M}(d) = \sigma(d)W V_{dl}(d)$$

where σ is the gas surface density (determined from the CO flux). W is the width of the dust lane (determined from high resolution multi-color images). and V_{dl} is the velocity of the gas along the dust lane (derived from Fabry-Perot Hα images and CO maps compared to galaxy models to correct for inclination). They find a mass inflow rate of 6 $M_\odot$/year. in excellent agreement with the estimates of Benedict. Smith. & Kenney (1996) derived for NGC 4314. Unfortunately. the large number of assumptions that had to be made for the galaxy model (mass-to-luminosity ratio. pattern speed. etc.) suggest that more measurements of this sort are needed to obtain more precise inflow rates for barred galaxies.

So overall it appears clear (both theoretically and observationally) that galactic bars are an excellent means of driving molecular gas into the nuclear regions where it can fuel nuclear activity. There is a problem with all of these models and calculations of gas flows in barred galaxies. in that the inner Lindblad resonance seems to be very effective at trapping molecular gas at the ILR radius (Combes & Gerin 1985; Athanassoula 1992). In a study of CO in four barred galaxy nuclei. Kenney et al. (1992) found that three of the galaxies exhibited a "twin peak" morphology (the

CO emission is confined to two peaks away from the center). consistent with what one might expect if the molecular gas was being trapped at the ILR radius as it flowed inward along the leading edge of the galactic bar. The fourth exhibited a central nuclear concentration. as if the galaxy had no ILR or the gas had found a way to get past it. The galaxy with the central peak of molecular gas is undergoing star formation. while the three twin peaked galaxies are not. This result suggests that ILRs may be a way of preventing molecular gas from traveling all the way into the nucleus of a barred galaxy. The double barred models discussed in the following sections provide a means of overcoming this gas trapping. It is the search for these nuclear bars that is the motivation for the remaining chapters of this thesis.

2.8 Double Barred Galaxy Models

The original theoretical study of nuclear bars (or double bars. or bars within bars) was performed by Shlosman. Frank. & Begelman (1989). They discuss the need for a mechanism that can transport molecular gas from the outer disks of galaxies. down to regions of a few pc. where it can be accreted by the black hole. The main difficulty in transporting gas in the outer disk of a galaxy (at tens of kpc from the nucleus) down to the regions surrounding a black hole (tens of pc) is that the specific angular momentum must be reduced by a factor of approximately 10^6. They show that viscous gas processes are not sufficient to transport enough material into the nuclei of galaxies to maintain the high luminosities of these AGN. They also note that a large scale bar alone could not be solely responsible for the gas transport into the nucleus. because the gas flows generally do not extend all the way in to the very centres of galaxies. In addition. ILRs can trap the gas on the way into the nucleus.

Shlosman. Frank. & Begelman (1989) propose that a large scale bar can collect molecular gas into a nuclear ring or disk. Subsequently. this ring or disk may also become unstable (Hohl 1971) and form yet another. smaller bar. interior to the ILR of the large scale bar. This nuclear bar may then transport material inward. until it encounters the ILR of the nuclear bar. at which point the process repeats itself until the gas is transported all the way into the centre of the galaxy through a series of nested bars. Thus. they conclude that large scale bars may be a necessary. but not sufficient condition for strong nuclear activity. They point out that nuclear bars may be prematurely disrupted by the onset of star formation in the molecular gas as it accumulates in the nuclear disk or ring. Thus. it may be that the formation (or lack of formation) of these nuclear bars determines the final state of activity in barred galaxies.

2.8.1 N-Body Models with Stars and Gas

Shaw et al. (1993) model galaxies as a 2D ensemble of stars and clouds. each as particles. The stars are collisionless and the clouds undergo energy loss and sticky collisions as described in §2.7.1 in the models of Combes & Gerin (1985). The results of their simulations show that a nuclear ring quickly forms. as has been seen in previous simulations. and the gas tries to settle into the x_2 orbits that run perpendicular to the bar inside the ILR radius. The gravitational torques caused by the large scale bar act to slow down the procession of this elongated ring. such that the gaseous ring begins to slide back into alignment with the large scale bar. but still leads it. Since the x_2 orbits are constantly being re-supplied with new gas from the disk. the steady state is a nuclear elongated ring that appears to lead the large scale bar by up to 30°. The gaseous ring may contain enough mass to draw some of the stars into these phase shifted orbits. explaining why the isophote twists are

visible in the near infrared (NIR) images. The whole system will rotate *at the same pattern speed*, with the inner part of bar (gas and stellar) leading, followed by the rest of the main bar (gas and stars). This model requires large amounts of molecular gas to reproduce the observed NIR isophote twists: 4-6% by mass. Without the gas, the stellar components of the models of Shaw et al. (1993) become kinematically heated very rapidly and destroy any nuclear structures that could be responsible for the NIR isophote twists.

In contrast, Friedli & Martinet (1993) propose that the nuclear bars must be kinematically distinct. If the nuclear bar and the large scale bar are rotating at the same pattern speed as proposed by Shaw et al. (1993) than the gravitational torques exerted by the large scale bar on the nuclear bar would act to pull the nuclear bar into alignment with the large scale bar. In addition, observations of NIR isophote twists show that the nuclear bar can either lead *or trail* the large scale bar, whereas the models of (Shaw et al. 1993) can only account for the nuclear bars that lead the large scale bar.

Friedli & Martinet (1993) model galaxies as a 3D stellar and gaseous system, with the stars treated as collisionless particles and the gas treated as a smooth fluid. Their simulations of double barred galaxies suggest in the models run without gas, any evidence of nuclear bars is quickly destroyed by the kinetic heating of the stars. When the gaseous component is added, the models evolve into a large scale bar and a nuclear bar, as the x_2 orbits of the primary bar are converted into the x_1 orbits of the nuclear bar. Eventually the nuclear bar gains enough mass to become kinematically distinct. It rotates with a pattern speed up to 3 times the pattern speed of the large scale bar. As the nuclear bar sweeps around, it slowly forms a nuclear ring. After approximately six rotations of the nuclear bar, the central region becomes chaotic, and the nuclear bar dissolves. The large scale bar and nuclear ring
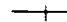
remain, since they are at. or beyond. the location of the inner Lindblad resonance. In order to create and sustain these nuclear bars. there must be a substantial gaseous component to prevent the kinematic heating of the stars. The galaxy must contain 10% gas by mass, or contain 2% (of the total mass) gas in the inner kpc.

In summary. these two models are both capable of re-creating the observed NIR isophote twists using two very different mechanisms. The one thing these models do have in common is the need to include rather large amounts of a dissipative material. such as molecular gas. In both models. the gas dissipation is rather arbitrarily set at some value that relates to an energy loss of $\sim 10\%$. Combes (1994) studied the effect of the gas dissipation on the simulations of double barred galaxies and shows that simulations containing higher viscosity gas tend to form kinematically distinct bars (like those of Friedli & Martinet 1993). Less viscous gas produces nuclear gas bars that lead the nuclear stellar bar by up to 30°. but rotate at the same pattern speed as the main bar of the galaxy (like those of Shaw et al. 1993). So this suggests that more detailed studies of the dissipative properties of molecular gas are needed to increase the accuracy of these models of barred galaxy nuclei.

2.8.2 Models Without Gas: Purely x_2 orbits

In order to bypass the complications introduced by attempting to model the gaseous component of barred galaxies accurately. a variety of groups have modeled NIR isophote twists using purely stellar models. As discussed already. the main cause of nuclear bars in the N-body models is the feeding of gas onto the x_2 orbits. Contopoulos & Papayannopoulos (1980) showed that the x_2 family of orbits are stable and may become populated by stars. This model neglects the self gravity of stars that tend to result in the kinematic heating as the stars interact deep in the potential well near the nucleus of the galaxies. If the nuclear bars are simply stars

that orbit in the x_2 orbits, then we should always see the nuclear bar perpendicular to the large scale bar. Is it possible that the observed variation in angles between the large scale and nuclear bar are simply the result of seeing these galaxies at various inclinations?

Friedli & Martinet (1993) compared a simple model of perpendicular x_1 and x_2 with observations of isophote twists in barred galaxies in an attempt to determine if these twists were the result of the stable stellar (x_2) orbits that run perpendicular to the main bar seen at various oblique angles. In their model, the barred galaxy would look like —+— (seen face-on and un-rotated) where the vertical line represents the x_2 orbits and the horizontal line is the main bar (comprised of the x_1 orbits). They found that projection of the perpendicular x_2 orbits cannot explain all the observed angles of NIR isophote twists and concluded that they must be time dependent systems (i.e. the inner bar rotating at a different pattern speed than the main bar).

So, if the galaxy consists of two kinematically distinct bars, is it possible that the average density of all the stars on their orbits in the time-varying potential adds up exactly to what is needed to give rise to the potential in which they move (i.e. can it be a self consistent model)? Recently, Maciejewski & Sparke (2000) performed a study of closed orbits of double barred galaxies with different pattern speeds for the large scale and nuclear bar. Following a similar approach as Contopoulos & Papayannopoulos (1980), they found that closed orbits do exist in these seemingly chaotic systems. The x_2 orbits are capable of supporting the nuclear bar as it rotates. They predict that the nuclear bar should change shape and axial ratio as it rotates, with the distortions induced by the gravitational tug of the large scale bar. The predicted shapes could be tested with observations of nuclear bars at sufficiently high resolution.

2.8.3 Triaxial Stellar Bulges

The original explanation of the isophote twists observed in the centres of early type galaxies does not require the existence of a nuclear bar at all. Kormendy (1979) proposed that the twists are the result of a stellar bulge that is triaxial in shape. The projection of this triaxial bulge would result in a twisting of the isophotes which could easily be mistaken as a secondary nuclear bar (see Figure 2.4).
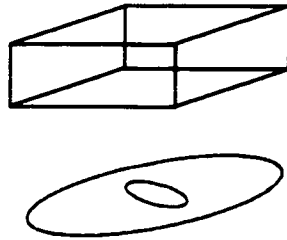
Figure 2.4: Schematic Diagram of How a Triaxial Bulge Results in Isophote Twists

In this example. we represent a triaxial stellar bulge with the triaxial box shown in the upper panel. If the box were luminous and transparent. the resulting isophotes would have orientations similar to those shown in the lower panel.

2.9 Observations of Double Barred Galaxies

2.9.1 Nuclear Bars in Active Galaxies as Seen from the Earth

The original observations of isophote twists in the nuclei of galaxies is traced back to de Vaucouleurs (1974) who identified isophote twists in the centres of NGC 1291 and NGC 1329. These isophote twists were attributed to the presence of a triaxial "spheroid" or stellar bulge by Kormendy (1979). In this picture. the isophote twists result from the projection of a triaxial bulge of older stars that surround the nucleus

of a galaxy seen as it appears in projection on the sky. A study of axial ratios of some of the isophote twists indicates that not all of these can be attributed to a triaxial stellar bulge. Some of them must be actual nuclear bars.

Wozniak et al. (1995) performed an optical survey of 36 galaxies that were thought to contain isophote twists or triaxial structures in their nuclei. They find that of these. 22 show signs of some form of triaxial structure. The dust obscuration at these optical wavelengths make determination of nuclear structures difficult. so in a second paper (Friedli et al. 1996) they present NIR observations of a sub-sample of 13 from the original 36 galaxies that showed evidence for a nuclear bar. The NIR images verified the existence of nuclear bars in these galaxies and they show that when deprojected. the primary bar and the nuclear bar have no preferred orientation with respect to each other. They also find that the ratio of the major axis of the primary bar to the nuclear bar ranges from 4 to 13. with an average of 7. The primary bar has an ellipticity of 0.58. while the nuclear bars are generally narrower with an ellipticity of 0.31. They find that the occurrence of Seyfert activity is high in these double barred galaxies (6 of 13).

Elmegreen et al. (1996) studied the NIR images of 21 barred galaxies that cover a wide range of morphological classifications. They find that isophote twists occur preferentially in earlier type galaxies[3]. Half of the early type galaxies (SBa-SBbc) and none of the later type galaxies (SBc-SBm) show signs of nuclear bars. Since the early type galaxies are known to be more likely to contain ILRs (Combes & Gerin 1985). the findings of this work suggest that bars may be associated with galaxies that contain ILRs. Elmegreen et al. (1996) do find galaxies that contain

---

[3]Early type galaxies are those which have larger bulges than later type galaxies. Early type galaxy classifications are suffixed with the letters 'a' or 'b'. while later types are marked with 'c' or 'm'.

rings (hence ILRs) but contain no nuclear bars. so it seems that the presence of an ILR is not sufficient condition for a nuclear bar.

The previous studies have been selecting target galaxies that are believed to contain nuclear bars based on previous observations. Thus. meaningful statistics on the occurrence of nuclear bars is difficult. The largest and most recent NIR survey of the nuclei of disk galaxies (spiral and barred) was undertaken by Jungwiert. Combes. & Axon (1997). They observed 72 galaxies closer than 40 Mpc and observed a wide range range of nuclear morphologies including 17 galaxies with either double nuclear bars or a nuclear bar nested in a triaxial bulges. as well as 3 nuclear bars in non-barred galaxies (as classified by RC3: de Vaucouleurs et al. 1991). Of the 56 galaxies in which they were able to perform deprojections. 37 of them contained evidence for some form of nuclear bar (either single or double). Of these. 9 were Seyferts.

It seems that there is an abundance of Seyfert activity in double barred galaxies. If we wish to address mechanisms that may be at work in the very centres of theses galaxies. we will need much higher resolution observations. Currently. the only instrument with the resolution to see the inner tens of parsecs of AGN is the Hubble Space Telescope.

2.9.2 Nuclear Bars in Active Galaxies with the Hubble Space Telescope

In an effort to determine if nuclear bars are prevalent in the nuclei of AGN. Regan & Mulchaey (1999) used the Hubble Space Telescope to observe the nuclei of 12 active galaxies. These galaxies were previously found to contain the NIR isophote twists that are thought to be the signature of a double barred galaxy. They argue that stellar light does not necessarily trace the gravitational potential in the nuclei

of galaxies because of its high velocity dispersion. They claim that gas and dust are better tracers of potential. and since current generation millimeter and submillimeter arrays do not have the resolution to map the details of the inner 3″ of these galaxies. they use color Hubble Space Telescope (HST) images to trace the nuclear dust distributions. They searched for the signature straight dust lanes associated with bars (see Figures 2.1 and 1.1 for example). They found the signature of bars in only 3 of the 12 galaxies. Two of the nuclei showed a ring structure while the rest (6) resembled the spiral arm patterns seen in large scale spiral galaxies. Regan & Mulchaey (1999) conclude that the nuclear bars are not the dominant fueling mechanism for AGNs. and suggest that perhaps nuclear spirals may be responsible.

In a similar study. Martini & Pogge (1999) observed the nuclei of 24 Seyfert 2 galaxies using the HST. Unlike the study of Regan & Mulchaey (1999) who chose their galaxy sample based on the existence evidence of nuclear bars. Martini & Pogge (1999) chose their sample from the CfA spectroscopic survey of AGN by Huchra & Burg (1992). They chose galaxies that were typically closer than 100 Mpc. which allows resolution down to at worst a few tens of parsecs with the HST. Using a technique similar to Regan & Mulchaey (1999). they use the color maps $(V - H)$ to search for dust lanes associated with bars in the nuclei of these 24 galaxies. They find that 20 of the 24 galaxies have nuclear spirals. 2 are nearly edge-on so their morphology cannot be determined. and the remaining two are very irregular and look like the remnants of a merger. They can therefore rule out nuclear bars in all but 4 of these galaxies.

It should be noted that the dust lanes do not always appear straight in barred galaxies. If the bar is weak. the dust lanes can take on a very curved appearance. similar to those of two-armed spiral galaxies (Athanassoula 1992: see Figure 2.3: lower middle panel). Thus the appearance of curved dust lanes does not necessarily

rule out the existence of weak or rapidly rotating nuclear bars (as predicted by the models of Friedli & Martinet (1993): see §2.8). In addition, using the interstellar medium (ISM: dust, gas) may not be the best indicator of gravitational potential. Recent results from the Berkeley Illinois Maryland Array Survey Of Nearby Galaxies (BIMA SONG) survey of molecular gas in galaxies shows a wide range of gas distributions in samples of galaxies with nearly identical stellar distributions, suggesting that other factors such as star formation may re-distribute the molecular gas in any number of distributions (Kartik Sheth: private communication). Molecular gas of different viscosities may also respond differently in similar gravitational fields (Combes 1994). More detailed studies of the effect of molecular gas conditions (such as density and temperature) on the viscosity of molecular gas are needed before we can use the ISM as a tracer of gravitational potential.

2.10 The Long Term Fate of Double Barred Galaxies

Pfenniger & Norman (1990) modeled barred galaxies containing black holes in their nuclei. They find gas inflow in barred galaxies (without ILRs) feeds the black hole, increasing its mass. As the black hole grows, it modifies the gravitational potential and changes the rotation curve such that ILRs eventually appear. Oddly, they find that mass accretion accelerates after the formation of an ILR. This is because the chaotic region interior to the ILR in these models grows as the central mass increases and pushes the ILR radius outward. Thus, the larger the chaotic region, the greater the accretion onto the black hole. As the black hole becomes stronger, so does the ILR, increasing the accretion rate. The material that crosses the ILR may form a disk around the central mass concentration. This disk may become bar unstable and form a nuclear bar. The nuclear bar accelerates the accretion onto the

black hole, which acts to sphericalize the gravitational potential, which eventually leads to the disruption of both bars. The end result would be a kinematically hot spheroid, that will eventually become weakly triaxial (Pfenniger & Norman 1990).

2.11 A Brief Description of the Galaxies Discussed in this Thesis

Here I briefly describe some of the past studies of the galaxies discussed in the following chapters. Much of this information was obtained using the NASA-IPAC Extragalactic Database (NED). These summaries are not intended to be complete, but are meant to give the reader a feel for the wide variety of galaxies that are contained in my sample. I will provide more details of each galaxy in the individual chapters when necessary. Images of the nuclear regions of these galaxies is shown in Figure 2.5. The images with the light greyscale and black contours are taken from Wozniak et al. (1995) (B and I) and Friedli et al. (1996) (J). The images with the dark greyscales with the white contours are taken from Mulchaey et al. (1997) and the images that are just black contours are from Shaw et al. (1993).

NGC 470: This galaxy is classified as SA(rs)b in de Vaucouleurs et al. 1991 but is found to have an elongated bar structure in the NIR images of Friedli et al. (1996). They also see evidence for nuclear isophote twists. The nucleus is undergoing starburst activity (Jogee 1998) and NGC 470 is probably interacting with NGC 474 (de Vaucouleurs 1974). It was mapped in ^{12}CO $J=1-0$ by Jogee (1998) and the molecular gas distribution follows the isophote twists seen by Friedli et al. (1996) suggesting that there really is a nuclear bar at the centre of this galaxy. The CO maps were kindly provided to us prior to publication by S. Jogee.
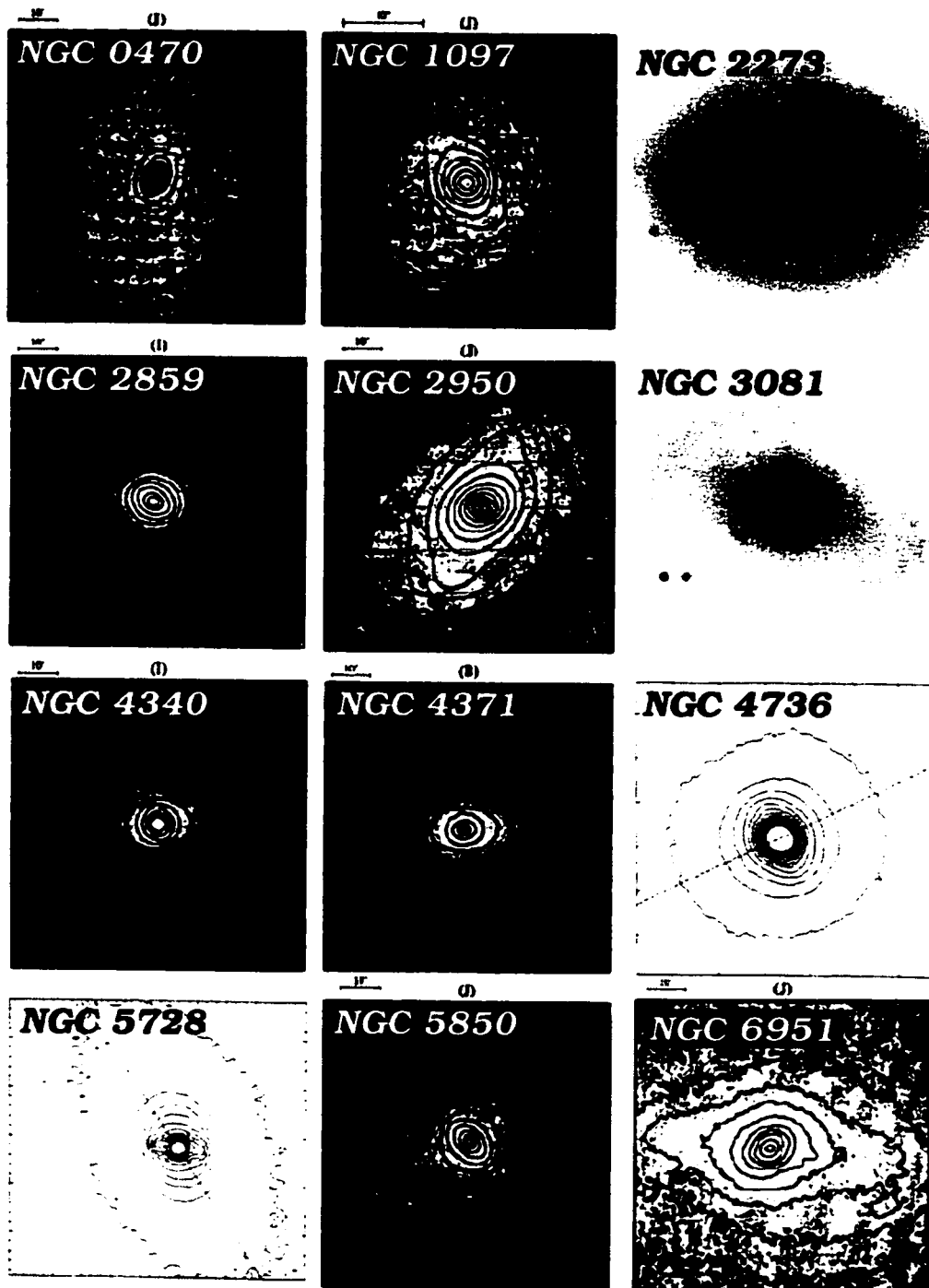
Figure 2.5: Optical and NIR images of the Galaxies Discussed in this Thesis
This figure shows the B-band and NIR images of the centres of galaxies that are considered double barred candidates based on the isophote twists at the very centres. Note how the outer isophotes have a different position angle than the isophotes near the nucleus. These are either caused by the presence of a true nuclear bar or are the result of a triaxial stellar bulge.

NGC 1097: This galaxy is classified as SB(s)b by de Vaucouleurs et al. (1991). It was originally thought to contain a LINER nucleus, but new observations suggest that it is actually a Seyfert 1 (Kinney et al. 1993; Friedli et al. 1996). It has a strong bar (possibly triggered by interaction with the companion galaxy NGC 1097A) with a bright circumnuclear ring with a radius of $10''$ that has been seen at a number of wavelengths including the low resolution CO maps of Gerin et al. (1988). The NIR images of Shaw et al. (1993) indicate the presence of a nuclear bar interior to the ring. No high resolution CO maps of this galaxy exist in the literature.

NGC 2273: Classified as a SB(r)a by (de Vaucouleurs et al. 1991), this galaxy contains a strong bar and a number of rings: a circumnuclear one and another one (perhaps two) near the bar ends (van Driel & Buta 1991). It is thought to contain a nuclear starburst based on its "M82-like" infrared properties (Young & Devereux 1991). The NIR images of this galaxy by Mulchaey, Regan, & Kundu (1997) show a nuclear bar nearly perpendicular to the large scale bar (see Figure 3.2). The wide emission lines seen by Huchra, Wyatt, & Davis (1982) suggest that it contains a Seyfert 2 nucleus.

NGC 2859: This galaxy that not been extensively studied in the past. It is classified as a (R)SB(r) galaxy by de Vaucouleurs et al. (1991). The "(R)" indicates the presence of an outer ring, while the "(r)" indicates a circumnuclear ring. There is no evidence in the literature that this galaxy contains any form of nuclear activity, but it was found to contain a nuclear bar in the images of Wozniak et al. (1995)

NGC 2950: Classified as a (R)SB(r) galaxy by de Vaucouleurs et al. (1991), this galaxy also contains an outer and inner ring. It, too, is relatively poorly studied. It is known to contain a very bright nucleus, but there is no evidence in the literature that it is undergoing any form of nuclear activity. It has been identified as a double bar galaxy candidate by the NIR survey of Friedli et al. (1996).

NGC 3081: This strongly barred SBa. Seyfert 2 galaxy (Kinney et al. 1993) has gained much attention recently. It was identified as a double bar candidate the in NIR survey of Friedli et al. (1996). It also contains a nuclear ring that surrounds the nuclear bar. It was one of the targets of the Hubble Space Telescope survey of nuclear bars undertaken by Regan & Mulchaey (1999). The appearance of the nuclear bar in their HST images is impressive. The nucleus of this galaxy resembles a scaled down version of the large scale galaxy rotated at a different position angle. It is one of only two galaxies that have nuclear bars in the HST survey of Regan & Mulchaey (1999).

NGC 4340: Yet another poorly studied. strongly barred galaxy. This one is classified SB(r) by de Vaucouleurs et al. (1991) and has no published record of its nuclear activity. It was observed to contain a nuclear bar in the NIR survey of Friedli et al. (1996).

NGC 4371: A poorly studied. strongly barred galaxy classified as SB0(r) by (de Vaucouleurs et al. 1991). It has no published published record of its nuclear activity. but it contains a very bright nucleus that may harbour Seyfert activity if studied spectroscopically. It was identified as a double barred galaxy by Wozniak et al. (1995).

NGC 4736: This is the closest galaxy in our sample (4.3 Mpc) and is also probably the best studied galaxy in our sample. It is better known as M94. Based on optical images. it has been classified as SAab (the "ab" means is is somewhere between "a" and "b"). The NIR images of Shaw et al. (1993) suggest that this galaxy may contain a slight large scale bar distortion. as well as a nuclear bar. It contains an expanding ring of star formation and is known to contain LINER activity in the nucleus (Kinney et al. 1993). High resolution CO maps of this galaxy (Wong & Blitz 2000) show an elongated central peak of emission that aligns with the NIR

isophote twists of Shaw et al. (1993). The higher resolution CO images of Sakamoto et al. (1999) show that this peak actually resolves into two peaks separated by 3″.

NGC 5728: This barred spiral galaxy is the most distant in our sample (37 Mpc). It is classified as SAB(r)a and also contains a Seyfert 2 nucleus (de Vaucouleurs et al. 1991). Color maps indicate the galaxy contains two blue rings of recent star formation, one in the nucleus ($r \approx 5''$: Wilson et al. 1993) and one near the main bar ends ($r \approx 55''$: Schommer et al. 1988). Two dust lanes emerge from just outside the nuclear ring and run parallel to the main bar of the galaxy. Near infrared images of this galaxy strongly suggest the presence of a nuclear bar (Shaw et al. 1993). Prada & Gutiérrez (1999) proposed that the nuclear bar in this galaxy may actually be counter-rotating.

NGC 5858: This galaxy is one of the most distant of our sample (34 Mpc) but fortunately, it is one of the biggest. It is classified as SB(r)b by de Vaucouleurs et al. (1991) and shows no evidence of starburst or Seyfert activity. It shows strong signs of a nuclear bar in the NIR images of Friedli et al. (1996). It has been mapped at low resolution in CO by Leon, Combes, & Friedli (2000), who find vast amounts of molecular gas in the large scale bar. They propose that the lack of star formation despite such a large reservoir of molecular gas may be the result of strong shearing in the bar that is disrupting the molecular clouds before stars can form. The high resolution CO maps of this galaxy (Leon, Combes, & Friedli 2000) show a single off-centre peak of emission that does not correspond with either the large scale or nuclear bar.

NGC 6951: This galaxy is classified as SAB(rs)bc by de Vaucouleurs et al. (1991) and contains a Seyfert 2 nucleus. It is classified as a having one (perhaps 2!) nuclear bars in the NIR images of Friedli et al. (1996). This galaxy has a circumnuclear ring of star formation whose radius coincides with twin peaks of dense

molecular gas upon which the star formation is likely feeding (Kohno. Kawabe. &

Vila-Vilaró 1999). These twin peaks of molecular gas are likely the result of gas

collection at the ILR in this barred galaxy.

Bibliography

Antonucci. R.. 1993. *ARAA* **31**. 473.

Athanassoula. E.. 1992. *MNRAS* **259**. 345.

Benedict. G. F.. Howell. D. A.. Jorgensen. I.. Smith. B. J.. & Kenney. J. D. P.. 2000. Ngc 4314 - a galaxy dynamicist's playground. In *AAS/Division of Dynamical Astronomy Meeting*. Volume 32. pp. 1102.

Benedict. G. F.. Smith. B. J.. & Kenney. J. D. P.. 1996. *AJ* **112**. 1318.

Binney. J. & Merrifield. M.. 1998. *Galactic astronomy*. Galactic astronomy / James Binney and Michael Merrifield. Princeton. NJ : Princeton University Press. 1998. (Princeton series in astrophysics).

Binney. J. & Tremaine. S.. 1987. *Galactic dynamics*. Princeton. NJ. Princeton University Press. 1987. 747 p.

Combes. F.. 1994. Nuclear gas flows in barred galaxies. In *Mass Transfer Induced Activity in Galaxies*. pp. 170. ed. I. Shlosman. Cambridge Univ. Press.

Combes. F. & Gerin. M.. 1985. *A&A* **150**. 327.

Contopoulos. G. & Papayannopoulos. T.. 1980. *A&A* **92**. 33.

de Vaucouleurs. G.. 1974. Structures of central bulges and nuclei of galaxies. In *IAU Symp. 58: The Formation and Dynamics of Galaxies*. Volume 58. pp. 335.

de Vaucouleurs. G.. de Vaucouleurs. A.. Corwin. H. G.. Buta. R. J.. Paturel. G.. & Fouque. P.. 1991. *Third Reference Catalogue of Bright Galaxies*. Volume 1-3. XII. 2069 pp. 7 figs.. Springer-Verlag Berlin Heidelberg New York.

de Vaucouleurs. G.. de Vaucouleurs. A.. & Corwin. J. R.. 1976. Second reference catalogue of bright galaxies. In *Second reference catalogue of bright galaxies. 1976. Austin: University of Texas Press.*

Dutil. Y. & Roy. J. .. 1999. *ApJ* **516**. 62.

Elmegreen. D. M.. Elmegreen. B. G.. Chromey. F. R.. Hasselbacher. D. A.. & Bissell. B. A.. 1996. *AJ* **111**. 1880.

Friedli. D. & Martinet. L.. 1993. *A&A* **277**. 27.

Friedli. D.. Wozniak. H.. Rieke. M.. Martinet. L.. & Bratschi. P.. 1996. *A&AS* **118**. 461.

Gerin. M.. Combes. F.. & Nakai. N.. 1988. *A&A* **203**. 44.

Hawarden. T. G.. Mountain. C. M.. Leggett. S. K.. & Puxley. P. J.. 1986. *MN-RAS* **221**. 41P.

Ho. L. C.. Filippenko. A. V.. & Sargent. W. L. W.. 1997a. *ApJ* **487**. 591.

Ho. L. C.. Filippenko. A. V.. & Sargent. W. L. W.. 1997b. *ApJ* **487**. 579.

Hohl. F.. 1971. *ApJ* **168**. 343.

Huchra. J. & Burg. R.. 1992. *APJ* **393**. 90.

Huchra. J. P.. Wyatt. W. F.. & Davis. M.. 1982. *AJ* **87**. 1628.

Jogee. S.. 1998. *Molecular Gas and Starbursts in the Circumnuclear Regions of Spiral Galaxies.* Ph.D. Thesis. Yale University.

Jungwiert. B.. Combes. F.. & Axon. D. J.. 1997. *A&AS* **125**. 479.

Kenney. J. D. P.. Wilson. C. D.. Scoville. N. Z.. Devereux. N. A.. & Young. J. S.. 1992. *ApJL* **395**. L7.

Kinney. A. L.. Bohlin. R. C.. Calzetti. D.. Panagia. N.. & Wyse. R. F. G.. 1993. *ApJSS* **86**. 5.

Knapen. J. H.. Shlosman. I.. & Peletier. R. F.. 2000. *ApJ* **529**. 93.

Kohno. K.. Kawabe. R.. & Vila-Vilaró. B.. 1999. *ApJ* **511**. 157.

Kormendy. J.. 1979. *ApJ* **227**. 714.

Kormendy. J. & Richstone. D.. 1995. *ARAA* **33**. 581.

Leon. S.. Combes. F.. & Friedli. D.. 2000. Single co peak in the double bar galaxy
    ngc 5850. In *ASP Conf. Ser. 197: Dynamics of Galaxies: from the Early
    Universe to the Present*. pp. 61.

Lin. C. C. & Shu. F. H.. 1964. *ApJ* **140**. 646.

Maciejewski. W. & Sparke. L. S.. 2000. *MNRAS* **313**. 745.

Martini. P. & Pogge. R. W.. 1999. *AJ* **118**. 2646.

McLeod. K. K. & Rieke. G. H.. 1995. *ApJ* **441**. 96.

Moles. M.. Marquez. I.. & Perez. E.. 1995. *ApJ* **438**. 604.

Mulchaey. J. S. & Regan. M. W.. 1997. *ApJ* **482**. L135.

Mulchaey. J. S.. Regan. M. W.. & Kundu. A.. 1997. *ApJSS* **110**. 299.

Ondrechen. M. P.. 1985. *AJ* **90**. 1474.

Ondrechen. M. P. & van der Hulst. J. M.. 1983. *ApJ* **269**. L47.

Ostriker. J. P. & Peebles. P. J. E.. 1973. *ApJ* **186**. 467.

Peletier. R. F.. Knapen. J. H.. Shlosman. I.. Pérez-Ramírez. D.. Nadeau. D..
    Doyon. R.. Espinosa. J. M. R.. & Garcia. A. M. P. .. 1999. *ApJS* **125**. 363.

Pence. W. D. & Blackman. C. P.. 1984. *MNRAS* **207**. 9.

Pfenniger. D. & Norman. C.. 1990. *ApJ* **363**. 391.

Prada. F. & Gutiérrez. C. M.. 1999. *ApJ* **517**. 123.

Quillen. A. C.. Frogel. J. A.. Kenney. J. D. P.. Pogge. R. W.. & Depoy. D. L..
    1995. *ApJ* **441**. 549.

Regan. M. W. & Mulchaey. J. S.. 1999. *AJ* **117**. 2676.

Regan. M. W.. Vogel. S. N.. & Teuben. P. J.. 1997. *ApJ* **482**. L143.

Roberts. W. W.. 1969. *ApJ* **158**. 123.

Sakamoto. K.. Okumura. S. K.. Ishizuki. S.. & Scoville. N. Z.. 1999. *ApJ* **525**. 691.

Schommer. R. A.. Caldwell. N.. Wilson. A. S.. Baldwin. J. A.. Phillips. M. M.. Williams. T. B.. & Turtle. A. J.. 1988. *ApJ* **324**. 154.

Seigar. M. S. & James. P. A.. 1998. *MNRAS* **299**. 672.

Sellwood. J. A.. 1981. *A&A* **99**. 362.

Shaw. M. A.. Combes. F.. Axon. D. J.. & Wright. G. S.. 1993. *A&A* **273**. 31.

Sheth. K.. 2000. *Molecular gas properties of barred spiral galaxies*. Ph.D. Thesis. University of Maryland.

Shlosman. I.. Frank. J.. & Begelman. M. C.. 1989. *Nature* **338**. 45.

Solomon. P. M.. Sanders. D. B.. & Scoville. N. Z.. 1979. *ApJ* **232**. L89.

Teuben. P. J.. Sanders. R. H.. Atherton. P. D.. & van Albada. G. D.. 1986. *MNRAS* **221**. 1.

van Driel. W. & Buta. R. J.. 1991. *A&A* **245**. 7.

Veron-Cetty. M. . & Veron. P.. 1991. *A Catalogue of quasars and active nuclei*. ESO Scientific Report. Garching: European Southern Observatory (ESO). 1991. 5th ed.

Vila-Costas. M. B. & Edmunds. M. G.. 1992. *MNRAS* **259**. 121.

Wilson. A. S.. Braatz. J. A.. Heckman. T. M.. Krolik. J. H.. & Miley. G. K.. 1993. *ApJL* **419**. L61.

Wong. T. & Blitz. L.. 2000. *ApJ* **540**. 771.

Wozniak. H.. Friedli. D.. Martinet. L.. Martin. P.. & Bratschi. P.. 1995. *A&AS* **111**. 115.

Young. J. S. & Devereux. N. A.. 1991. *ApJ* **373**. 414.

Chapter 3

Molecular Gas in Double Barred Galaxies I. The Diverse Morphology and Dynamics of NGC 2273 and NGC 5728

Abstract

Double bars have been proposed as a means of transporting molecular gas past inner Lindblad resonances into the nuclear regions. where it can fuel active or starburst nuclei. Thus far. the existence of double bars has been determined by isophote twists seen in the near infrared. which could probe the bulge properties of these galaxies rather than the disk properties. We have observed two double bar galaxy candidates (NGC 2273 and NGC 5728) in ^{12}CO $J=1-0$ with the Caltech Millimeter Array. Despite the similar near infrared images of the two galaxies. we see rather different nuclear morphologies in the CO maps. NGC 2273 shows evidence of a nuclear bar misaligned from the main stellar bar by $\sim$90°. and aligned with the near infrared isophote twists observed by Shaw et al. (1993). NGC 5728 shows an arc of CO clumps that peaks just to the south-west of the dynamical center and curves to the south-east where it follows the dust lane to the south. Models of double-barred

galaxies suggest that these galaxies should contain a large fraction (5-10%) of their mass in the form of molecular gas. Our calculations suggest that NGC 2273 and NGC 5728 contain sufficient amounts of gas. but NGC 5728 is contains a smaller fraction (6%) than NGC 2273 (20%). If the dissipative nature of the gas has been overestimated in the models. the gas mass fraction could explain why we see a nuclear bar in NGC 2273 and no such structure in NGC 5728. The lack of a nuclear bar in the CO maps of NGC 5728 may be evidence that it is in a later stage of evolution. Bar dissolution may have just begun. and the gas has responded first. which may explain why we see a nuclear bar in the near infrared images of NGC 5728. but not in the CO maps.

keywords: Galaxies: starburst - galaxies: active - galaxies: ISM - galaxies: kinematics and dynamics - galaxies: nuclei

3.1 Introduction

The nuclei of barred spiral galaxies are often the setting for extraordinary events such as starbursts. molecular rings. inflow. and even Seyfert activity. The need to understand the mechanisms driving these phenomena has inspired a great number of observations and computer simulations. Models suggest that bars in galaxies can drive molecular gas into the nucleus where it can fuel the vigorous star formation activity that would otherwise exhaust the molecular gas content on timescales much shorter than observed (e.g. Combes 1994). Bars can only drive molecular gas inward until it reaches the Inner Lindblad Resonance (ILR: see Fig. 3.1). where it will accumulate into a ring that will halt the inflow. To overcome this. Shlosman. Frank. & Begelman (1989) proposed that the ring may become unstable and form a secondary bar inside the radius of the ILR. which could allow gas to reach much farther into the nucleus and possibly be the driving mechanism behind Seyfert nuclei.
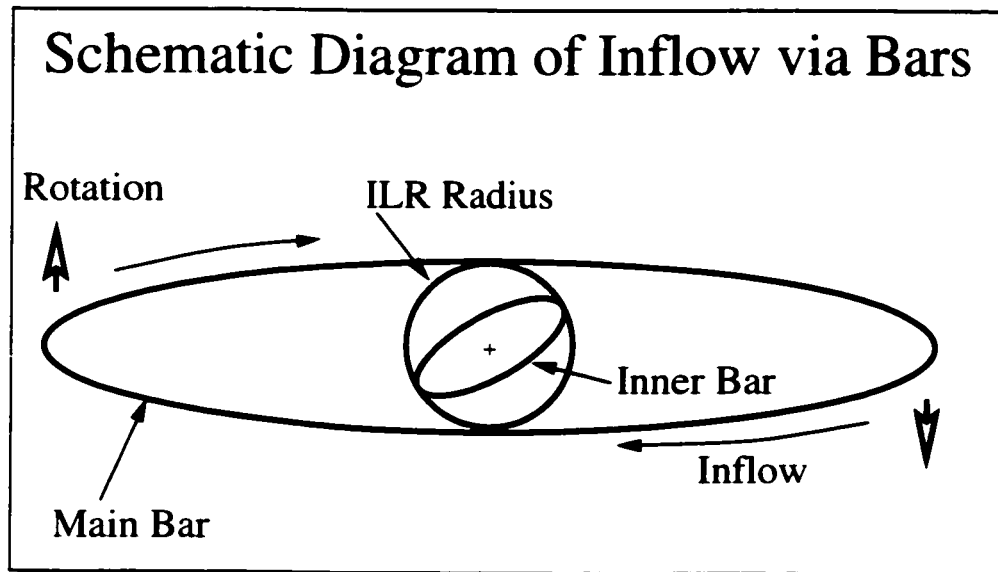
Figure 3.1: Schematic Diagram of a Double-Barred Galaxy

Schematic diagram of how a large scale bar (Main Bar) passing though a disk can transport material towards the nucleus of the galaxy. It is difficult for simulations to transport material all the way to the center because it tends to get trapped at the Inner Lindblad Resonance (ILR). This figure shows the Inner Bar that may form interior to the ILR and transport material all the way to the nucleus.

Recent near infrared (NIR) surveys reveal isophote twists in the central regions of barred galaxies which may be the signature of this 'bar within a bar' (e.g. Mulchaey. Regan. & Kundu 1997). There are three mechanisms which can account for NIR isophotal twists (Elmegreen et al. 1996). The first mechanism (hereafter called Model 1). proposed by Shaw et al. (1993). suggests the isophote twists are the result of an inner stellar bar triggered by a dissipative gaseous component and misaligned from the main bar. Their numerical simulations suggest that in the presence of two ILRs a nuclear ring can become elongated perpendicular to the main bar (along the $x2$ orbits). Gas dissipation steals angular momentum which can cause the inner part of the perpendicular gaseous ring to become more aligned with the main bar. resulting in the appearance of an elongated nuclear ring that leads the main bar. This gas ring exerts a torque on the stellar component of the bar. pulling it out of alignment also. The whole system would then rotate with the same angular frequency. with the inner gaseous ring and nuclear stellar bar leading the main bar[1]. The second mechanism (hereafter Model 2) suggests that the twists are the result of a kinematically distinct inner bar (Friedli & Martinet 1993). Their N-body simulation (with stars and gas) suggests gas inflow along the bar can accumulate enough mass that the inner part of the gas bar can become nearly self-gravitating and decouple from the main bar. The inner bar may rotate with a pattern speed of up to 6 times that of the main bar. The third mechanism (Model 3) suggests that the NIR isophote twists may be the result of a triaxial stellar bulge (Kormendy 1979).

These models can be tested through observations of the molecular gas morphology and dynamics. Model 1 would exhibit an inner gaseous bar that leads the inner

---

[1]Note: Shaw et al. (1993) suggest that the NIR isophote twists are *not* the result of a *distinct* nuclear bar. but simply a distortion of the main bar. For ease of comparison with the other models. we will. however. also refer to this main bar distortion as a nuclear bar.

stellar bar slightly. but has the same rotation speed as the main bar. Model 2 would show a gaseous inner bar that is rotating with a different pattern speed than the main bar. Thus. molecular gas dynamics should allow us to distinguish between these models. Model 3 is associated with the stellar bulge. Since there is very little gas in the bulge compared to the disk of a galaxy. the isophote twists should not be visible in the CO maps. Both the first and second models require the galaxy contain about 5-10% gas (by mass) in order to produce long-lived nuclear bars. Without this large gas fraction. there is not enough dissipation in the models. and the observed structures do not last long enough to be as common as they are observed to be (Shaw et al. 1993: Friedli & Martinet 1993).

This paper presents observations taken with the Caltech Millimeter Array of two galaxies that exhibit such NIR isophote twists: NGC 2273 and NGC 5728. NGC 2273 is a SB(r)a galaxy that has a Seyfert 2 nucleus. nuclear star formation (Mulchaey. Wilson. & Tsvetanov 1996). and a nuclear ring of dust ($r \approx 5''$: Yankulova 1999). It has a recession velocity of 1841 km s^{-1} (de Vaucouleurs et al. 1991) which implies that it is 24.5 Mpc away (assuming $H_0 = 75$ km s^{-1} Mpc^{-1}). It also has three outer rings which appear to be made by separate sets of spiral arms at $r \approx 0.'4$. 1.'1 and 1.'0. HI observations indicate that it is not very gas rich for a barred spiral galaxy with such a wide variety of nuclear activity (van Driel & Buta 1991). This observation is supported by the ^{12}CO $J=1-0$ spectra taken by Young & Devereux (1991). who find very narrow CO linewidths and conclude that most of the molecular gas must be contained in the central few arcseconds of the nuclei of NGC 2273. Color maps of the inner regions of NGC 2273 suggest that there is a reddened ring of dusty material ($r \sim 5''$) surrounding a region of high ionization (Yankulova 1999). NGC 5728 is a southern hemisphere barred spiral galaxy classified as SAB(r)a that also contains a Seyfert 2 nucleus. Its recession velocity of 2788

Table 3.1: Adopted Properties of NGC 2273 and NGC 5728

Property	NGC 2273	NGC 5728	References
R.A. (2000.0)	$06^h50^m08\overset{s}{.}7$	$14^h42^m24\overset{s}{.}0$	1
Dec. (2000.0)	$+60°50'45\overset{''}{.}1$	$-17°15'10\overset{''}{.}8$	1
Classification	SB(r)a	SAB(r)a	2
Optical Diameter	3′3	3′1	1, 2
Nuclear Ring Diameter	~10″	~10″	3, 4
Outer Ring Diameter(s)	0′7, 2′2, 3′1	55″	4, 5
Inclination	41°	48°	2, 4
Main Bar PA	~115°	~38°	4, 6
NIR Isophote Twist PA	~45°	~90°	6, 7
Heliocentric Velocity	1841km s^{-1}	2788km s^{-1}	2
Assumed Distance	24.5 Mpc	37.2 Mpc	8
Linear Scale	1″ = 120 pc	1″ = 180 pc	8

(1) NASA/IPAC Extragalactic Database; (2) de Vaucouleurs, de Vaucouleurs, Corwin, Buta, Paturel, & Fouque 1991; (3) Yankulova 1999; (4) Schommer et al. 1988; (5) van Driel & Buta 1991; (6) Mulchaey, Regan, & Kundu 1997; (7) Shaw et al. (1993); (8) Assumes $H_0 = 75$ km s^{-1} Mpc^{-1}

km s^{-1} (de Vaucouleurs et al. 1991) suggests it is located at a distance of 37.2 Mpc. Color maps indicate the galaxy contains two blue rings of recent star formation, one in the nucleus ($r \approx 5''$: Wilson et al. 1993) and one near the main bar ends ($r \approx 55''$: Schommer et al. 1988). Two dust lanes emerge from just outside the nuclear ring and run parallel to the main bar of the galaxy. Table 3.1 summarizes the properties and adopted parameters for these galaxies. These two galaxies were chosen as targets for this study because of the similarity in their nuclear and large scale morphologies: both galaxies are classified as Seyfert 2 galaxies and contain nuclear rings (which suggest the presence of an ILR), and, most importantly, both galaxies exhibit the NIR isophote twists thought to be the signature of a nuclear bar as discussed above.

In §3.2 we discuss the observations and data reduction techniques. In §3.3.1 and §3.3.2 we discuss the molecular gas distribution and dynamics, respectively. In

§3.4 we discuss the molecular gas mass determined from the ^{12}CO J=1−0 flux in comparison with the amount of molecular gas required by the models to produce the observed features. In §3.5 we compare our results to models of double barred galaxies, previous observations of these galaxies, and to observations of other galaxies. The paper is summarized in §3.6.

3.2 Observations and Data Reduction

We have observed the barred galaxies NGC 2273 and NGC 5728 in ^{12}CO J=1−0 (115.3 GHz) using the Caltech Millimeter Array. For NGC 2273 we have 3 tracks, two in the low-resolution (L) configuration, and one in the high-resolution configuration (H). For NGC 5728 we have four tracks (two H, one L, and one in the equatorial (E) configuration). Preliminary calibration was done using the calibration package MMA (Scoville et al. 1993). Only baselines with a coherence >0.5 were used. The quasars 0642+449 and 1334−127 were used for gain calibration and Neptune and 3C273 were used for flux calibration.

For NGC 2273, we used α(2000) = 06^{h}50^{m}08^{s}7, δ(2000) = +60°50′45″1 for the pointing center and the spectrometer was centered at V_{lsr} = 1841 km s^{-1}. For NGC 5728 we used the pointing center of α(2000) = 14^{h}42^{m}24^{s}0, δ(2000) = −17°15′10″8 and a recession velocity of V_{lsr} = 2930 km s^{-1}. In both cases, the spectrometer had a bandwidth of 240 MHz which corresponds to a velocity coverage of ∼620 km s^{-1}. The frequency resolution was 2 MHz, which gives a velocity resolution of 5.2 km s^{-1} at 115 GHz; however, we have binned the data to a resolution of 10.4 km s^{-1} to increase the signal to noise ratio.

For map making we used the data reduction software MIRIAD (Sault, Teuben, & Wright 1995). Data with unusually high visibilities were clipped, the maps were

naturally weighted and the inner quarter CLEANed to 1σ. The resulting synthesized beam is $3\overset{''}{.}0 \times 2\overset{''}{.}5$ (PA=21°) for NGC 2273 and $4\overset{''}{.}5 \times 3\overset{''}{.}0$ (PA=−12°) for NGC 5728. The rms noise in the maps is 3.09 Jy/beam km s^{-1} for NGC 2273 and 2.65 Jy/beam km s^{-1} for NGC 5728. The maps cover a 60″×60″ area. but only the regions with significant emission are shown in Figures 3.2 and 3.5.

3.3 Molecular Gas Distribution, Dynamics, and Comparisons to Models

3.3.1 Morphology

Figure 3.2 shows the NIR image (top panel) of Mulchaey. Regan. & Kundu (1997) as well as the integrated intensity ^{12}CO $J=1-0$ map (bottom panel) for NGC 2273. In the NIR image the contours start at 17 mag arcsec^{-2} (K_S band) and are in 0.5 mag increments. while in the CO map contours start at 3.1 Jy/beam km s^{-1} and increase in steps of 3.1 Jy/beam km s^{-1} (1σ). The CO emission is integrated over the velocity range where we see emission. namely from 1669 km s^{-1} to 1981 km s^{-1}. The ^{12}CO $J=1-0$ integrated intensity map (Fig 3.2) shows a small bar-like structure (P.A. ∼40°) that is approximately perpendicular to the main bar of the galaxy (P.A. ∼115°). Comparing the size of the CO bar with the synthesized beam. we see that the bar is resolved along its major axis. but may not be fully resolved along its minor axis. The integrated intensity map also shows finger-like structures protruding to the north and south of the CO bar. Assuming trailing spiral arms. these fingers line up with the leading edge of the main galactic bar.

The integrated intensity map only shows a two-dimensional view. If we want to see the details of how the molecular gas is distributed. we need to use the velocity
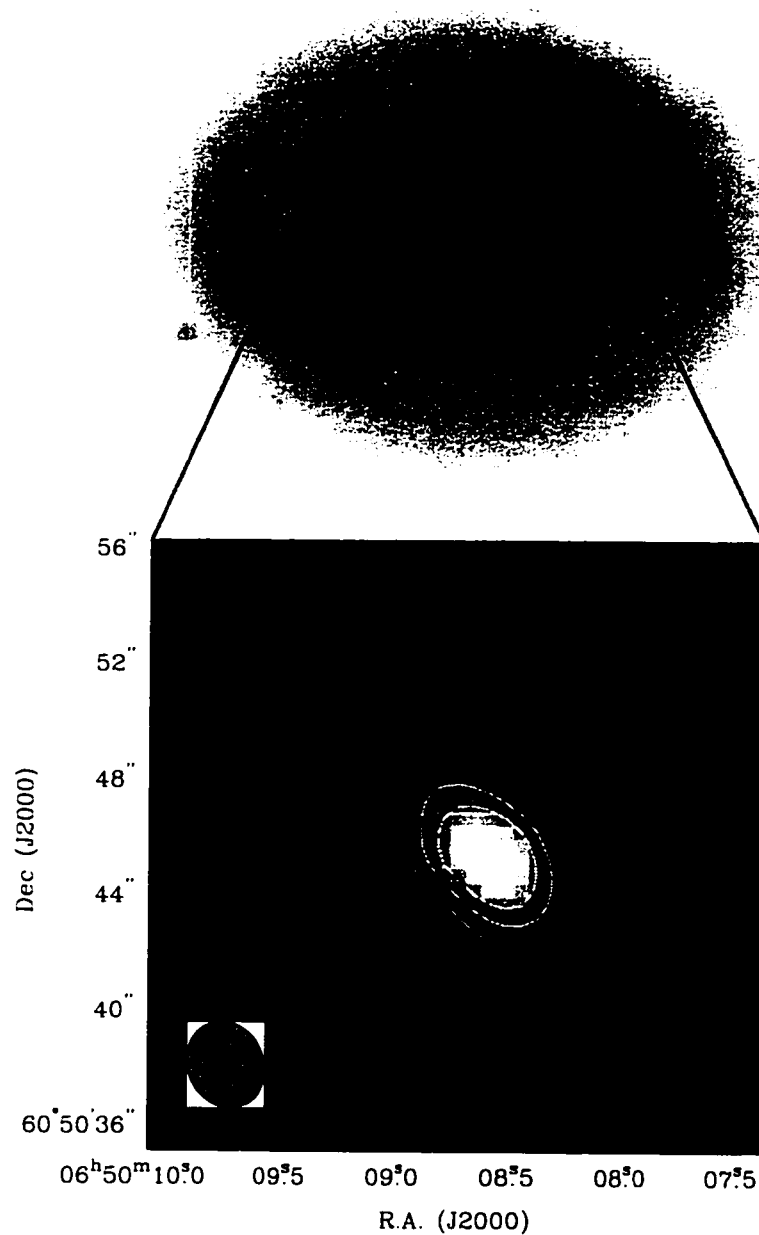
Figure 3.2: NIR and CO Images of NGC 2273

Integrated intensity map of ^{12}CO $J=1-0$ emission in NGC 2273. The CO map of NGC 2273 shows a nuclear bar aligned with the NIR isophote twists of Mulchaey et al. (1997). This result suggests that in NGC 2273, these NIR isophote twists are the result of a true nuclear bar. The fingers of emission to the north and south of the nuclear CO bar suggest evidence of inflow onto the inner bar along the leading edge of the main bar. The rms noise in the map is 3.1 Jy/beam km s^{-1} and the contour levels for the CO integrated intensity map start at 1σ and increase in steps of 1σ. The beam size of $3'' \times 2.5''$ with a PA of $21°$ is shown in the lower left corner.

information. The channel maps (Fig. 3.3) show that the CO bar is actually three dynamically separate clumps that merge into a bar-like structure when we average the emission over all channels. In order to emphasize the three individual clumps. we have used the clumpfind algorithm (Williams. de Geus. & Blitz 1994) and plotted the individual clumps in Fig. 3.4. The two clumps near the ends of the CO bar are brighter than the central peak. which suggests that molecular gas may be flowing in along the main bar. but is actually being collected into clumps which are presumably the location of the ILR. Similar CO morphologies have been seen in other barred galaxies such as the 'twin peaks' galaxies of Kenney et al. (1992) and the nearby starburst galaxy M82 (e.g. Shen & Lo 1995). We will discuss the importance of these similarities in §3.5.

The NIR image of NGC 2273 (top panel Figure 3.2: Mulchaey. Regan. & Kundu 1997) shows isophote twists in the inner $10 \times 10''$ misaligned from the main bar by $\sim 90°$. The ^{12}CO $J=1-0$ integrated intensity map (bottom panel: Figure 3.2) shows a nuclear bar that aligns with the NIR isophote twists. This result rules out the triaxial bulge explanation of the NIR isophote twists for NGC 2273 (Model 3: Kormendy 1979). The models of Shaw et al. (1993) predict that we should see the nuclear molecular component leading the nuclear isophote twists observed in the NIR by up to 20°. The models of Friedli & Martinet (1993) predict that the gaseous nuclear bar leading the gaseous stellar bar by up to 10°. In NGC 2273. there is no clear evidence that the gaseous inner bar is leading the stellar inner bar by any significant amount. However. this observation does not rule out either model. since Shaw et al. (1993) and Friedli & Martinet (1993) predict deviation angles between the gaseous and stellar bars as small as 5°. which is smaller than we can measure accurately from the maps.
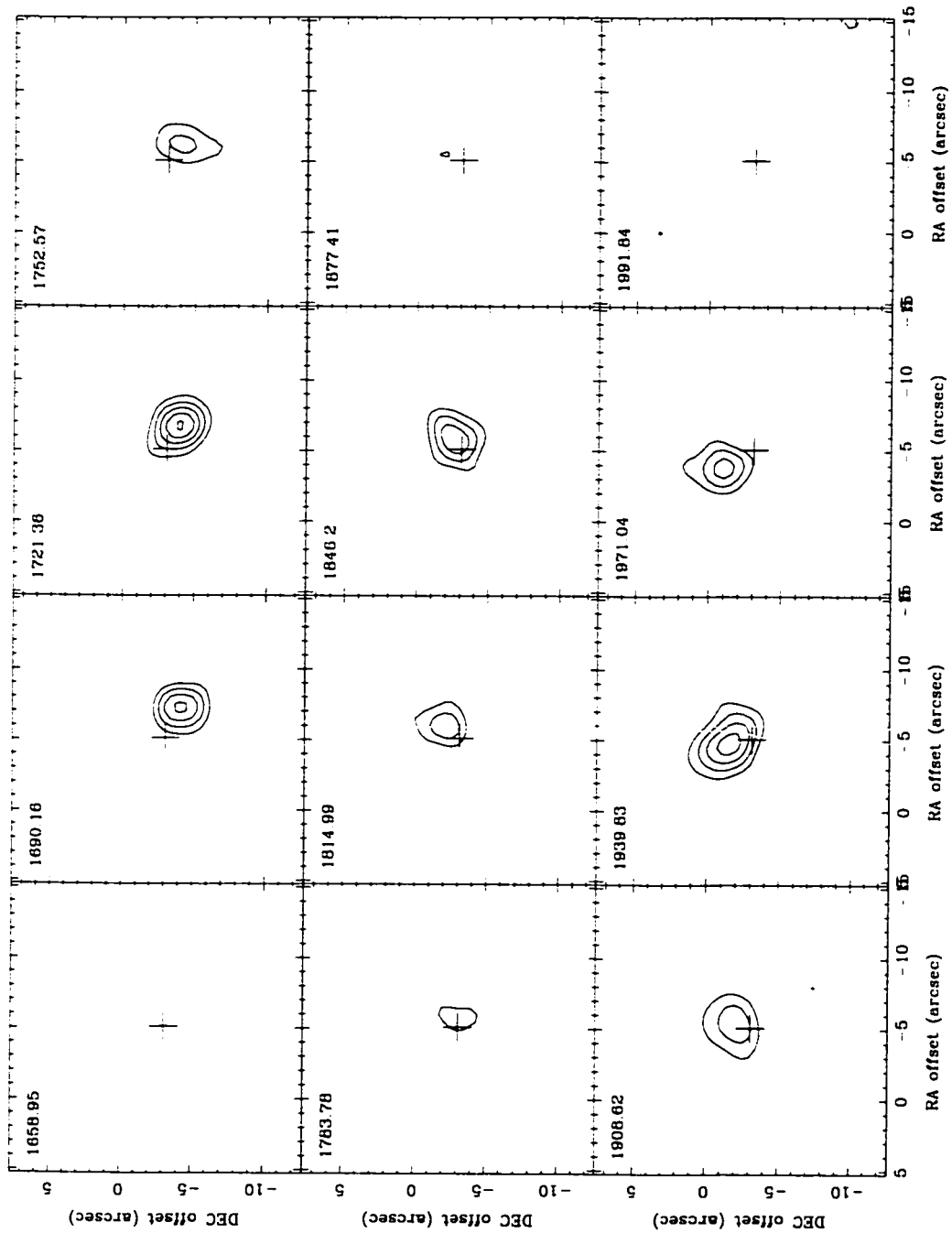
Figure 3.3: CO Channel Map of NGC 2273

The CO bar seen in Fig. 3.2 is actually comprised of three separate clumps. The contour levels are 0.04. 0.06. 0.08 ... Jy/beam (2. 3. 4 ... σ). The plus sign indicates the map center. The panels are shown at 31.2 km s^{-1} intervals and are binned to 31.2 km s^{-1} wide bins.
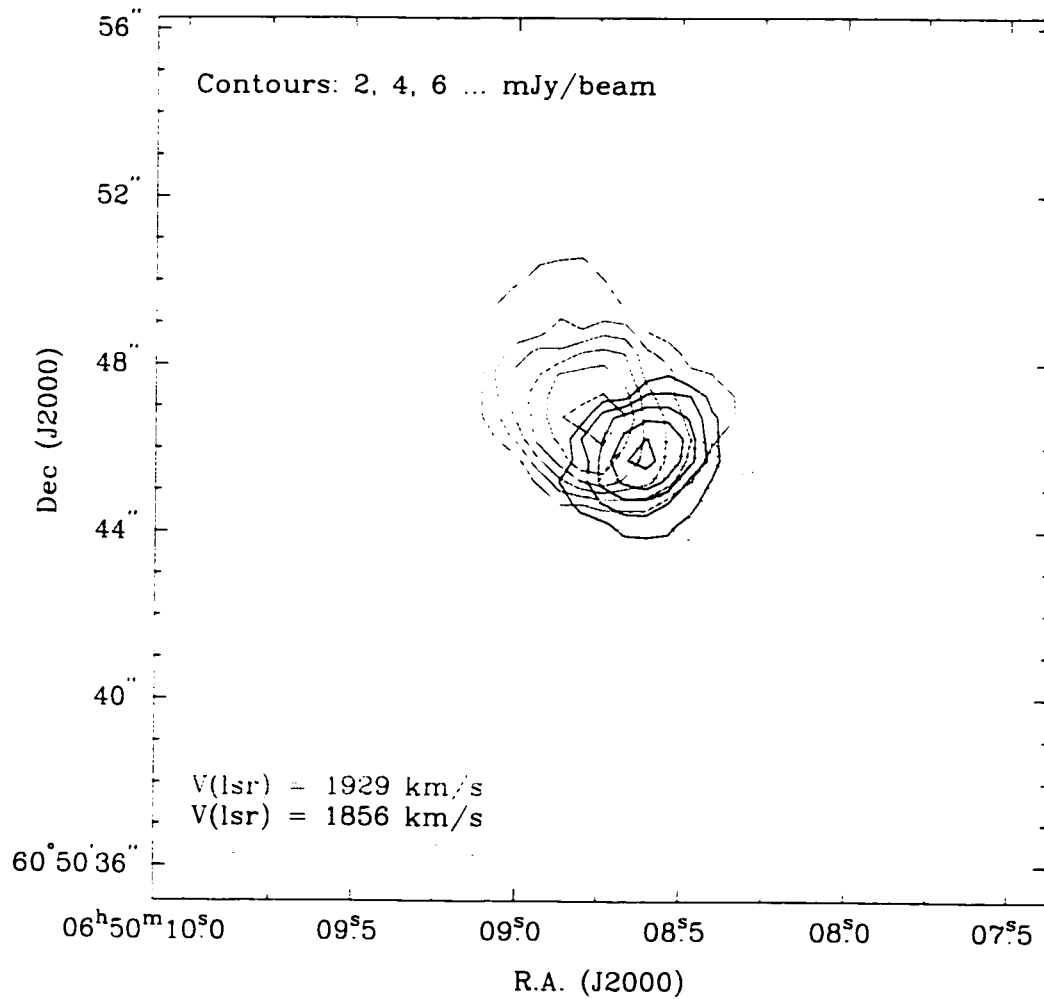
Figure 3.4: Individual CO Clumps in NGC 2273

This figure shows the output from the clumpfind algorithm. It shows the three main clumps of CO emission that combine to produce the bar seen in the integrated intensity map (Fig.3.2).

Figure 3.5 shows the I-band image (top panel) of Prada & Gutiérrez (1999) as well as the integrated intensity ^{12}CO $J=1-0$ map (bottom panel) of NGC 5728. The CO contours start at 1.3 Jy/beam km s^{-1} and increase in steps of 1.3 Jy/beam km s^{-1} (0.5σ). The emission is integrated over the velocity range of 2650 km s^{-1} to 2980 km s^{-1}. The ^{12}CO $J=1-0$ map of NGC 5728 (Fig. 3.5) does *not* show an obvious nuclear bar as seen in NGC 2273. It contains several individual clumps of emission that seem to form an arc with a radius of 6$''$. If this arc is part of a molecular ring, then the CO ring is not aligned with the galactic center, nor is it aligned with the ring structure surrounding ionization cones seen in the HST images by Wilson et al. (1993). The brightest peak in the CO map of Fig. 3.5 is located $\sim 2''$ to the SW of the brightest peak seen in the VLA and Hα maps of Schommer et al. (1988). The smaller CO clumps that run counter-clockwise to the SE of the brightest peak line up with the dust lane that runs out of the nucleus and along the main bar of the galaxy (Schommer et al. 1988). We reserve discussion of the physical interpretation of these features for §3.5.2.

At first glance, it appears that our CO map is offset from the galaxy center (marked with a '+' in Fig. 3.5) determined by Schommer et al. (1988). It should be noted that the spectral lines in the nucleus of NGC 5728 cover such a large range of velocities that we have missed velocities lower than 2630 km s^{-1}. The Hα maps of Schommer et al. (1988) show that there are some velocities as low as 2600 km s^{-1} and as high as 3010 km s^{-1} in the nucleus of NGC 5728. The lowest velocity regions are located to the north-east of the dynamical center, so if there is strong CO emission at 2600 to 2630 km s^{-1}, we will have missed it in our maps, perhaps creating the observed non-symmetric appearance. There is definitely evidence of bright CO emission near the low velocity end of our spectrometer. It can be seen as
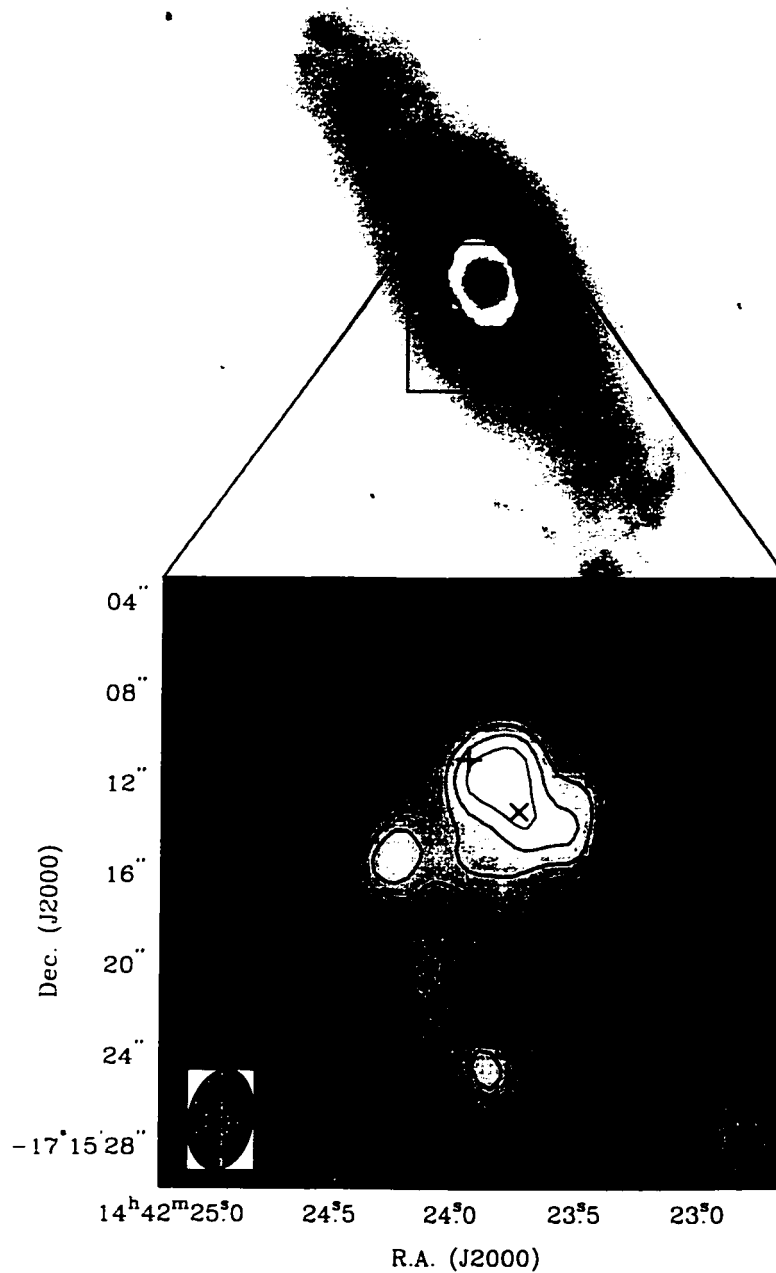
Figure 3.5: NIR and CO Images of NGC 5728

The top panel shows the NIR image of NGC 5728 by Prada & Gutiérrez 1999. The lower panel is the ^{12}CO J=1−0 integrated intensity map for the nucleus of NGC 5728. Note that we do *not* see an inner bar as we do for NGC 2273. The emission appears be asymmetric with respect to the dynamical center of the galaxy (marked by the +) determined by Schommer et al. 1988. The rms noise in the map is 2.65 Jy/beam km s^{-1}, and the contours start at 0.5σ and increase in steps of 0.5σ. The beam size is $4.5'' \times 3''$ with a PA=$-12°$ and is shown in the lower left corner. The × symbols indicate the clumps used to determine the dynamical mass discussed in §3.3.2.

a faint peak in Fig. 3.5 at RA $= 14^h42^m24\overset{s}{.}2$. $\delta = -17°15'07\overset{''}{.}6$ (it is the NE clump that was used in the dynamical mass calculation of §3.3.2).

To test whether the asymmetry seen in the CO map of NGC 5728 is caused by the exclusion of the lowest 30 km s^{-1} of the spectral data, we cropped the highest 30 km s^{-1} from the spectra and recreated the moment maps. This process reduces the intensity of the brightest peak to the west of the dynamical center, but the peak is still more than twice as bright as the emission peak on the north-east side of the dynamical center. Thus, it is likely that the asymmetric appearance of the CO maps is real, and not an artifact of missing low velocity emission.

The NIR image of NGC 5728 Shaw et al. (1993) shows isophote twists in the nuclear region similar to those of NGC 2273, but our CO map of NGC 5728 shows no clear evidence for the existence of a nuclear bar. This result suggests that in NGC 5728, the NIR isophote twists may not be the result of the nuclear bar, but may be caused by a triaxial stellar bulge as predicted by Kormendy (1979). We give a more detailed discussion of the possible causes of the NIR isophote twists in §3.5.2.

3.3.2 Dynamics

The position-velocity diagram (Fig. 3.6) taken along the axis of the CO bar in NGC 2273 shown in Fig. 3.2 indicates that the bar is rotating at approximately 570 km s^{-1} kpc^{-1} (870 km s^{-1} kpc^{-1} deprojected). Since we have no detections beyond the inner bar shown in Fig. 3.2, and there are no rotation curves published for the inner 1', we cannot determine yet if the CO inner bar is kinematically distinct as predicted by Model (2) or if it is rotating at the same angular frequency as the main bar as predicted by Model (1).

Position–Velocity Diagram Along the Nuclear CO Bar of NGC 2273
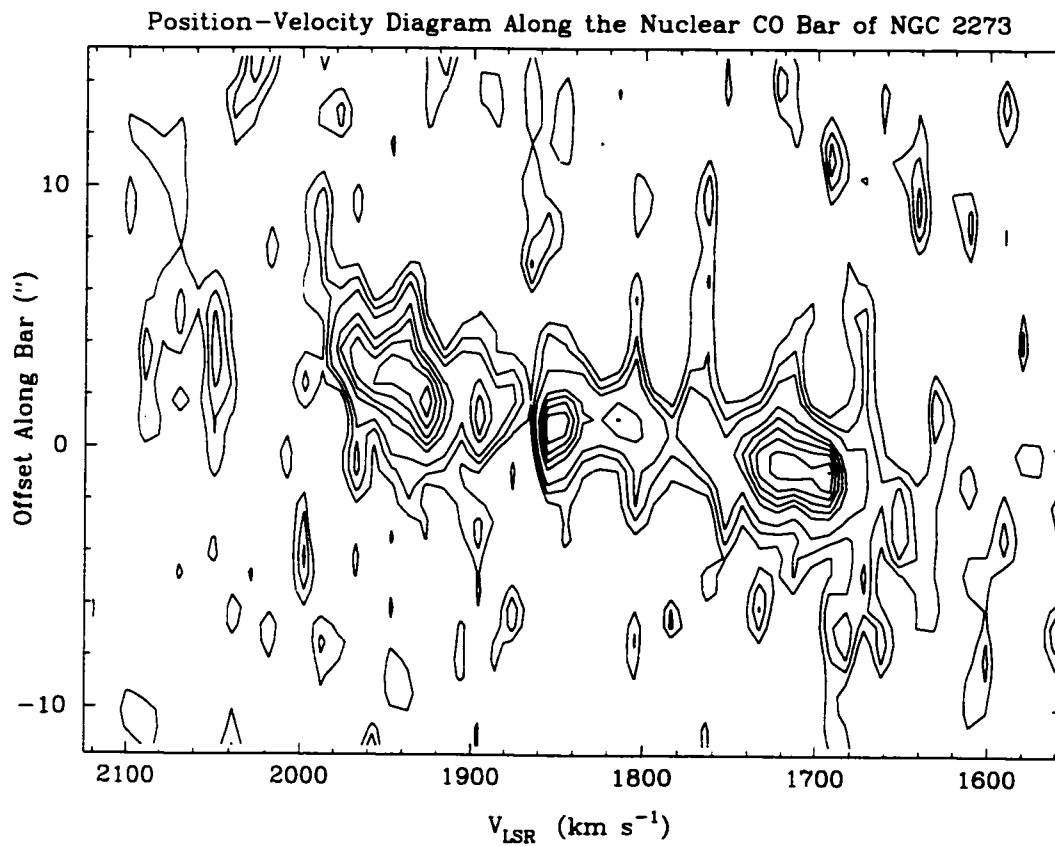
Figure 3.6: Position-Velocity Plot Along the CO Bar of NGC 2273
Position-velocity diagram for a slice along the major axis of the CO bar in Fig. 3.2. It rotates as a solid body with a projected angular frequency of 570 km/s/kpc. Contours indicate 10%. 20%. 30% ... of the peak. Positive offsets are toward the north-east end of the bar.

Assuming Keplerian rotation. we have

$$M_{\rm dyn} = \left(\frac{V_{\rm circ}}{\sin i}\right)^2 \left(\frac{R}{G}\right)$$

where $M_{\rm dyn}$ is the mass interior to radius R. $V_{\rm circ}$ is the circular velocity of the material at radius R. i is the galaxy's inclination and G is the gravitational constant. Contributions from non-circular velocities can only cause deviations of approximately 30% in the calculated mass (e.g. Sakamoto et al. 1999). Using Figure 3.4 to obtain velocities at the bar ends. and assuming the inclination to be 41°. we find the dynamical mass of the nuclear molecular bar to be 1.6×10^9 M$_\odot$.

The channel maps of NGC 5728 (Figure 3.7) show a much less ordered appearance. Careful examination of the velocity of the clumps suggests that the southern-most clump has the highest recession velocity and the velocities of the clumps decrease as you move clockwise around the arc (ignoring the CO emission associated with the dust lane to the far south). This is consistent with the velocity field determined by the Hα maps of Schommer et al. (1988). The CO emission is very clumpy with some of the features seen in the integrated intensity map of Figure 3.5 being made up of numerous CO features that are separated in velocity space. The brightest peak is actually a superposition of many less bright peaks at different velocities. There is no evidence in our CO maps of NGC 5728 for a bar interior to the ring as reported by Prada & Gutiérrez (1999). so naturally we cannot confirm the reports that this inner bar may be counter-rotating.

Our CO data for NGC 5728 are not sufficient to create a high quality position-velocity map as we did for NGC 2273. but we can use the channel maps to determine the position and velocity for the two bright clumps that lie along the major axis
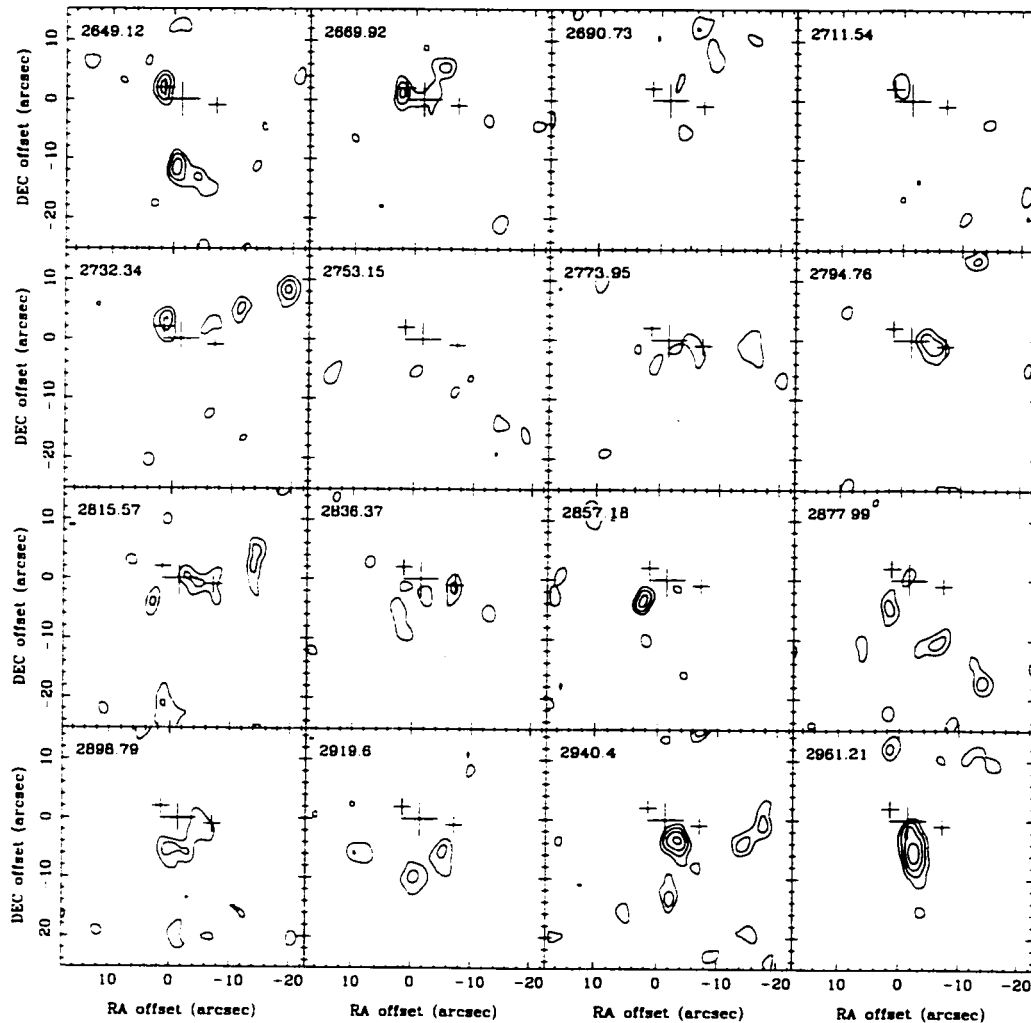
Figure 3.7: CO Channel Map of NGC 5728

Note how there is not strong evidence for large scale ordered motion. The large plus sign indicates the galaxy center determined by Schommer et al. (1988). The smaller plus signs mark the locations of the peaks used to calculate the dynamical mass. Contours levels are 0.04, 0.06, 0.08, ... Jy/beam (1.5, 2.3, 3 ... σ). The panels are shown at 20.8 km s^{-1} intervals and are binned to 20.8 km s^{-1} wide bins.

of NGC 5728 and straddle the dynamical center[2]. Using the same equations as for NGC 2273. we calculate a dynamical mass of 6.3×10^9 M$_\odot$ for the inner 8'' of NGC 5728.

Thus far we have concentrated our comparisons predominantly on the models of double barred galaxies that are comprised of both stars and gas. There is another class of models that attempt to explain nuclear NIR isophote twists using purely stellar orbits (Maciejewski & Sparke 2000). It is known that there are different classes of orbits in a barred potential. The two important ones are the x1 family that runs parallel to the bar major axis. and the x2 family. that runs perpendicular (e.g. Athanassoula 1992). It was thought that the x2 orbits of the large scale bar near the nucleus could form the x1 orbits of the smaller nuclear bar and the corotation radius of the nuclear bar could correspond to the ILR of the large scale bar. In this picture. the nuclear bar must *always* be aligned perpendicular to the main bar. Friedli & Martinet (1993) rule out this model by studying a large sample of double-barred galaxies. since they found that not all the observed offset angles between the nuclear bar and the main bar can be explained by inclination effects. Recently. Maciejewski & Sparke (2000) find that there exist orbits in which particles in a double-barred potential remain on closed orbits and may form the building blocks of long-lived double-barred galaxies without the need for a gaseous component. The particle nature of this model renders it untestable with our molecular gas observations. since it is unlikely that molecular gas will orbit in a particle-like manner. We mention it here solely as a possible explanation as to why NGC 5728 shows nuclear bars in the NIR images. but not in the CO maps.

---

[2]The north east peak is at RA = $14^h42^m24\overset{s}{.}2$. δ =-17°15'07''6 and has a central velocity of 2660 km s^{-1}. The south west peak is at RA = $14^h42^m23\overset{s}{.}75$. δ = -17°15'13''0 and has a central velocity of 2960 km s^{-1}. These points are indicated in Figure 3.5 by x's.

3.4 Molecular Gas Mass and Gas Mass Fraction

We use the CO flux over the entire nuclear bar of NGC 2273 to estimate the molecular gas mass in the nuclear region. We adopt

$$M_{gas} = 1.6 \times 10^4 \left(\frac{D}{Mpc}\right)^2 \left(\frac{S_{CO(1-0)}}{Jy\ km\ s^{-1}}\right)\left(\frac{X}{X_{Gal}}\right)$$

(Wilson 1995). where D is the distance to the galaxy. $S_{CO(1-0)}$ is the ^{12}CO $J=1-0$ flux. X is the CO-to-H_2 conversion factor compared to the Galactic value (X_{Gal}). The constant at the start of the equation contains a factor of 1.36 to account for other elements besides hydrogen. For lack of evidence to the contrary. we adopt the Galactic value of the CO-to-H_2 conversion factor of 3×10^{20} cm^{-2} (K km s^{-1})$^{-1}$ (Scoville & Sanders 1987) for the galaxies studied in this paper. The total CO flux for the nuclear CO bar of NGC 2273 is 48.6 Jy km s^{-1}. which corresponds to a molecular mass of 4.7×10^8 M$_\odot$. If we repeat this calculation using only the region interior to the locations used in the dynamical mass calculation ($\sim$ 1 kpc along the length of the CO bar) we measure a flux of 38.0 Jy km s^{-1}. which corresponds to a molecular mass of 3.6×10^8 M$_\odot$. This mass constitutes approximately 20% of the nuclear bar's dynamical mass (§3.3.2).

Of course. the estimate for the molecular gas mass is only a lower limit since the interferometer is insensitive to the large scale structure that may be present in the nuclear regions of this barred galaxy. Single dish ^{12}CO $J=1-0$ spectra of the inner 55″ of NGC 2273 taken by Young et al. (1995) show a flux of 137 ± 24 Jy km s^{-1}. suggesting that our interferometry maps may be missing up to 65% of the CO emission. Also important is the effect of the uncertainties in the individual measurements used to calculate this ratio. For example. in §3.3.2. if we assume that V_{circ}. i. and R each have a conservative $\sim$10% uncertainty. this results in a $\sim$25% uncertainty in M_{dyn}. Similarly for the molecular gas mass. if we assume a $\sim$10%

uncertainty for each measured value. we obtain an uncertainty in $M_{\rm gas}$ of $\sim 20\%$. The final value for the ratio $M_{\rm gas}/M_{\rm dyn}$ is $(20\pm 6)\%$.

Yankulova (1999) find that the nuclear ring of NGC 2273 is very dusty and calculate the mass of this dust to be $\sim 10^5$ $M_\odot$. Comparing this to our molecular gas mass. we find that the gas-to-dust ratio is approximately 3600 in the center of this Seyfert 2 galaxy. This ratio is higher than found for nearby spiral galaxies ($M_{\rm gas}/M_{\rm dust} \sim 1000$: Devereux & Young 1990). It may not be surprising that the ratio of gas to dust is higher in the center of this barred galaxy. where we might expect an increase of nuclear molecular gas (caused by inflow along the bar) as well as a decrease in dust due to the strong ionizing nuclear source (Yankulova 1999).

The CO flux for the inner $8\times 8''$ of NGC 5728 is 25.6 Jy km s^{-1}. which indicates a molecular mass of 5.7×10^8 $M_\odot$. Using our dynamical mass data we find that the molecular gas in the nucleus of NGC 5728 constitutes 9% of the total mass. We believe that our determination of the dynamical mass in such a complicated environment is likely unreliable. Our dynamical mass determined in §3.3.2 is lower than the value determined by Rubin (1980) through model fits of the velocity data over the entire galaxy. Due to the complexity of our data and the simplicity of the models assumed in §3.3.2. we will adopt the value determined by Rubin (1980). She finds the total dynamical mass of the galaxy in the inner $10''$ diameter (1.8 kpc) is $\sim 1 \times 10^{10}$ $M_\odot$. This estimate lowers the mass fraction of molecular gas to $6\pm 2\%$. Again. this result is a lower limit because the interferometer will miss large scale structure. There are no single dish ^{12}CO $J=1-0$ spectra for NGC 5728 published. so we cannot directly estimate the flux missed by our interferometric maps. Single dish ^{12}CO $J=2-1$ spectra of the inner $22''$ of NGC 5728 (Petitpas & Wilson. in prep.) show fluxes of 62 Jy km s^{-1}. Assuming a ^{12}CO $J=2-1/J=1-0$ ratio of 0.7 (Sakamoto et al. 1995) we obtain a ^{12}CO $J=1-0$ flux of 89 Jy km s^{-1}. Comparing

this to the CO flux in the interferometric map of 30 Jy km s^{-1} for this region, we find that the interferometric maps are missing ~67% of the flux detected by a single dish.

A requirement of both the models of Shaw et al. (1993) and Friedli & Martinet (1993) is that the entire galaxy contain ~5-10% molecular gas by mass. Friedli & Martinet (1993) found that they could also create nuclear bars if the *total* (atomic + molecular) gas to total mass ratio is 10%, or if 2% of the total mass interior to 1 kpc (diameter) is molecular. Shaw et al. (1993) only require that 4-6% of the entire galaxy mass be gaseous. The high gas contents in these two models are required to provide enough dissipation so that the nuclear ring can become phase shifted out of its stable orbit and collapse into a nuclear bar. Both galaxies meet the molecular gas mass requirements of the models, yet only NGC 2273 shows evidence for a nuclear molecular bar. It is interesting that we find ~20% gas (by mass) in the nucleus of NGC 2273, where we see a nuclear bar, yet we only see ~6% (by mass) in NGC 5728, where we see no evidence in our CO maps for a nuclear bar. This comparison suggests that perhaps the models of Shaw et al. (1993) and Friedli & Martinet (1993) are correct, but the parameters they adopted to model the gas dissipation may not be correct. For example, if they were to decrease the amount of dissipation in the gas slightly, it is possible that they could still create nuclear CO bars in galaxies that contain 20% gas, yet galaxies with lower mass fractions such as NGC 5728 would not have enough dissipation to create long-lived nuclear bars.

A recent interferometric ^{12}CO J=1−0 survey by Sakamoto et al. (1999) suggests that typical gas mass fractions range from 0.9% to 31.5% in the inner 500 pc radius of a sample of 17 galaxies, with no apparent correlation with galaxy type. Since we have used the same techniques to determine the gas mass fraction, it is worthwhile to compare our results with those of a larger sample. For NGC 2273, we calculate

the molecular gas mass fraction over the entire length of the bar for which we see emission in the position velocity plot (Figure 3.6), which corresponds to the inner 720×720 pc. For NGC 5728, we measured the molecular gas mass fraction over an area of 8×8"which corresponds to the inner 1.4×1.4 kpc. NGC 2273 has a nuclear gas mass fraction of 20% and NGC 5728 has 6% molecular gas. Sakamoto et al. (1999) find evidence that HII nuclei have higher ratios of gas to dynamical masses (~18% average) compared to Seyfert and LINER galaxies (~6% average). NGC 5728 is in agreement with the previously observed range for its type of nuclear activity, while NGC 2273 seems to have a higher molecular gas fraction than the other Seyfert 2 galaxies in the sample obtained by Sakamoto et al. (1999). A distinct classification of NGC 2273 into one particular category is difficult in light of current observations which suggest that, in addition to its Seyfert 2 activity, NGC 2273 is undergoing nuclear star formation (Mulchaey, Wilson, & Tsvetanov 1996). These observations suggest that NGC 2273 may be an intermediate object that should fall somewhere between the HII and Seyfert 2 classifications of Sakamoto, Okumura, Ishizuki, & Scoville 1999, in which case it is in the expected intermediate range of gas mass fraction for such an object. In any case, our observed gas mass fraction for NGC 2273 does not compromise the results of Sakamoto et al. (1999).

3.5 Discussion

3.5.1 Comparison to Previous Studies of NGC 2273

It has long been known that bars are a good way to transport material into the nuclear region of a galaxy (e.g. Combes 1994) by allowing material to flow inward along the leading edge of the bar. Indications of such an inflow are visible in the CO

map of NGC 2273, seen as fingers extending NW and SE from the top and bottom (respectively) of the CO bar. This observation suggests that inflow along the main bar of NGC 2273 is depositing material onto the ends of the nuclear bar seen in the CO maps. This material would then be free to flow along the nuclear bar into the central regions, and could possibly supply the nucleus with enough material to sustain the observed Seyfert and starburst activity.

The channel maps of NGC 2273 show that the bar seen in the integrated intensity maps is actually composed of three separate structures. These structures are barely spatially resolved in our maps (if at all), but they are clearly resolved in velocity (as seen in Fig. 3.3). Similar nuclear CO distributions have been seen previously in regular (non-double) barred galaxies such as NGC 5383 and M82 (Sheth et al. 2000; Neininger et al. 1998). In NGC 5383, Sheth et al. (2000) see bright CO emission from "twin peaks" that coincide with the ILR radius, as well as a central concentration near the nucleus. High resolution observations suggest that the nuclear structure of NGC 5383 is actually a nuclear spiral when viewed with the Hubble Space Telescope (Sheth et al. 2000), which casts some doubt on the identification of nuclear bars with lower resolution, ground-based images.

HST images (Malkan, Gorjian, & Tam 1998) and narrow-band color maps (Yankulova 1999) of NGC 2273 show that the nucleus contains a ring elongated in the same direction as our nuclear CO bar. The HST (WFPC2, F606W) images show a central bright spot and indications of what may be flocculent spiral arms and a ring. The bright blobs at the ends of the nuclear CO bar correspond with the edges of the ring seen by Malkan, Gorjian, & Tam (1998) and Yankulova (1999). It is likely that this ring indicates the location of the ILR of the main bar, and thus, our nuclear bar ends occur at the ILR radius as predicted by the models of Friedli & Martinet (1993) and Shaw et al. (1993). If we assume that the corotation radius of the nuclear bar

occurs near the ILR of the main bar (Pfenniger & Norman 1990: see Fig. 3.1). then the CO peaks at the ends of the nuclear bar are analogous to the condensations that collect at the corotation resonance of large-scale bars (Garcia-Burillo et al. 1998). This result suggests that nuclear bars may share many of the same properties as large-scale bars and that modeling nuclear bars may be done using scaled-down versions of the large-scale barred potentials that are currently used in barred galaxy models.

3.5.2 Comparison to Previous Studies of NGC 5728

HST images of the nucleus of NGC 5728 show what appears to be an off-center ring of young stars circling two ionization cones that seem to originate from a point $\sim3''$ west-north-west ($-60°$) from the center of our maps (Wilson et al. 1993). These images also show a bar-like structure that is oriented at a position angle of $\sim90°$ which Wilson et al. (1993) suggest may be comprised of older stars. Our CO map shows no bright emission peak at the vertex of the ionization cones of the HST maps. The bright and faint CO peaks (used in §3.3.2 to determine the dynamical mass) that straddle the map center are roughly perpendicular to the ionization cones. The other peaks in the maps (curving to the south) are associated with the dust lanes that run along the leading edge of the main bar (Schommer et al. 1988). Our CO maps also do not show any strong evidence of a bar structure oriented at PA $= \sim90°$ which might correspond to the bar suggested by the NIR images of Shaw et al. (1993). If we assume that the clumps (marked by x's in Figure 3.5) that straddle the dynamical center (indicated by the +) correspond to similar nuclear bar end enhancements as seen in NGC 2273 (Figure 3.2) then the nuclear CO bar in NGC 5728 would be leading the stellar nuclear bar seen in the NIR images by $\sim45°$. This angle is greater than the offsets predicted by Shaw et al. (1993) and Friedli

& Martinet (1993) for which a 20° maximum offset is predicted. If the nuclear stellar bar is counter rotating as reported by Prada & Gutiérrez (1999). then the nuclear CO bar is trailing the main bar. which is not predicted in any of the models discussed in this paper.

Unfortunately, the integrated intensity maps and the channel maps of the nucleus of NGC 5728 show no *conclusive* evidence for a nuclear bar in our data either aligned or misaligned with the NIR isophote twists. This result suggests that if the NIR isophote twists of Shaw et al. (1993) are the result of a nuclear bar. it is mostly stellar and contains little molecular gas. This observation counters the finding of Shaw et al. (1993) and Friedli & Martinet (1993) whose models require that these nuclear bars contain lots of molecular material in order to provide enough dissipation.

3.5.3 Comparison with Other Nuclear Barred and NIR Isophote Twist Galaxies

Considering all barred galaxies (not just the ones containing NIR isophote twists) there are currently nine barred galaxies that show evidence for a nuclear molecular bar (Devereux et al. 1992: Kenney et al. 1992: this work). It seems that the identification of a gaseous nuclear bar may be ambiguous: there may be confusion between what is considered a "twin peak" galaxy and what is considered a nuclear bar. Unresolved twin peak galaxies will appear as galaxies with a nuclear CO bar. For example. NGC 3351 is classified as a twin peak galaxy by Kenney et al. (1992) but considered to have a nuclear CO bar by Devereux. Kenney. & Young (1992). Twin peak galaxies are believed to be caused by gas collecting at an ILR as it flows inward along the leading edge of the main bar of a galaxy (Kenney et al. 1992). These galaxies are thought to be *preventing* molecular gas from reaching all the way into the nucleus. while nuclear bar galaxies are thought to *assist* molecular gas flow

into the nucleus by transporting it interior to the ILR (Kenney et al. 1992; Shlosman, Frank, & Begelman 1989). We will need a larger sample of galaxies containing unambiguous nuclear bars so we can determine their properties in comparison to twin peak galaxies.

From the NIR surveys that have detected the isophote twists originally thought to be the signature of a nuclear bar (e.g. Mulchaey, Regan, & Kundu 1997; Shaw et al. 1993; Wozniak et al. 1995; Jarvis et al. 1988; Elmegreen et al. 1996; Friedli & Martinet 1993), only a handful of galaxies have high resolution CO maps published: NGC 4736, NGC 6951, NGC 5728, and NGC 2273 (Sakamoto et al. 1999; Kenney et al. 1992; this work). NGC 2273 and NGC 6951 contain two peaks at the ILR radius with more CO emission interior to these peaks. CO maps of NGC 4736 show what may be a weak twin peak structure, with a bright central concentration (Sakamoto et al. 1999). NGC 5728 has a bright, off-center peak of emission, with other emitting regions that do not seem to line up with other features or the ILR radius. Only NGC 5728 does not show evidence for a twin peaked or bar structure elongated in the same direction as the nuclear NIR isophote twists.

To explain why there is no nuclear CO bar in NGC 5728, we need to examine the time evolution of the models. The models of Shaw et al. (1993) were only run until they reached a steady state, so comparisons of our CO maps with the predictions for the lifetimes of nuclear bars is not possible. Friedli & Martinet (1993) show that after the nuclear bar forms, it usually remains present for over 5 turns of the nuclear bar (approximately 2 turns of the main bar; ~500 Myr). The double-bar phase can transport the molecular gas inward, which eventually results in the disruption of the nuclear bar; often even the large-scale bar is disrupted by bulge growth (Pfenniger & Norman 1990) or central mass concentration (Hasan & Norman 1990) which changes the barred gravitational potential into a more spherical potential. In this picture,

NGC 5728 may represent a older double-barred galaxy that has already undergone a molecular nuclear bar stage which has modified the gravitation potential through the creation of a high mass central object (perhaps the cause of the jets seen in the HST images of Wilson et al. (1993)). The molecular gas could have responded to the change in the potential faster than the stellar component. which may explain why we see evidence for a nuclear bar in the NIR images but not in the CO maps.

Additional support for this scenario is found when we consider the star formation activity of each of these galaxies. NGC 2273 and NGC 6951 have active nuclear star formation and the CO maps show a strong CO bar and a distorted twin peak structure with faint central concentration. respectively (Kohno et al. 1999; Kenney et al. 1992). In NGC 4736. there is evidence for a recent starburst phase. and the CO maps show a weak twin peaked structure as well as a bright central concentration (Kinney et al. 1993; Sakamoto et al. 1999). A summary of these observations is given in Table 3.2. These results suggest that NGC 2273 and NGC 6951 may be in a earlier stage of evolution. where the nuclear molecular bar is still visible. NGC 4736 may be just finishing its double bar phase and the molecular gas (and stars) are beginning to return to a single barred galaxy phase. NGC 5728 may have been finished with its double bar phase for quite a while. The molecular gas has lost its nuclear barred appearance. while the stars have not. The models of Friedli & Martinet (1993) show no evidence for the evolutionary sequence proposed here. Their models suggest that the gas and stars in a nuclear bar behave similarly on timescales of a few million years: thus *if* evolution is responsible for the variation in nuclear stellar and CO morphologies *and* the models are correct. then it is unlikely that we should see such a variety in our small sample of galaxies.

Another explanation for the variety of CO morphologies may be that there are different physics at work in the molecular gas in each galaxy. It is interesting that the

Table 3.2: Properties NIR Isophote Twist Galaxies

Galaxy	M_{gas}/M_{dyn}	Nuclear Activity	CO morph.	Refs
NGC 2273	20%	Star formation. Seyfert 2 activity	Obvious bar/triple peaks	1, 2
NGC 4736	2%	Star formation in ring outside nucleus. LINER	Central peak, weak signs of twin peaks?	3, 4
NGC 5728	6%	Evidence of past star formation. Seyfert 2	Non-centralized peaks, no bar?	1, 5
NGC 6951	29%	Star formation	Twin (triple?) peak/ elongated ring?	6

1) this paper; 2) Mulchaey, Wilson, & Tsvetanov (1996); 3) Sakamoto, Okumura, Ishizuki, & Scoville (1999); 4) Kinney, Bohlin, Calzetti, Panagia, & Wyse (1993); 5) Wilson, Braatz, Heckman, Krolik, & Miley (1993); 6) Kohno, Kawabe, & Vila-Vilaró (1999)

NIR images of all four galaxies look remarkably similar, while the CO maps look remarkably different. The similarity in the NIR images suggests that the stellar distribution in these galaxies is similar. The differences in the CO morphology suggest that there is something different about the molecular gas in each galaxy, which causes it to respond differently to the galactic stellar potential. We are in the process of obtaining multi-line CO data at the JCMT in order to place constraints on the molecular gas temperatures and densities in a sample of starburst and non-starburst Seyfert 2 galaxies, which may help shed some light on the different CO morphologies observed in the double barred galaxies.

3.6 Summary

We have mapped the barred galaxies NGC 2273 and NGC 5728 in ^{12}CO J=1-0 with the Caltech Millimeter Array. These galaxies are known to contain NIR nuclear isophote twists, which are thought to be the signature of a nuclear bar. The main results are summarized as follows:

1) In NGC 2273 we see a nuclear molecular bar approximately perpendicular to the large scale galactic bar. The CO bar is aligned with the NIR isophote twists suggesting that in NGC 2273, the twists are caused by the presence of a real nuclear bar, and are not the result of a triaxial stellar bulge. Such a feature is predicted by the simulations of NIR isophote twist galaxies by Shaw et al. (1993) and Friedli & Martinet (1993). Friedli & Martinet (1993) predict a kinematically distinct nuclear bar that rotates with a pattern speed greated than the main bar, while Shaw et al. (1993) predict that the nuclear structure will have the same pattern speed as the main bar. Unfortunately, the lack of a detailed rotation curve for the inner regions of NGC 2273 prevents us from determining if the nuclear bar is kinematically separate from the rest of the galaxy.

2) In the nucleus NGC 5728 we see a series of clumps of emission that do not seem to align with any of the features previously observed at other wavelengths. CO emission is detected coincident with the dust lane to the south of the nucleus. The peak of the CO map is not aligned with the galactic center, nor is it located at the center of the offset nuclear ring seen in the HST images of Wilson et al. (1993). We do not see evidence for a nuclear bar in the CO maps, which suggests that, if there is a real nuclear bar in the nucleus of NGC 5728, it must contain little or no molecular gas. This result is contrary to current simulations of double barred galaxies, which require large amounts of dissipative material to produce long-lived nuclear bars. It is possible that the NIR isophote twists in NGC 5728 are caused by either a triaxial stellar bulge or are scattered light from the jets observed in the HST images of Wilson et al. (1993).

3) We have calculated the molecular gas mass over the entire nuclear bar of NGC 2273 and find that it contains 4.7×10^8 $M_\odot$ of molecular gas. The inner 1.4×1.4 kpc of NGC 5728 contains 5.7×10^8 $M_\odot$ of molecular gas. Assuming Keplerian motion,

we find that the dynamical mass of the inner $10''$ of NGC 2273 is 1.9×10^9 M$_\odot$. which translates into a molecular gas mass fraction of 20% for NGC 2273. Adopting the dynamical mass value determined by Rubin (1980) we calculate the molecular mass fraction to be 6% for NGC 5728.

4) Comparing our observations to models of double-barred galaxies. it seems that both galaxies contain sufficient molecular gas for the models of Shaw et al. (1993) and Friedli & Martinet 1993. However. we only see a nuclear gas bar in NGC 2273. One possibility is that the gas dissipation in the models may be overestimated. Reducing the viscosity of the gas in the models could permit nuclear bars to form in galaxies with a 20% gas mass fraction. but not in galaxies with 6% gas mass fraction.

5) Another possible explanation for the differing CO morphologies may be galaxy evolution. When comparing our results with other double barred galaxies. we find evidence that NGC 5728 may represent an older double-barred galaxy in the final stages before nuclear bar dissolution. It is possible that the inflow has already modified the galactic potential. and the molecular gas has responded to the changes before the stellar component. This may explain why we see a nuclear bar in the NIR images of NGC 5728. but not in the CO maps.

6) The similarity in the NIR images and the differences in the CO maps suggest that the molecular gas may have different physical properties in each galaxy, which allows it to respond differently in similar gravitational potentials. These differences could be the result of nuclear starburst activity heating the gas. which could make it less viscous. Multi-line data are currently being obtained to test this hypothesis.

Bibliography

Athanassoula. E.. 1992. *MNRAS* **259**. 345.

Combes. F.. 1994. Nuclear gas flows in barred galaxies. In *Mass Transfer Induced Activity in Galaxies*. pp. 170. ed. I. Shlosman. Cambridge Univ. Press.

de Vaucouleurs. G.. de Vaucouleurs. A.. Corwin. H. G.. Buta. R. J.. Paturel. G.. & Fouque. P.. 1991. *Third Reference Catalogue of Bright Galaxies*. Volume 1-3. XII. 2069 pp. 7 figs.. Springer-Verlag Berlin Heidelberg New York.

Devereux. N. A.. Kenney. J. D.. & Young. J. S.. 1992. *AJ* **103**. 784.

Devereux. N. A. & Young. J. S.. 1990. *ApJ* **359**. 42.

Elmegreen. D. M.. Elmegreen. B. G.. Chromey. F. R.. Hasselbacher. D. A.. & Bissell. B. A.. 1996. *AJ* **111**. 1880.

Friedli. D. & Martinet. L.. 1993. *A&A* **277**. 27.

Garcia-Burillo. S.. Sempere. M. J.. Combes. F.. & Neri. R.. 1998. *A&A* **333**. 864.

Hasan. H. & Norman. C.. 1990. *ApJ* **361**. 69.

Jarvis. B. J.. Dubath. P.. Martinet. L.. & Bacon. R.. 1988. *A&AS* **74**. 513.

Kenney. J. D. P.. Wilson. C. D.. Scoville. N. Z.. Devereux. N. A.. & Young. J. S.. 1992. *ApJL* **395**. L7.

Kinney. A. L.. Bohlin. R. C.. Calzetti. D.. Panagia. N.. & Wyse. R. F. G.. 1993. *ApJSS* **86**. 5.

Kohno. K.. Kawabe. R.. & Vila-Vilaró. B.. 1999. *ApJ* **511**. 157.

Kormendy. J.. 1979. *ApJ* **227**. 714.

Maciejewski. W. & Sparke. L. S.. 2000. *MNRAS* **313**. 745.

Malkan. M. A.. Gorjian. V.. & Tam. R.. 1998. *ApJSS* **117**. 25.

Mulchaey. J. S.. Regan. M. W.. & Kundu. A.. 1997. *ApJSS* **110**. 299.

Mulchaey. J. S.. Wilson. A. S.. & Tsvetanov. Z.. 1996. *ApJ* **467**. 197.

Neininger. N.. Guelin. M.. Klein. U.. Garcia-Burillo. S.. & Wielebinski. R.. 1998.
    A&A **339**. 737.

Pfenniger. D. & Norman. C.. 1990. *ApJ* **363**. 391.

Prada. F. & Gutiérrez. C. M.. 1999. *ApJ* **517**. 123.

Rubin. V. C.. 1980. *ApJ* **238**. 808.

Sakamoto. K.. Okumura. S. K.. Ishizuki. S.. & Scoville. N. Z.. 1999. *ApJ* **525**.
    691.

Sakamoto. S.. Hasegawa. T.. Hayashi. M.. Handa. T.. & Oka. T.. 1995.
    ApJSS **100**. 125.

Sault. R. J.. Teuben. P. J.. & Wright. M. C. H.. 1995. A retrospective view
    of miriad. In *ASP Conf. Ser. 77: Astronomical Data Analysis Software and
    Systems IV*. Volume 4. pp. 433.

Schommer. R. A.. Caldwell. N.. Wilson. A. S.. Baldwin. J. A.. Phillips. M. M..
    Williams. T. B.. & Turtle. A. J.. 1988. *ApJ* **324**. 154.

Scoville. N. Z.. Carlstrom. J. E.. Chandler. C. J.. Phillips. J. A.. Scott. S. L..
    Tilanus. R. P. J.. & Wang. Z.. 1993. *PASP* **105**. 1482.

Scoville. N. Z. & Sanders. D. B.. 1987. H2 in the galaxy. In *ASSL Vol. 134:
    Interstellar Processes*. pp. 21.

Shaw. M. A.. Combes. F.. Axon. D. J.. & Wright. G. S.. 1993. *A&A* **273**. 31.

Shen. J. & Lo. K. Y.. 1995. *ApJ* **445**. L99.

Sheth, K., Regan, M. W., Vogel, S. N., & Teuben, P. J., 2000. *ApJ* **532**, 221.

Shlosman, I., Frank, J., & Begelman, M. C., 1989. *Nature* **338**, 45.

van Driel, W. & Buta, R. J., 1991. *A&A* **245**, 7.

Williams, J. P., de Geus, E. J., & Blitz, L., 1994. *ApJ* **428**, 693.

Wilson, A. S., Braatz, J. A., Heckman, T. M., Krolik, J. H., & Miley, G. K., 1993. *ApJL* **419**, L61.

Wilson, C. D., 1995. *ApJL* **448**, L97.

Wozniak, H., Friedli, D., Martinet, L., Martin, P., & Bratschi, P., 1995. *A&AS* **111**, 115.

Yankulova, I. M., 1999. *A&A* **344**, 36.

Young, J. S. & Devereux, N. A., 1991. *ApJ* **373**, 414.

Young, J. S., Xie, S., Tacconi, L., Knezek, P., Viscuso, P., Tacconi-Garman, L., Scoville, N., Schneider, S., Schloerb, F. P., Lord, S., Lesser, A., Kenney, J., Huang, Y., Devereux, N., Claussen, M., Case, J., Carpenter, J., Berry, M., & Allen, L., 1995. *ApJSS* **98**, 219.

Chapter 4

Molecular Gas in Double Barred Galaxies II. Cooler Gas in Nuclear CO Bars

Draft of a paper that will be submitted to the Astrophysical Journal

Abstract

Near infrared galaxy surveys have revealed the existence of nuclear bars in a large number of barred or lenticular galaxies. High resolution CO maps of these galaxies exhibit a wide range of morphologies. The similarity in near infrared images combined with the wide variety of CO morphologies suggests that the molecular gas may have different properties that allow it to respond differently to similar gravitational potentials. We have performed a multi-transition CO study of the nuclei of seven double barred galaxies that exhibit a variety of molecular gas morphologies in order to determine if the molecular gas properties are correlated with the nuclear structure and activity. We find that the ^{12}CO $J=3-2/J=2-1$ line ratio is lower in galaxies with molecular bars in the nucleus and higher in galaxies with CO emission dispersed around the galactic center in rings and peaks. The $^{13}CO/^{12}CO$ $J=2-1$ line ratios are similar for all galaxies, which indicates that the $J=3-2/J=2-1$ line ratio is tracing variations in gas temperature and density, rather than variation in optical depth. The molecular gas in galaxies with nuclear molecular bars is cooler

(and perhaps more viscous) enhancing the gas's ability to clump together and flow inwards. The molecular gas conditions. combined with the star formation activity and models of double barred galaxies suggest that the varation in molecular gas distributions and physical conditions may be the result of galaxy evolution though the double barred phase.

keywords: Galaxies: starburst - galaxies: active

4.1 Introduction

Recent near infrared (NIR) surveys reveal isophote twists in the central regions of barred galaxies which are thought to be the signature of a bar within a bar (e.g. Mulchaey. Regan. & Kundu 1997). Recent models of double barred galaxies have had some success in reproducing relatively long lived nuclear features that can explain the isophote twists. Shaw et al. (1993) model galaxies as gravitational stars and dissipative gas clouds and find that the NIR isophote twists are caused by viscous and gravitational torques that drag the nuclear regions of the main bar out of alignment with the rest of the bar. Friedli & Martinet (1993) suggest that the NIR isophote twists are the result of a kinematically distinct nuclear bar that can rotate with up to six times the pattern speed of the large scale bar. The one thing these models have in common is the need for dissipation. Both groups have to include large amounts of molecular gas in order for the models to be able to reproduce the observed features. To date. the best observational test of how accurately these models are taking into account the gaseous component is the assumed gas mass to total mass ratio (usually adopted as 5 to 10%. in agreement with observations). The models of barred galaxies by Combes & Gerin (1985). Shaw et al. (1993). and Friedli & Martinet (1993) produce very different nuclear morphologies by adding a

gaseous component. In fact. the models of Combes (1994) exhibit different nuclear morphologies by simply changing the dissipative properties of the gas.

In an attempt to test these models. we recently undertook a study of the molecular gas morphologies in a sample of galaxies containing NIR isophote twists (Petitpas & Wilson 2001: Paper 1). We find that in a sample of double barred galaxies the CO maps have different morphologies while the NIR images are similar. For example. the CO maps of NGC 2273 and NGC 4736 exhibit nuclear bars that align with the nuclear NIR isophote twists (Petitpas & Wilson 2001: Wong & Blitz 2000). while NGC 6951 shows twin peaks of molecular gas collecting at an inner Lindblad resonance (Kohno. Kawabe. & Vila-Vilaró 1999). NGC 5728 shows a very disordered CO structure where the clumps of CO emission do not seem to align with any structures seen at other wavelengths (Petitpas & Wilson 2001: ?). This variety of gas distributions in galaxies with similar NIR morphologies suggests that there may be differences in the molecular gas physical conditions that allow it to respond differently to similar gravitational potentials. In this paper we present the results of a multi-line ^{12}CO and ^{13}CO survey of the nuclei of seven of these double barred galaxies.

Previous surveys of galaxy nuclei using optically thin tracers such as ^{13}CO have been performed primarily in either galaxies that contain enhanced activity (such as mergers or starburst galaxies) or are very nearby (such as M31 and M51). One of the first ^{13}CO surveys of galaxies was undertaken by Encrenaz et al. (1979). They find the ^{12}CO/^{13}CO $J=1-0$ line ratio in a sample of five nearby galaxies has a mean value of 12.5 ± 3.2. Later. Young & Sanders (1986) studied the ^{12}CO/^{13}CO line ratio in six more galaxies and found it similar to those of Encrenaz et al. (1979). with an average value of 10.4 and 11 for the disks and nuclei of these galaxies. respectively. Young & Sanders (1986) also observed a correlation between the dust

temperature (derived from IRAS f_{60}/f_{100} flux ratio) and the $^{12}CO/^{13}CO$ line ratio. with galaxies with higher dust temperatures tending to have higher $^{12}CO/^{13}CO$ line ratios. They claim that the same intense stellar radiation that heats the dust is also heating surface of the molecular clouds. lowering the optical depth at the clouds surface. which is believed to be the region probed by the (usually) optically thick ^{12}CO.

Aalto et al. (1991) performed $^{12}CO/^{13}CO$ survey of 21 galaxies of mixed types and find the ratio is much higher (> 20) in the four galaxies that are mergers. They also find that the dust temperatures in these merging systems is higher than normal. in agreement with the findings of Young & Sanders (1986). They too suggest that this may reflect a decrease in the mean optical depth of these clouds compared to non-merging systems. For the non-interacting galaxies in their sample. they find a mean line ratio of ∼11. in agreement with the previous studies of ^{13}CO in isolated galaxies.

Casoli. Dupraz. & Combes (1992) measured the $^{12}CO/^{13}CO$ J=2−1 and J=1−0 ratio in a sample of six merging systems. They found that the $^{12}CO/^{13}CO$ line ratios are approximately 30 and 40 for the J=1−0 and J=2−1 transitions. respectively. Using both the J=1−0 and J=2−1 transitions. they are able to rule out optical depth effects as the cause of these very high $^{12}CO/^{13}CO$ line ratios. They propose that these ratios are the result of a depletion of ^{13}CO in these systems through either by photodissociation. inflow of unprocessed gas. or. selective nucleosynthesis. in these merging systems.

Aalto et al. (1995) performed a similar survey of $^{12}CO/^{13}CO$ J=1−0 and J=2−1 line ratios in a sample of 32 galaxies of mixed type (mergers and starbursts) and found both the $^{12}CO/^{13}CO$ J=1−0 and J=2−1 ratios to be ∼13 (i.e. slightly higher than for a sample of isolated galaxies due to the inclusion of a few merging systems).

They also observed $C^{18}O$ and HCN in these galaxies to aid in the line ratio analysis and conclude that ^{12}CO emission is not mostly optically thick in the galaxies with very high $^{12}CO/^{13}CO$ line ratios. as has been assumed in the previous studies. It has an optical depth of ~ 1. indicating that more careful modeling of the molecular gas clouds is necessary in order to create a more accurate picture of the physical condition in these active systems.

Previous multi-J transition studies of just ^{12}CO in normal galaxy nuclei have shown only small variations of line ratios with other tracers of star formation (such as IRAS fluxes). For example. Braine & Combes (1992) undertook a brightness and distance limited ^{12}CO $J=1-0$ and $J=2-1$ survey of 81 nearby spiral galaxies. They found that the mean ^{12}CO $J=2-1/J=1-0$ ratio was 0.89 ± 0.06 suggesting that. on average. the molecular gas in the inner kpc was thermalized and optically thick. with an excitation temperature of 20 - 30 K for both CO transitions. They did not find any significant correlation between the ^{12}CO $J=2-1/J=1-0$ line ratio with the f_{60}/f_{100} ratio determined from the IRAS data when using the entire galaxy sample as a uniform set. but they did note a weak tendency for galaxies with higher f_{60}/f_{100} ratios to have higher ^{12}CO $J=2-1/J=1-0$ ratios when galaxies where binned by Hubble and RC3 classifications. They did not find any correlations between their CO line ratios and Seyfert. LINER or starburst activity.

More recently. Mauersberger et al. (1999) performed a ^{12}CO $J=3-2$ survey of 28 nearby galaxies and from these data created beam matched ^{12}CO $J=3-2/J=1-0$ line ratios. They found no correlations between CO line ratios and dust temperatures or infrared luminosities. They note. however. that most galaxies have line ratios less than 0.7. but those with ^{12}CO $J=3-2/J=1-0$ line ratios exceeding this also have high dust temperatures (in excess of 35 K) and infrared luminosities. Neither of these survey had observations of optically thin tracers such as ^{13}CO that will help

Table 4.1: Galaxy Properties

Galaxy	RA (2000)	dec (2000)	V_{LSR} (km s^{-1})	d (Mpc)	RC3 Class.	Nuclear Activity
NGC 0470	$01^h19^m44\overset{s}{.}8$	$+03°24'35''$	2374	32	SA(rs)b	starburst
NGC 1097	$02^h46^m19\overset{s}{.}0$	$-30°16'29''$	1275	17	(R'$_1$)SB(r'l)b	Seyfert 1
NGC 2273	$06^h50^m08\overset{s}{.}7$	$+60°50'45''$	1871	25	SB(r)a	Seyfert 2
NGC 3081	$09^h59^m29\overset{s}{.}5$	$-22°49'35''$	2385	32	(R$_1$)SAB(r)0/a	Seyfert 2
NGC 4736	$12^h50^m53\overset{s}{.}0$	$+41°07'14''$	308	4	(R)SA(r)ab	LINER
NGC 5728	$14^h42^m23\overset{s}{.}9$	$-17°15'10''$	2788	37	(R$_1$)SAB(r)a	Seyfert 2
NGC 6951	$20^h37^m14\overset{s}{.}5$	$+66°06'20''$	1424	19	SAB(rs)bc	Seyfert 2

All Data taken from the NASA IPAC Extragalactic Database. Distances are derived assuming $H_0 = 75$ km s^{-1} kpc^{-1}.

us determine the optical depth and place stronger constraints on the molecular gas properties determined by modeling CO line ratios.

The goal of this paper is two-fold. First, we wish to obtain a complete set of molecular gas data for a sample of barred galaxies containing 'bars within bars'. We have chosen 7 galaxies that are known to contain NIR isophote twists (thought to be the signature of a double barred galaxy) for which 5 have high resolution ^{12}CO $J=1-0$ data published. The properties of these galaxies are summarized in Table 4.1. This sample will allow us to determine if variations in the molecular gas physical conditions can explain why we see such a wide variety of CO morphologies in a sample of galaxies with similar NIR morphologies.

The second question that we wish to address is if the gas properties determine whether a double barred galaxy exhibits starburst or Seyfert activity. Shlosman, Frank, & Begelman (1989) suggest that, in double barred galaxies, the type of activity depends on whether or not star formation occurs as the gas is transported along the inner bar towards the galactic center. If star formation occurs, inflow is halted and a starburst galaxy is born. If star formation does not occur, the

inflow can continue to the center and accrete onto a central massive object and fuel an active galactic nuclei (AGN). A comparison of the physical conditions of the gas (e.g. density, column density, temperature) in the AGN, starburst, and non-starburst galaxies will provide valuable insight into what determines if a barred galaxy transporting material into the nucleus forms an AGN or a starburst galaxy.

In §4.2 we discuss the observations and data reduction techniques. In §4.3 we use the ^{12}CO $J=2-1$ fluxes to determine the molecular gas masses in the nuclei of these galaxies. In §4.4 we compare our CO line ratios with the high resolution CO morphology, dust temperatures, nuclear activity and large scale morphology of these galaxies. In §4.5 we determine the molecular gas physical condition using the Local Thermodynamic Equilibrium (LTE) and Large Velocity Gradient (LVG) approximations in order to provide a physical basis for the correlations discussed in §4.4. This work is summarized in §4.6.

4.2 Observations and Data Reduction

The nuclei of seven double barred galaxies were observed using the James Clerk Maxwell Telescope (JCMT)[1] over the period of 1998 - 2001. We have obtained ^{12}CO $J=2-1$, ^{13}CO $J=2-1$, and ^{12}CO $J=3-2$ detections for all galaxies except ^{13}CO $J=2-1$ in NGC 3081 and NGC 5728. The half-power beamwidth of the JCMT is $21''$ at 230 GHz (^{12}CO $J=2-1$) and $14''$ at 345 GHz (^{12}CO $J=3-2$). ^{12}CO $J=3-2$ data were obtained on a five-point cross offset by $7''$ in order to allow convolution to match the $21''$ beam of the JCMT at 230/220 GHz. All observations were obtained

---

[1]The JCMT is operated by the Joint Astronomy Centre in Hilo, Hawaii on behalf of the parent organizations Particle Physics and Astronomy Research Council in the United Kingdom, the National Research Council of Canada and The Netherlands Organization for Scientific Research.

using the Digital Autocorrelation Spectrometer. The calibration was monitored by frequently observing spectral line calibrators. The spectral line calibrators showed very little scatter from the values published on the JCMT webpage with individual measurements differing by typically $< 15\%$ from standard spectra. Thus, we adopt the normal main beam efficiencies from the JCMT Users Guide of 0.69 at 230/220 GHz and 0.63 at 345 GHz.

Initially, similar data sets were averaged together using the software package SPECX. Spectra were output to FITS files and then the data were further reduced using the Bell Labs data reduction package COMB. The data were binned to 10 km s^{-1} resolution (7.8 and 11.5 MHz at 230 and 345 GHz respectively) and and zeroth (horizontal) or first order (linear sloped) baselines were removed. The emitting regions were quite wide (> 200 km s^{-1}) but the spectrometer bandwidth was at least 800 km s^{-1}, which allowed for accurate baseline determination. The exception is NGC 5728 which had lines that were more than 450 km s^{-1} wide and the ^{12}CO $J=2-1$ spectra ran off the low velocity end of the spectrometer. For this reason, only the high velocity continuum was used in baseline removal. Finally, the five ^{12}CO $J=3-2$ spectra were then convolved to simulate a 21″ beam. The spectra for each galaxy are shown in Figures 4.1-4.7, and the spectral line intensities are summarized in Table 4.2.

The data were then binned to 20 km s^{-1} resolution. This allowed the calculation of line ratios for each channel within the spectral line. The ratios for each channel were averaged to obtain the final line ratios. Only those channels with a signal-to-noise ratio of at least two in the line ratio were used in the calculation. This method helps reduce errors introduced by the existence of poor baselines or weak signals. The uncertainty in the line ratio is taken as the standard deviation of the mean. As a final step, the spectra and line ratios were scaled to the main beam temperature
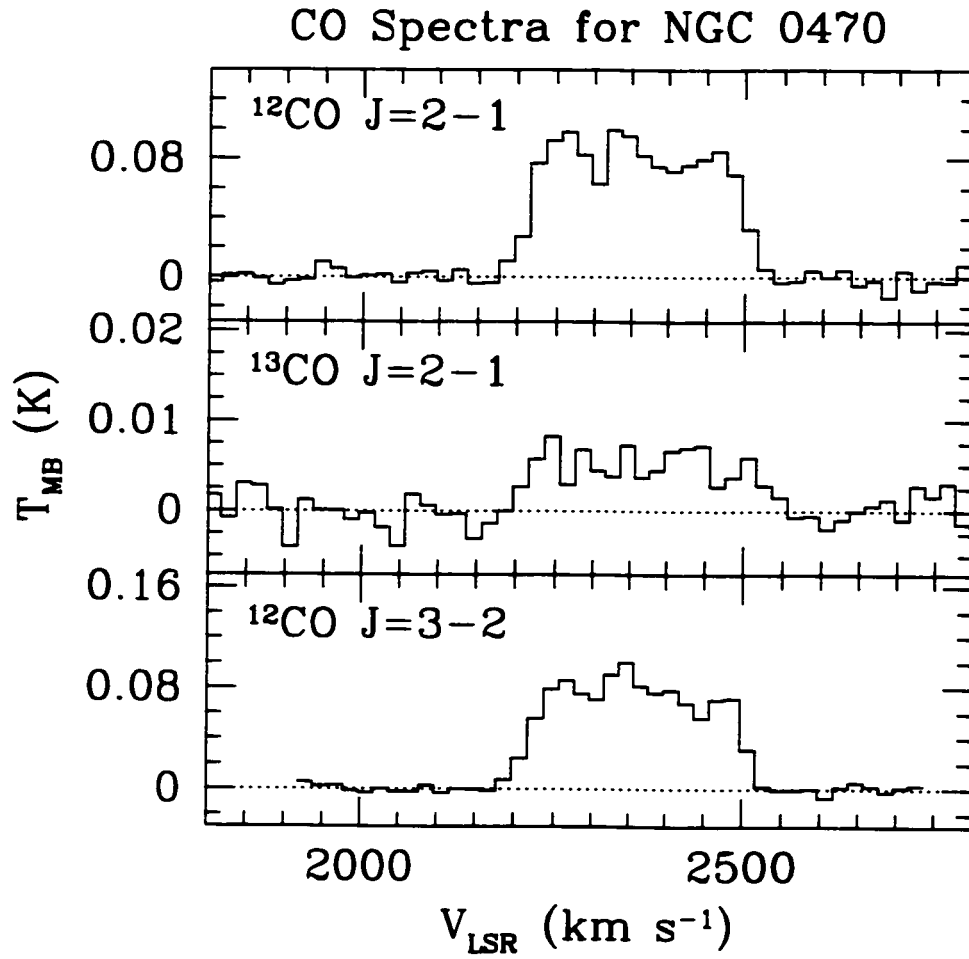
Figure 4.1: CO spectra for the inner 21″ of NGC 470

Individual spectra for the inner 21″ of NGC 470. The top panel shows ^{12}CO J=2–1: the middle panel shows ^{13}CO J=2–1: the bottom panel shows ^{12}CO J=3–2 (convolved to 21″ resolution.
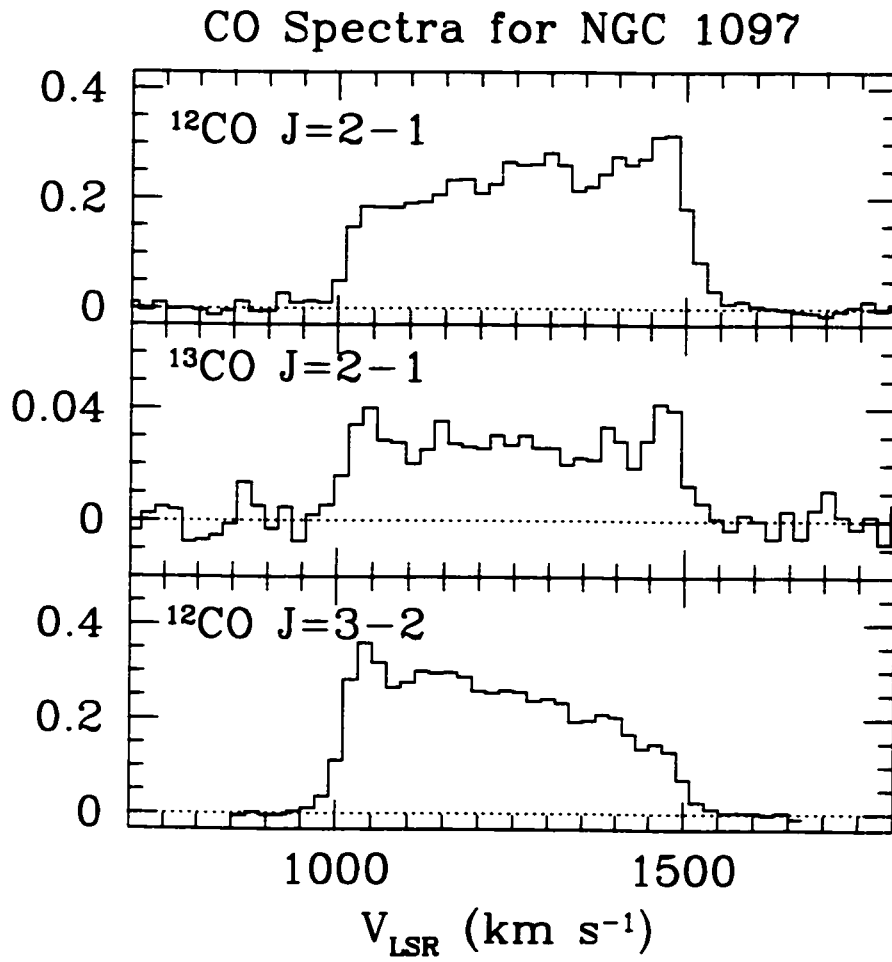
Figure 4.2: CO spectra for the inner 21″ of NGC 1097
Same as Figure 4.1, except for NGC 1097.
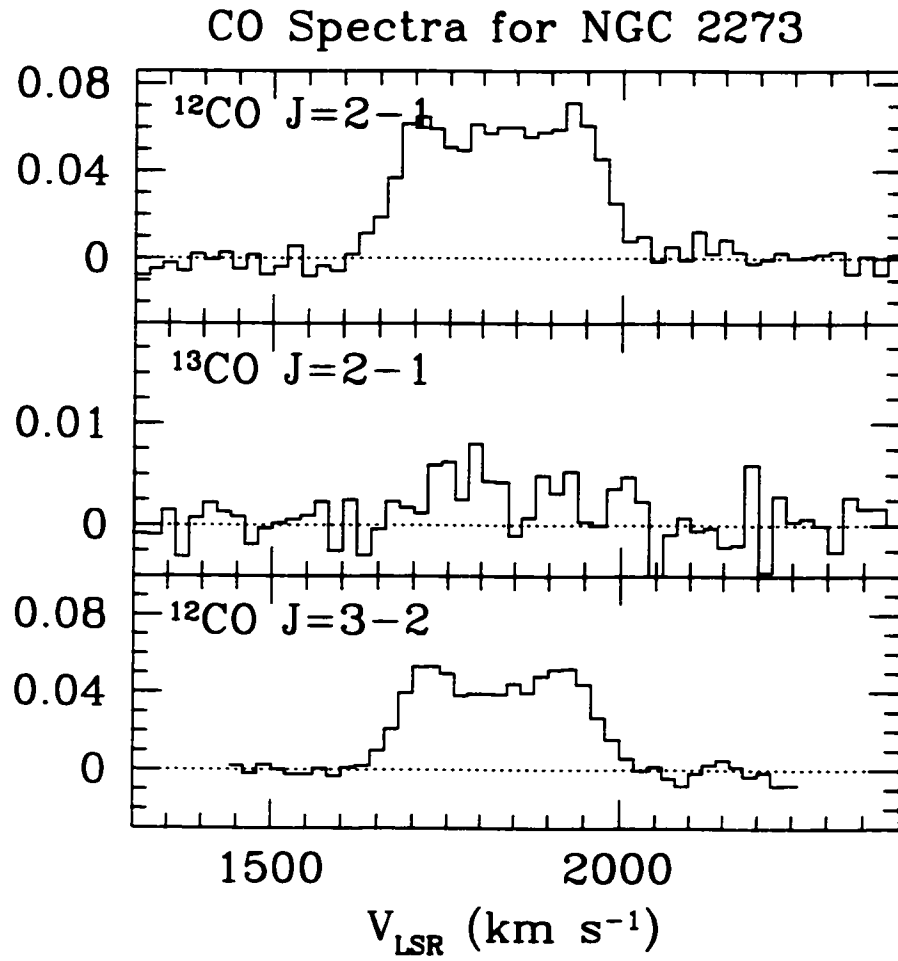
Figure 4.3: CO spectra for the inner 21″ of NGC 2273
Same as Figure 4.1. except for NGC 2273.
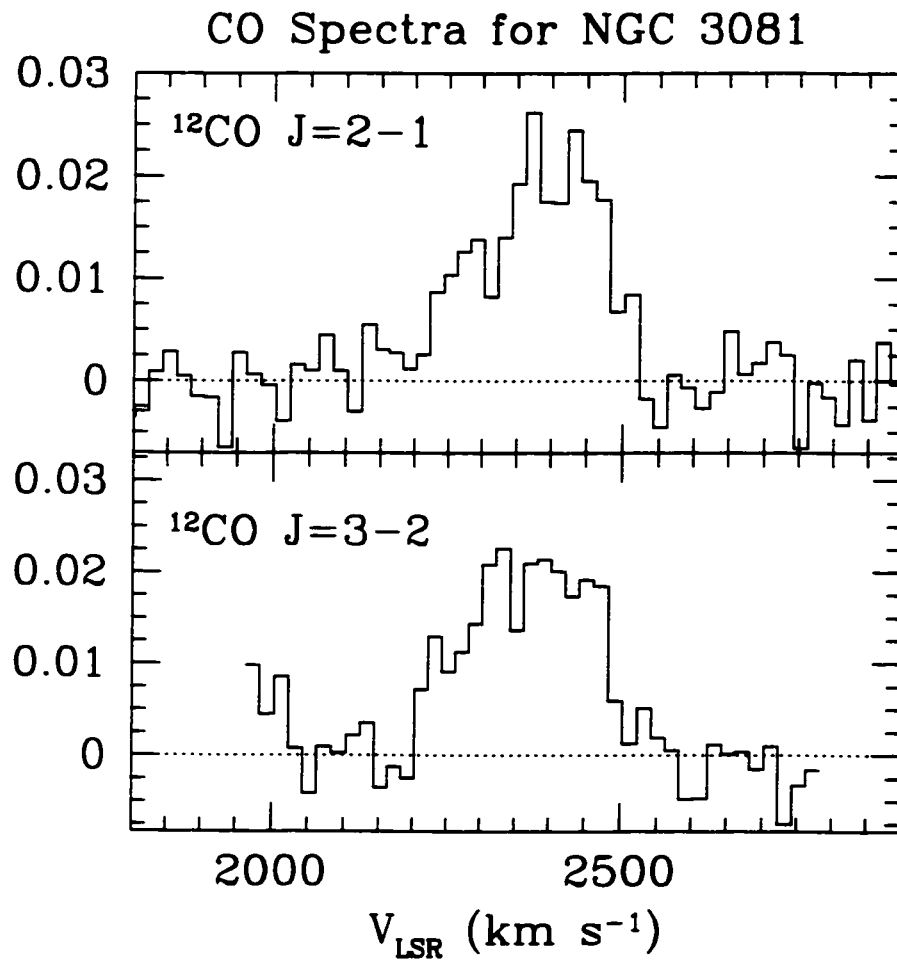
Figure 4.4: CO spectra for the inner 21″ of NGC 3081
Same as Figure 4.1. except for NGC 3081.
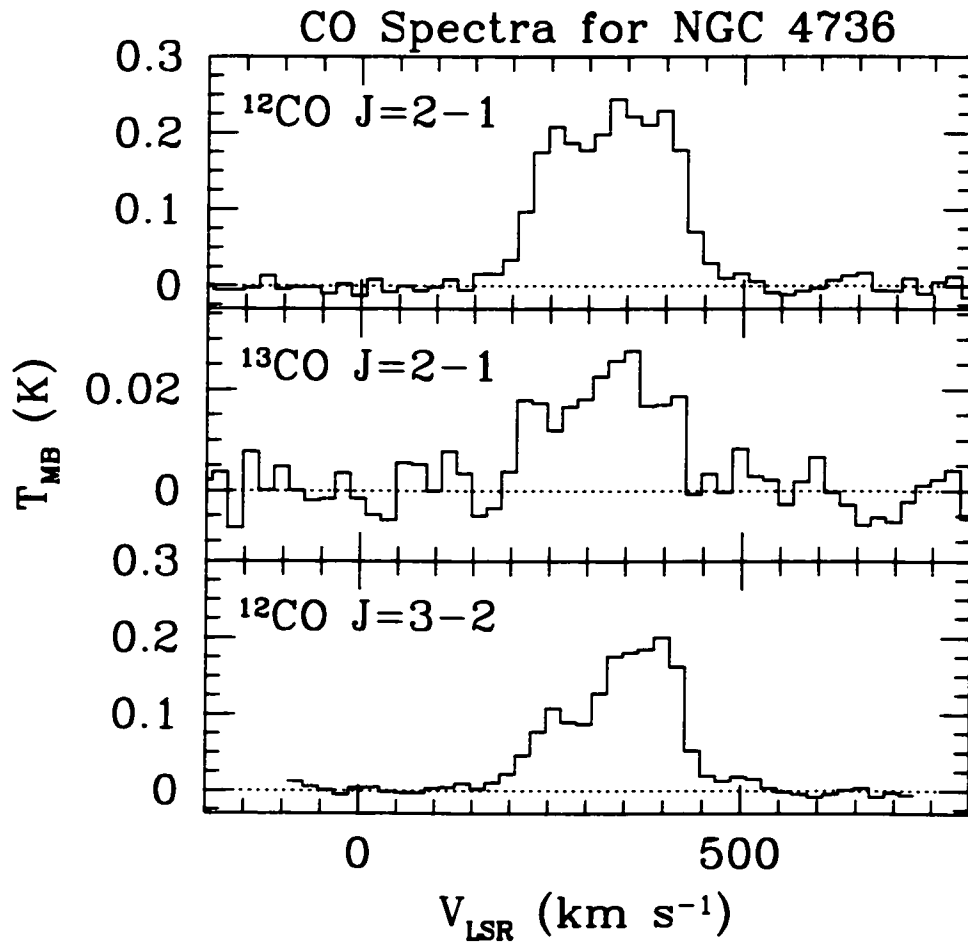
Figure 4.5: CO spectra for the inner 21″ of NGC 4736
Same as Figure 4.1. except for NGC 4736.
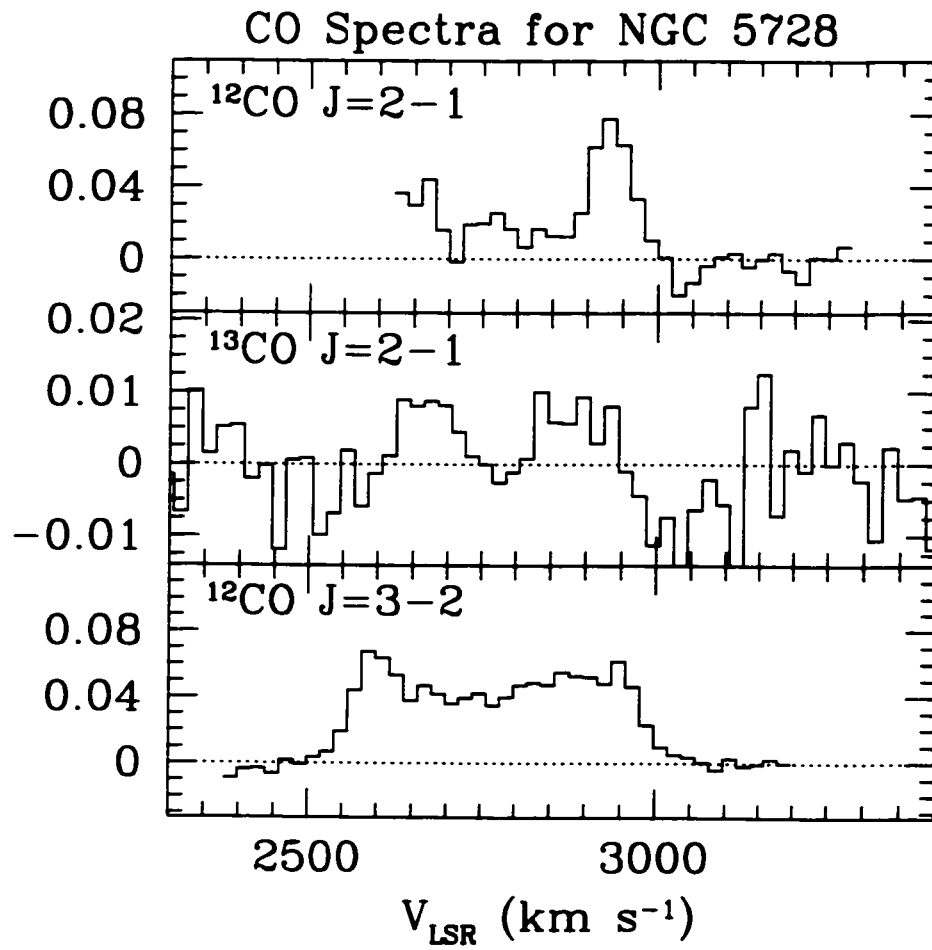
Figure 4.6: CO spectra for the inner 21″ of NGC 5728
Same as Figure 4.1. except for NGC 5728.
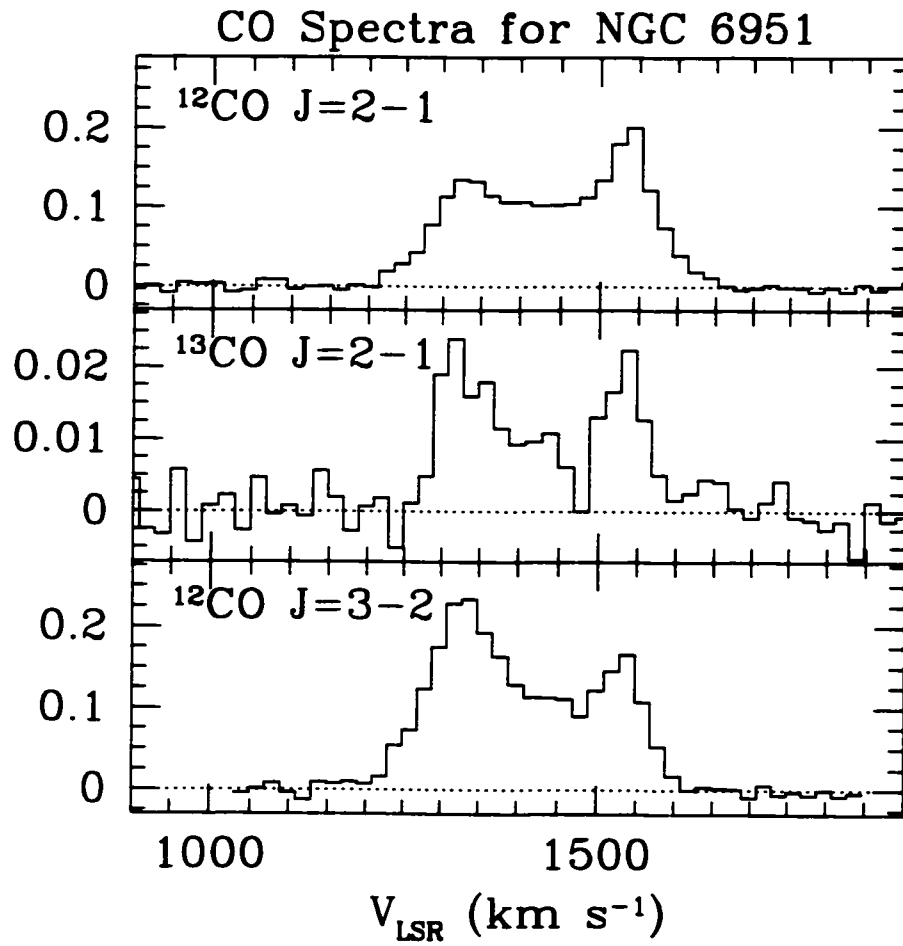
Figure 4.7: CO spectra for the inner 21″ of NGC 6951
Same as Figure 4.1. except for NGC 6951.

Table 4.2: Spectral Line Parameters

Galaxy	^{12}CO J=2-1 (21″)	^{13}CO J=2-1 (21″)	^{12}CO J=3-2 (21″)	^{12}CO J=3-2 (16″)	^{12}CO J=1-0	Refs
NGC 0470	24.2 ± 0.5	1.8 ± 0.2	22.4 ± 0.3	24.9 ± 0.6	19.3 (16″)	1
NGC 1097	121 ± 1	14.6 ± 0.6	121.7 ± 0.5	137.5 ± 0.8	80 (16″)	2
NGC 2273	19.7 ± 0.5	1.2 ± 0.2	14.3 ± 0.3	17.9 ± 0.5	22.5 (22″)	3
NGC 3081	4.6 ± 0.3	...	4.9 ± 0.3	7.4 ± 0.5	...	...
NGC 4736	46.1 ± 0.8	4.6 ± 0.4	31.9 ± 0.4	32.9 ± 0.5	32.5 (16″)	4
NGC 5728	9.5 ± 0.6	(0.8 ± 0.8)	21.5 ± 0.4	26.5 ± 0.8	9.74 (16″)	2
NGC 6951	41.7 ± 0.6	4.2 ± 0.4	48.8 ± 0.5	59.4 ± 0.8	71 (16″)	5

All CO line strengths given in T_{MB}. The beam size for the first four columns are stated below the transition. The ^{12}CO J=1−0 beam sizes are given beside the flux value.

(1) Sofue. Wakamatsu. Taniguchi. & Nakai (1993): (2) Vila-Vilaró. Taniguchi. & Nakai (1998): (3) Kruegel. Chini. & Steppe (1990): (4) Kohno. Kawabe. & Vila-Vilaró (1999)

scale using the appropriate values for η_{MB} (see below). A summary of the line ratios is given in Table 4.3 and a channel by channel histograms of the ratios are shown in Figures 4.8-4.14. We note that the ^{12}CO J=2−1 spectral line for NGC 5728 is truncated somewhat (see Figure 4.6). We feel that the truncation of the J=2−1 spectra will have less effect on our CO line ratio. since they were calculated channel by channel. rather than integrated intensity over the entire spectral line.

For §4.5.2. the Large Velocity Gradient models contain four free parameters. so we need more line ratios in order to place stronger constraints on the molecular gas physical conditions. We have searched the literature and have obtained ^{12}CO J=1−0 line strengths for all galaxies except NGC 3081. All ^{12}CO J=1−0 spectra were taken with the Nobeyama Radio Observatory (NRO) with 16″ resolution except for NGC 2273 which was taken at the IRAM 30 m telescope with a 22″ beam (see Table 4.2 for references). Since our JCMT ^{12}CO J=2−1 data are taken at 21″ resolution. we have created beam matched ^{12}CO J=3−2/J=1−0 data with the JCMT and NRO
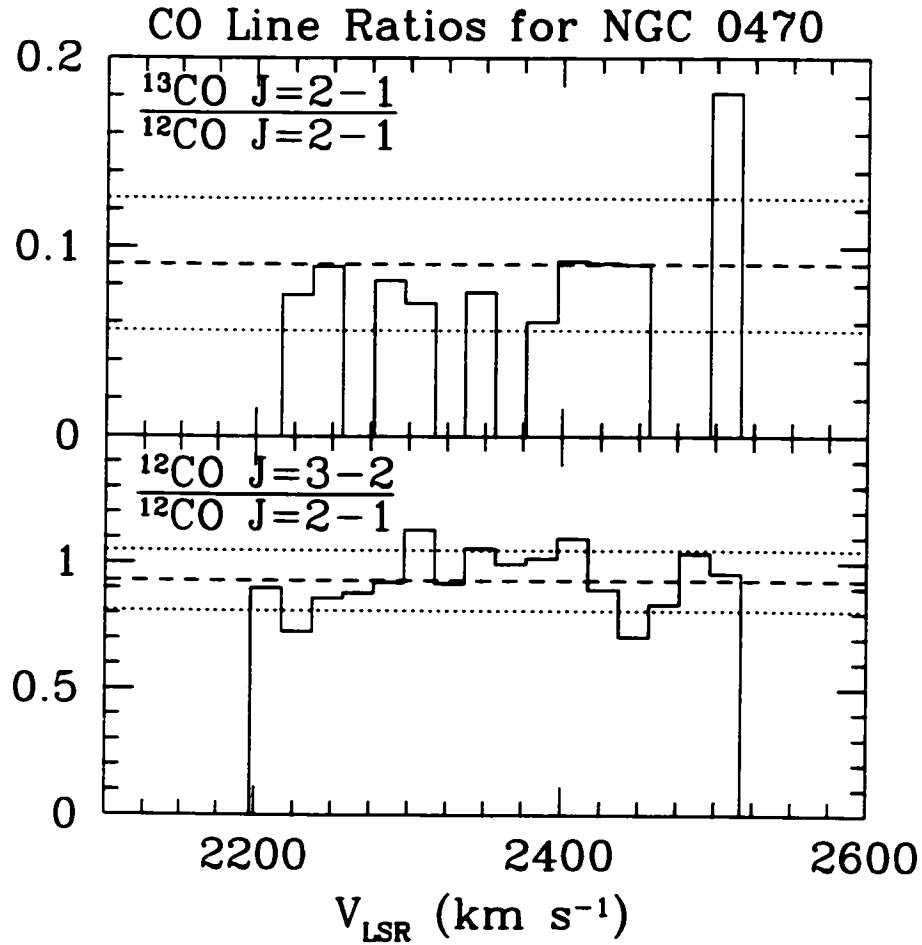
Figure 4.8: Channel by channel CO line ratios for NGC 0470

Channel by channel line ratios for NGC 470. The top panel shows the $^{13}CO/^{12}CO$ $J=2-1$ ratio and the bottom panel shows the ^{12}CO $J=3-2/J=2-1$ ratio. Only those channels with a combined SNR > 2 are shown. The dashed line is the average over all channels, the dotted line is the root-mean-square of the scatter. The values for the ratios listed in Table 4.3 are the average value over all channels shows here, and the uncertainty is the standard deviation in the mean.

CO Line Ratios for NGC 1097
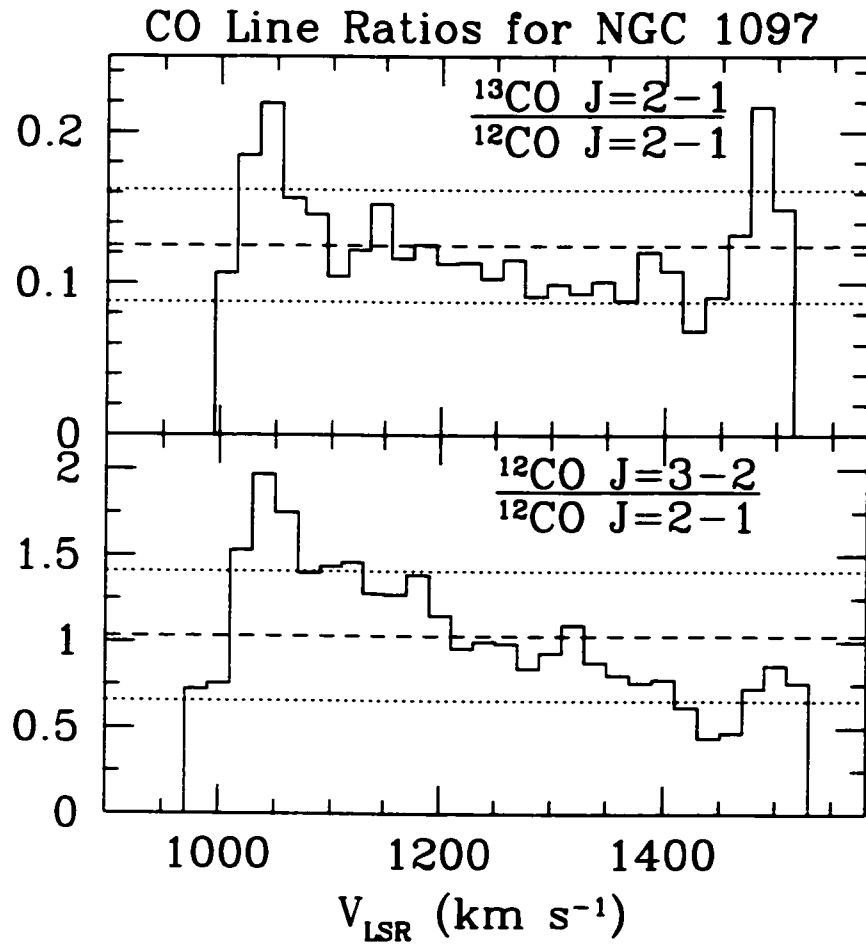
Figure 4.9: Channel by channel CO line ratios for NGC 1097
Same as Figure 4.8, except for NGC 1097.
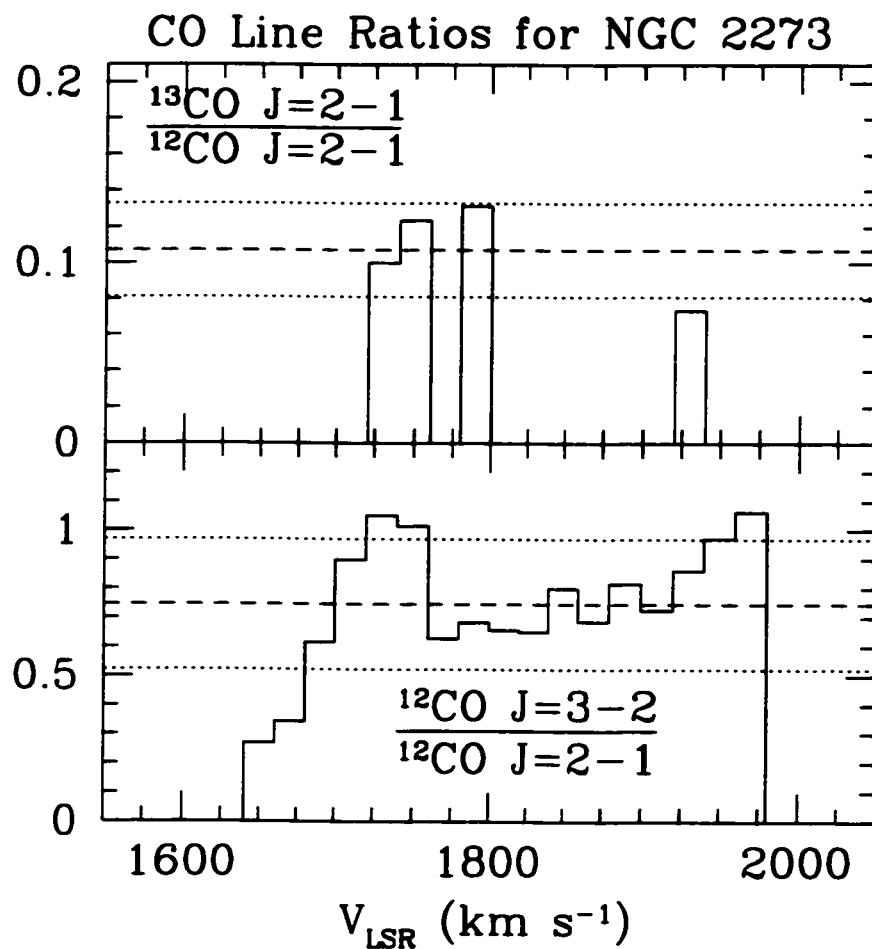
Figure 4.10: Channel by channel CO line ratios for NGC 2273
Same as Figure 4.8. except for NGC 2273.

CO Line Ratios for NGC 3081
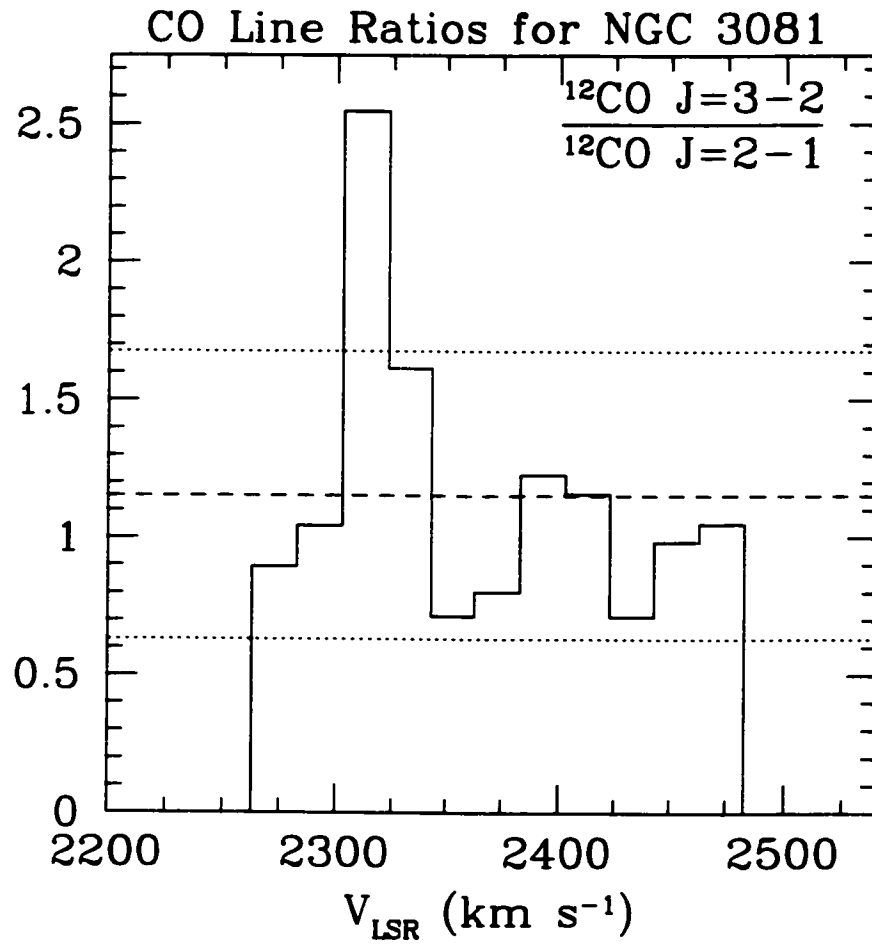
Figure 4.11: Channel by channel CO line ratios for NGC 3081
Same as Figure 4.8. except for NGC 3081.
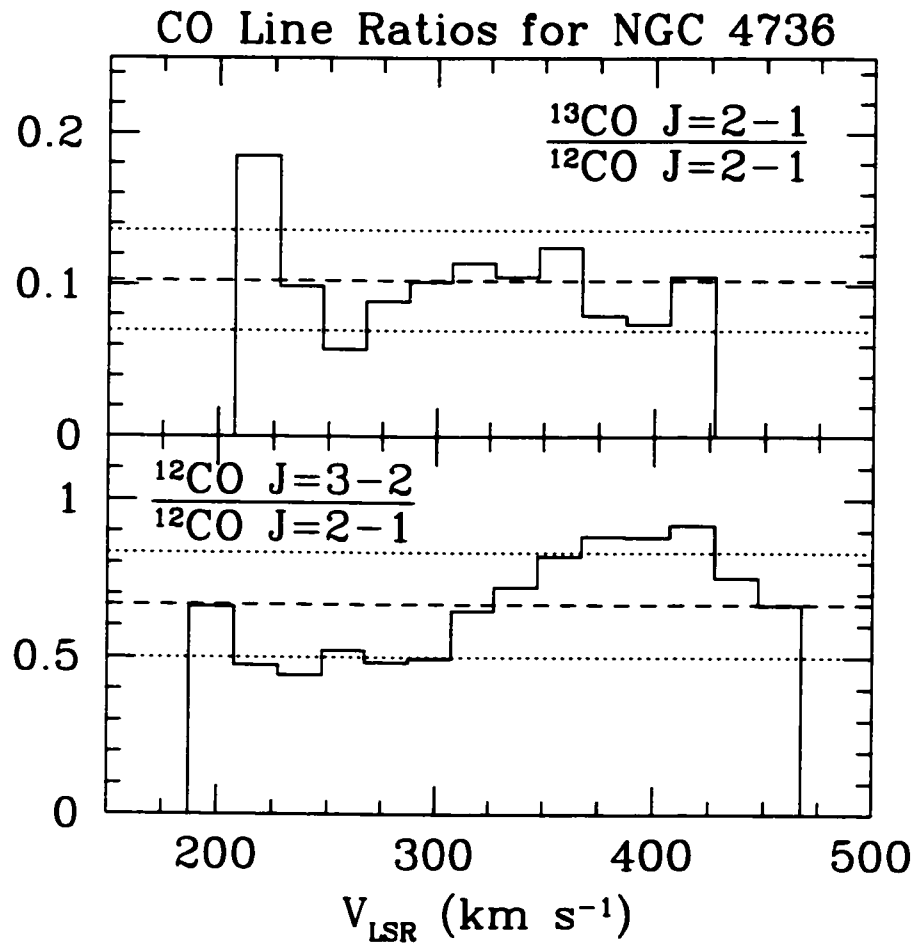
Figure 4.12: Channel by channel CO line ratios for NGC 4736
Same as Figure 4.8. except for NGC 4736.
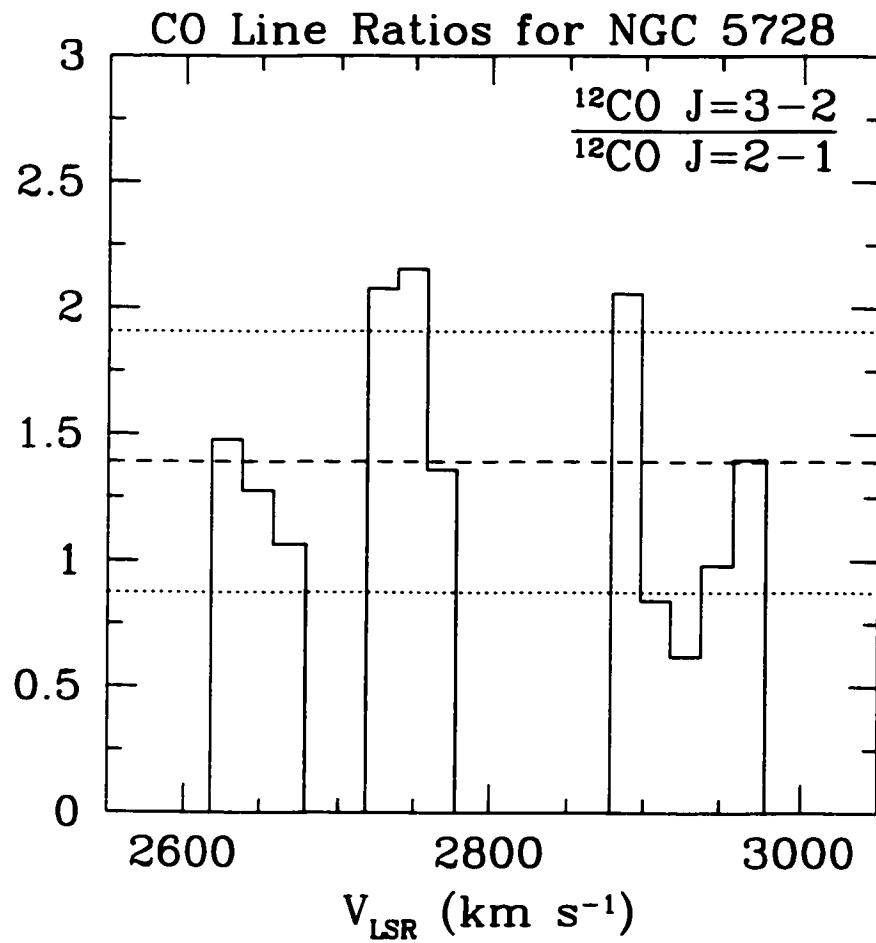
Figure 4.13: Channel by channel CO line ratios for NGC 5728
Same as Figure 4.8. except for NGC 5728.
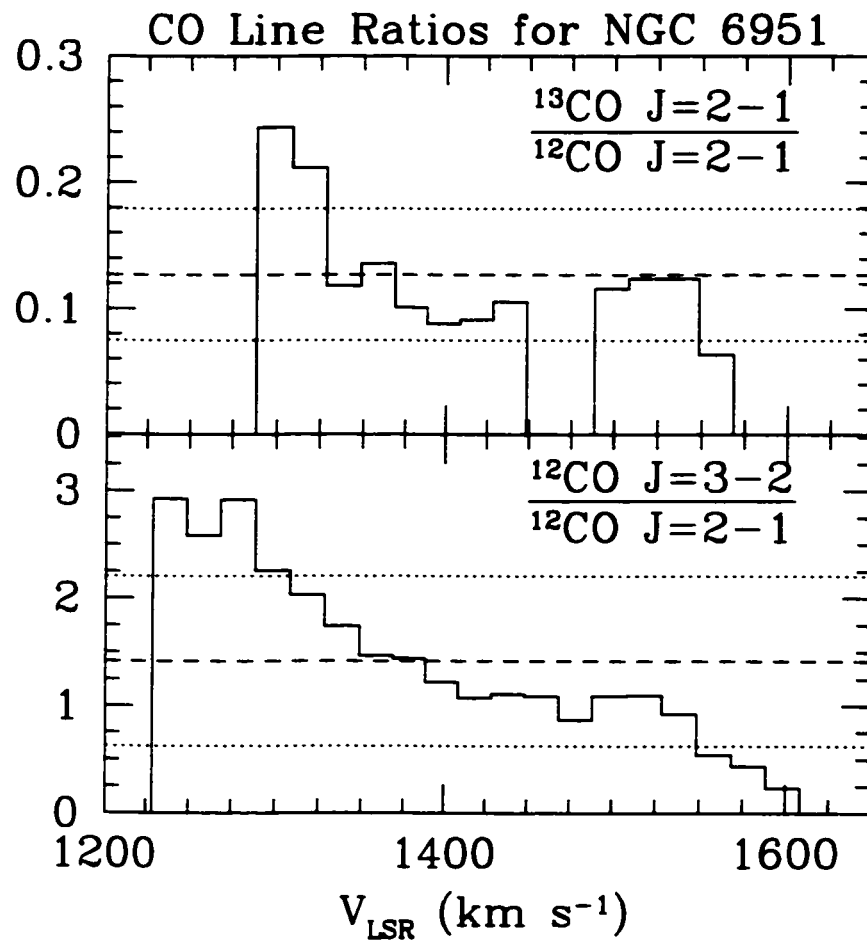
Figure 4.14: Channel by channel CO line ratios for NGC 6951
Same as Figure 4.8. except for NGC 6951.

Table 4.3: CO Line Ratios and Nuclear Characteristics

Galaxy	$\frac{^{13}CO\,J=2-1}{^{12}CO\,J=2-1}$	$\frac{^{12}CO\,J=3-2}{^{12}CO\,J=2-1}$	$\frac{^{12}CO\,J=2-1}{^{12}CO\,J=1-0}$	CO Morph	Act.	Refs
NGC 0470	0.09±0.01	0.93±0.03	1.38±0.42	bar	SB	1,2
NGC 1097	0.13±0.01	1.03±0.07	1.67±0.50	ring?	S1	3,4
NGC 2273	0.11±0.01	0.75±0.05	0.88±0.26	bar	S2	3,5,6
NGC 3081	...	1.15±0.16	...	?	S2	7
NGC 4736	0.10±0.01	0.67±0.04	0.70±0.14	peaked	L	8,9
NGC 5728	< 0.09	1.39±0.16	1.96±0.59	blobs	S2	3,6
NGC 6951	0.13±0.02	1.42±0.18	0.59±0.18	spiral	S2	3,10,11

All data for columns 2 and 3 are taken with the JCMT. The line ratio calculation is described in the text. The ^{12}CO J=1−0 data for NGC 2273 is taken with the IRAM 30 m telescope with a 22″ beam. The line ratio for NGC 4736 is taken from Gerin. Casoli. & Combes (1991) with a 22″ beam. The remaining ratios are a combination of ^{12}CO J=3−2 data taken with the JCMT (16″ beam) and ^{12}CO J=1−0 data taken with the Nobeyama 45 m telescope (16″ beam). The ^{12}CO J=3−2/J=1−0 ratio is scaled to the ^{12}CO J=2−1/J=1−0 ratio by dividing by the ^{12}CO J=3−2/J=2−1 ratio in column 3. All ratios are given in T_{MB}.

SB = Starburst: S1 = Seyfert 1; S2 = Seyfert 2; L = LINER (Classification taken from NASA-IPAC Extragalactic Database)

(1) Sofue et al. (1993); (2) Jogee (1998); (3) Vila-Vilaró. Taniguchi. & Nakai (1998); (4) Gerin. Combes. & Nakai (1988); (5) Kruegel. Chini. & Steppe (1990); (6) Petit-pas & Wilson (2001); (7) Phillips. Charles. & Baldwin (1983); (8) Gerin. Casoli. & Combes (1991); (9) Sakamoto et al. (1999); (10) Aalto et al. (1995); (11) Kenney et al. (1992)

and divided them by our beam matched ^{12}CO $J=3-2/J=2-1$ ratio. In the case of NGC 4736. we used the ^{12}CO $J=2-1/J=1-0$ line ratio taken at IRAM with a 22″ beam by Gerin. Casoli. & Combes (1991) (since they did not publish the individual line strengths). For the line ratios we took from the literature or created using JCMT and published data. we adopt a 30% uncertainty to account for cross calibration uncertainties.

Since the line strengths we are comparing are measured with the same beam diameter. using the T_R^* temperature scale would ensure that our observed line ratios are equal to the true radiation temperature ratios. However. conversion to T_R^* from T_A^* requires knowledge of the forward scattering and spillover (η_{FSS}). which is difficult to measure and was not attempted during the observing run. As a result. we do not know if it is safe to adopt the published values of η_{FSS}. On the other hand. we do have good values for the main beam efficiencies and so an accurate conversion to main beam temperature (T_{MB}) is possible. Using the T_{MB} scale instead of T_R^* scale only changes the ^{12}CO $J=3-2/J=2-1$ line ratio by ~5% under normal calibration conditions. For this reason. we will use the main beam temperature scale for the line ratios throughout this paper.

4.3 Molecular Gas Mass

The double barred galaxy models of Friedli & Martinet (1993) suggest the molecular gas inflow in these double barred galaxies should accumulate enough mass so that the nuclear bar can become kinematically distinct. Thus, we may expect to see a higher molecular gas mass in the galaxies that (still) possess nuclear molecular

bars. The intensity of the CO emission can be related to the molecular mass using the equation

$$M_{mol} = 1.61 \times 10^4 \left(\frac{\alpha}{\alpha_{Gal}} \right) \left(\frac{115 \text{ GHz}}{\nu} \right)^2 d^2_{Mpc} \frac{S_{CO}}{R} M_\odot \qquad (4.1)$$

(Wilson & Scoville 1990; Wilson 1995) where S_{CO} is the ^{12}CO J=2−1 flux in Jy km s^{-1}. R is the ^{12}CO J=2−1/J=1−0 line ratio. ν is the frequency of the emission (230 GHz for the J=2−1 transition). d_{Mpc} is the distance to the galaxy in Mpc. α is the CO-to-H$_2$ conversion factor for the galaxy. and α_{Gal} is the Galactic value $(3 \pm 1 \times 10^{20}$ cm^{-2}(K km s^{-1})$^{-1}$. Strong et al. (1988); Scoville & Sanders 1987). We use 29.4 Jy K^{-1} (η_{ap}= 0.53) to convert the JCMT data from Kelvins (T^*_A) to Janskys (Kraus 1986). We assume a coupling efficiency (η_c) of 0.7 to correct our observed fluxes to true fluxes. The CO-to-H$_2$ conversion factor (α) is a globally averaged property of the galaxy and hence there are uncertainties involved in its use in one specific region of the galaxy and it is only accurate to within ∼ 30%. Our fluxes are typically accurate to about 10%. We therefore adopt a total uncertainty of 40%. The results are shown in Table 4.4. The molecular gas masses determined using the above equation show good agreement with independent determinations for galaxies with published high resolution CO maps (Kohno. Kawabe. & Vila-Vilaró 1999: Gerin. Combes. & Nakai 1988: Sakamoto et al. 1999: Petitpas & Wilson 2001).

We see no correlation between molecular gas mass and the presence of bars in the CO maps. In fact the lowest CO mass is found in the center of NGC 4736. which is claimed to contain a nuclear molecular bar (Wong & Blitz 2000). We point out that the range in galaxy distances indicates that the beam of the JCMT covers different physical areas of the galaxies. In order to reduce this effect. we have normalized our gas masses to the physical size of our beam at the distance of the galaxy. We point out that this is not a true surface density (as in, for example Wong

Table 4.4: Molecular Gas Mass for the Inner 21″

Galaxy	Mass $(M_\odot)$	Scale $(pc/″)$	Beam Area (kpc^2)	Normalized to Beam $(M_\odot/kpc^2)$
NGC 0470	2.1×10^9	155	12.0	1.8×10^8
NGC 1097	2.4×10^9	82	3.4	7.1×10^8
NGC 2273	1.6×10^9	121	7.3	2.2×10^8
NGC 3081	0.8×10^9	155	12.0	0.7×10^8
NGC 4736	0.1×10^9	19	0.18	5.6×10^8
NGC 5728	0.8×10^9	179	16.0	0.5×10^8
NGC 6951	3.0×10^9	92	4.2	7.1×10^8

We have assumed a ^{12}CO $J{=}2{-}1/J{=}1{-}0$ ratio of 0.7 for NGC 3081. The last column is not a true surface density since it is not corrected for inclination. nor is it corrected for HI.

& Blitz 2000) since we have not corrected for inclination nor have we attempted to include HI mass. We see from Table 4.4 that the molecular mass determination for NGC 4736 was likely affected by its proximity and thus the small physical area covered by our beam. We see that the galaxies that contained the highest molecular gas masses (NGC 6951 and NGC 1097) retain their number one and two ranking even when normalized to beam area. Our sample of galaxies includes some with circumnuclear rings of star formation (e.g. NGC 2273. NGC 470. NGC 1097, and NGC 6951: Yankulova 1999: Jogee 1998: Barth et al. 1995). The CO emission in NGC 1097 and NGC 6951 also originates from predominantly in the nuclear ring. whereas NGC 2273 and NGC 470 have molecular emission originating from inside the ring. It is possible that the strong CO lines actually indicate the presence of large amounts of molecular gas. and this gas is responsible for the star formation in these galaxies.

4.4 Discussion

In this section we will discuss any trends that appear when we compare the CO integrated intensity line ratios with other properties such as nuclear activity, dust temperatures, and nuclear CO mass and distribution. In order to reduce the uncertainties introduced by combining observations made with different telescopes, we will limit our analysis to the interpretation of only those CO line ratios taken with the JCMT, namely $^{13}CO/^{12}CO$ $J=2-1$ and ^{12}CO $J=3-2/J=2-1$.

It is clear from Table 4.3 that the $^{13}CO/^{12}CO$ $J=2-1$ ratio is uniform at the 2σ level across all five of the galaxies for which we have a ^{13}CO $J=2-1$ detection. The constant $^{12}CO/^{13}CO$ $J=2-1$ ratio across all galaxies, while interesting, renders it useless for comparing differences in molecular gas properties between the galaxies. There is a wide range of variation in the ^{12}CO $J=3-2/J=2-1$ line ratio, so in the following sections, we will compare the $J=3-2/J=2-1$ integrated intensity line ratio with other galactic properties and tracers of star formation. The LTE and LVG models discussed in §4.5.1 and §4.5.2 (respectively) rely on basic assumptions that may not be valid in all galaxy nuclei. Thus, we will initially use the ^{12}CO $J=3-2/J=2-1$ ratio as a direct probe of the molecular gas properties.

Figure 4.15 shows the ^{12}CO $J=3-2/J=2-1$ integrated intensity line ratio for each galaxy plotted as a function of the f_{60}/f_{100} ratio taken from IRAS data (Soifer et al. 1989; Moshir 1990). Along the right side are different classifications for each galaxy. The first column is the type of nuclear activity harbored by each galaxy. The second column is the galaxy morphological type taken from RC3 (de Vaucouleurs et al. 1991). The last column is the molecular gas distributions of the inner $21''$ of each galaxy. These will be discussed in more detail in the following sections.
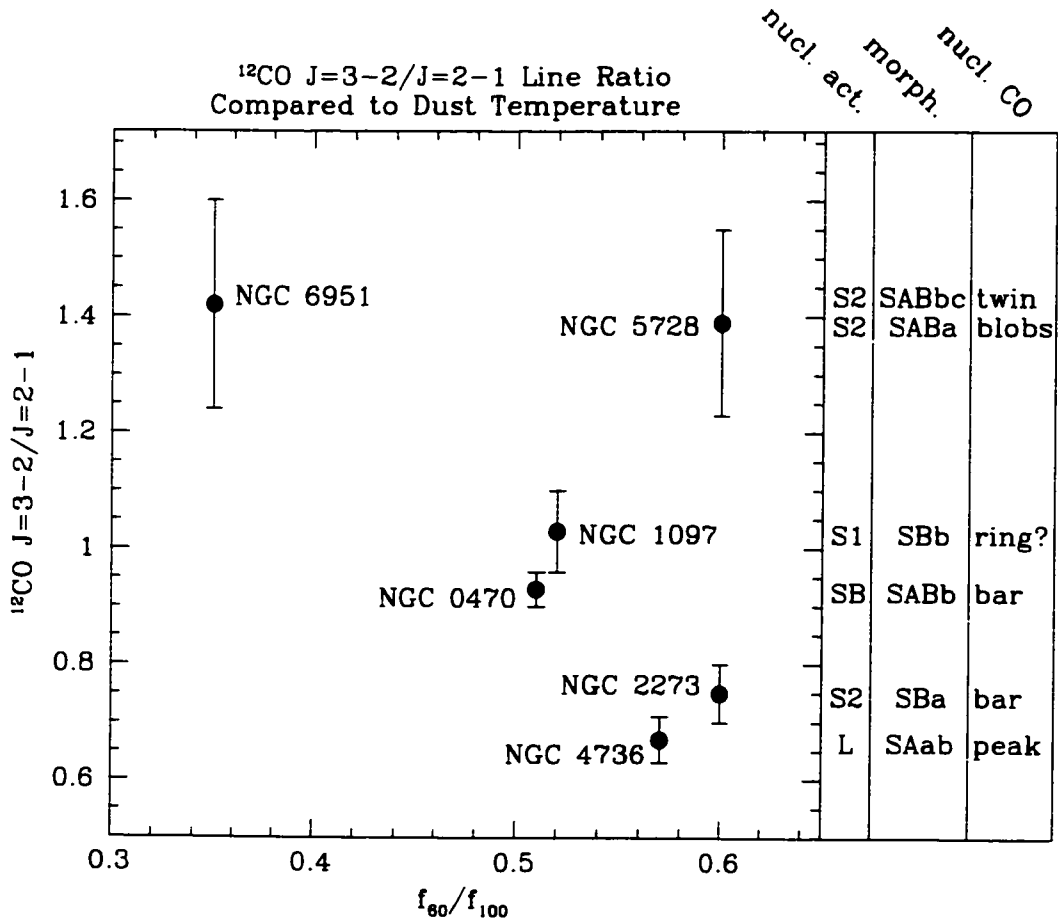
Figure 4.15: ^{12}CO J=3−2/J=2−1 Line Ratio Comapared to Galaxy Parameters

Our ^{12}CO J=3−2/J=2−1 line ratio taken at the JCMT (convolved to 21″) compared to the ratio of IRAS fluxes at 60 μm and 100 μm. Higher f_{60}/f_{100} indicates higher dust temperatures. The additional columns on the right indicate the nuclear activity. RC3 classification and nuclear CO morphology described in Table 4.3.

4.4.1 Comparison with Dust Temperature

Figure 4.15 shows the ^{12}CO $J=3-2/J=2-1$ integrated intensity ratio plotted against the IRAS f_{60}/f_{100} ratio. An obvious caveat in such a comparison is the effect of the different areas covered by the different beam sizes of IRAS and the JCMT. As discussed in §4.5.1 the unknown filling factor of the emission within the beam is partially cancelled out by the comparison of flux ratios. Also. as noted by Mauersberger et al. (1999). the beam dilution effects are partially cancelled out by the tendency for the f_{60}/f_{100} and ^{12}CO $J=3-2/J=2-1$ ratios to trace warmer material that is probably less dominant in the outer disk of these galaxies.

We see no correlation in the CO $J=3-2/J=2-1$ line ratio with f_{60}/f_{100} ratios (hence dust temperature). This result agrees with the findings of Mauersberger et al. (1999) who find no correlation between ^{12}CO $J=3-2/J=1-0$ line ratios and dust temperatures. They do note that the few galaxies in their sample that have ^{12}CO $J=3-2/J=1-0$ ratios > 0.7 also have dust temperatures > 35 K. For the galaxies where we are capable of creating beam matched ^{12}CO $J=3-2/J=1-0$ ratios. all of our galaxies have ratios > 0.7. Of these. only NGC 6951. (which has the lowest $J=3-2/J=1-0$ of our sample at 0.83) has a dust temperature less than 35 K assuming a dust emissivity $\beta = 1$.

The lack of correlation suggests that the molecular gas temperature is independent of the dust temperature as previously suggested by Mauersberger et al. (1999). We note. however. that the few galaxies in our sample cover a rather small range in f_{60}/f_{100} ratio. whereas Mauersberger et al. (1999) have a much larger sample of galaxies that cover a much wider range of dust temperatures. In fact. most of the galaxies discussed here have $S_{60}/S_{100} > 0.5$. unlike those in Braine & Combes (1992). We find that our sample of galaxies has f_{60}/f_{100} ratios similar to the 'disturbed' classification of Braine & Combes (1992). This suggests that double barred

galaxies have enhanced star formation activity, comparable to that of interacting galaxies.

It is interesting to note that our galaxies, which all have $f_{60}/f_{100} \sim 0.5 \pm 0.1$, also all have $^{12}CO/^{13}CO$ $J=2-1$ line ratios near 10. Thus, the similarity in the CO line ratios among our galaxies should not be surprising considering the similarities in their dust temperatures. The previous studies comparing the $^{12}CO/^{13}CO$ $J=1-0$ line ratios and dust temperatures saw a strong correlation, with higher line ratios in galaxies with higher dust temperatures (e.g. Young & Sanders 1986). It has also been shown that the $^{12}CO/^{13}CO$ $J=1-0$ and $^{12}CO/^{13}CO$ $J=2-1$ line ratios are, on average, equal (Aalto et al. 1995). Therefore, given the similarities in the dust temperatures in our galaxies, we should expect (at least empirically) that the $^{12}CO/^{13}CO$ $J=2-1$ line ratio should also be similar. The six galaxies discussed in this work for which we have ^{13}CO $J=2-1$ detections fit nicely into the f_{60}/f_{100} vs. $^{12}CO/^{13}CO$ plots of the previous studies of isolated galaxies (Young & Sanders 1986; Aalto et al. 1991).

4.4.2 Comparison with Nuclear CO Morphology

The right-most column of Figure 4.15 lists the nuclear CO morphologies for six of the galaxies in our sample. NGC 5728 exhibits a clumpy CO structure that is not centered on the galactic center. It appears that it may be a lumpy circumnuclear ring that joins up with the southern-most dust lane (Petitpas & Wilson 2001). High resolution CO maps of NGC 6951 show a "twin peaked" structure that may be collections of molecular gas at the Inner Lindblad Resonance (ILR;Kenney et al. 1992; Kohno et al. 1999). NGC 470 and NGC 2273 show what could be described as nuclear CO bars (Petitpas & Wilson 2001; Jogee 1998) both of which coincide with the nuclear stellar bars seen in the NIR images of Wozniak et al. (1995) and

Mulchaey. Regan. & Kundu (1997). The high resolution CO maps of the inner

21″ of NGC 4736 show an elongated central peak which has been interpreted as a

nuclear CO bar by Wong & Blitz (2000) and Sakamoto et al. (1999). We note that

it is more centrally concentrated that the nuclear bars seen in NGC 2273 and NGC

470.

There are currently no published high resolution CO maps of NGC 3081 and

NGC 1097 (likely because of their low declination). As such. we cannot include

NGC 3081 in our comparison. but there are single dish CO maps of NGC 1097 by

Gerin. Combes. & Nakai (1988) that strongly suggest a circumnuclear ring of CO.

with a radius of $\sim 8''$. This is confirmed by the HI maps by Ondrechen. van der

Hulst. & Hummel (1989). so we will include this galaxy in our comparisons.

Figure 4.15 shows that galaxies containing nuclear molecular bars have lower

^{12}CO $J=3-2/J=2-1$ integrated intensity line ratios. The $J = 1$. $J = 2$. and

$J = 3$ levels of CO lie at 5.5. 17. and 33 K above the ground state respectively. In

addition. in the optically thin limit where all CO emission escapes the cloud. the

critical densities of H_2 needed to collisionally excite ^{12}CO at the same rate that it

spontaneously decays are $\sim 10^3$. 10^4. and 10^5 cm^{-3} for the $J=1-0$. $J=2-1$. and

$J=3-2$ transitions respectively. So. fundamentally. the lower ^{12}CO $J=3-2/J=2-1$

line ratio suggests that the molecular gas is cooler in the galaxies with nuclear bars.

If the ^{12}CO is optically thin. then this correlation suggests that the gas is also less

dense in nuclear CO bar galaxies. We will see in §4.5.1 and §4.5.2 that the optically

thin assumption may not be valid.

Previous models have indicated that in order to create and sustain nuclear bars

and rings. there must be some form of viscous gas component that can dissipate

energy (Combes & Gerin 1985; Athanassoula 1992; Friedli & Martinet 1993; Shaw

et al. 1993). These models have reproduced many of the large variety of nuclear

morphologies seen in regular and double barred galaxies by varying the models parameters such as bar pattern speed. main bar strength. ILR strength. etc.. None of these models have attempted to vary the gas parameters. which is usually assumed to be some numerical viscosity or some percentage of energy loss during cloud collision and kept constant for all trials. Our observational result is the first detection of how gas properties may be responsible for the variety of molecular gas morphologies seen in the nuclei of double barred galaxies. Future models of double barred galaxies may wish to study the effects of gas properties on the gas morphology to see if nuclear bars preferentially form in galaxies with cooler (perhaps more viscous) gas.

We point out that there is currently no studies of how actual gas conditions relate to viscosity (as modeled in the simulations). It seems feasible that cooler gas would tend to be more viscous than warmer gas. since most of the CO and other molecular would be in lower energy states. The cooler gas may aborb more energy in cloud collisions by bumping molecules into the still empty higher energy levels. whereas warmer gas would not have these higher levels available. Clearly. much more study of the energy of molecular clouds and cloud collisions is needed before we can say that cooler gas clouds are more viscous.

Another possible explanation for the variation of line ratios with galaxy type is that perhaps the galaxies without molecular counterparts to their nuclear bars are undergoing (or underwent) vigorous star formation activity which disperses (or dispersed) the molecular gas. NGC 2273 and NGC 470 have active nuclear star formation and the CO maps show a molecular bar (Jogee 1998: Petitpas & Wilson 2001). In NGC 4736. there is evidence for a circumnuclear starburst phase, and the CO maps show a weak nuclear bar structure with a bright central concentration and many peaks of emission that are neither associated with the nuclear bar. nor with the spiral arms (Kinney et al. 1993: Wong & Blitz 2000). NGC 6951 and NGC

1097 show signs of star formation in a circumnuclear ring and the CO maps exhibit a "twin peak" and ring morphology, respectively, with no strong CO emission in the very center of the galaxy (Kenney et al. 1992; Kohno et al. 1999; Gerin et al. 1988). NGC 5728 shows evidence of past star formation activity, and the molecular gas is distributed in a rather chaotic pattern about the nucleus, with peaks that do not align with any features observed at other wavelengths.

NGC 470 and NGC 2273 may represent an earlier stage of evolution, and are still in the process of forming new stars from the material in the molecular bar. This star formation may exhaust the gas in the bar, and the supernovae resulting from this starburst may heat and compress the remaining molecular gas. The result of this process could be a CO morphology similar to that of NGC 5728. The past star formation history of NGC 5728 may be responsible for the lack of a nuclear molecular bar in that galaxy. NGC 6951 and NGC 1097 may represent intermediate stages, where the starburst is still ongoing, yet the nuclear CO bar has begun to disperse.

Confirmation of this hypothesis is found in the models of Friedli & Martinet (1993) who predict that the double bar phase of galaxy evolution is a temporary state. For their models of double barred galaxies with ILRs (their set II), they find that the double bar phase gradually evolves into a ringed galaxy and the nuclear bar dissolves. The nuclear ring will slowly become more elliptical as it become dominated by the x_2 (perpendicular to the large scale bar) orbits inside the ILR. Eventually, due to mass concentration in the nucleus, both the nuclear and primary bars are dissolved.

If the variety of nuclear CO morphologies and ^{12}CO $J=3-2/J=2-1$ line ratios are caused by different evolutionary stages, then in this picture we might expect the oldest galaxies to have the lowest gas surface densities, as they have already

exhausted much of their gas content by the formation of stars or feeding of AGN. For NGC 5728, we see that the low gas mass corroborates the evolutionary hypothesis. Following the above arguments, NGC 2273, NGC 470, and perhaps NGC 4736 are predicted to be in the earliest stage of evolution and should show the most molecular gas according to the evolutionary scenario. In reality, these galaxies have gas surface densities that are lower than NGC 6951 and NGC 1097. The CO emission from both NGC 1097 and NGC 6951 originate near the rings of active star formation (Gerin, Combes, & Nakai 1988; Kohno, Kawabe, & Vila-Vilaró 1999), and it is possible that the star formation is heating or compressing the molecular gas, effecting its emissivity (Sakamoto 1996). A more detailed analysis of the impact of star formation on the properties of molecular clouds will help disentagle these potential ambiguities.

In summary, these CO line ratios combined with the star formation activity and high resolution CO morphology of these galaxies suggest that NGC 2273, NGC 470, and NGC 4736 may be in a earlier stage of evolution, where the nuclear molecular bar is still visible and star formation is just getting underway. NGC 1097 may be near the end stages of evolution, as suggested by the presence of the nuclear ring (Gerin, Combes, & Nakai 1988; Friedli & Martinet 1993). NGC 6951 has been undergoing star formation for a longer time, and the gas has been heated and the molecular bar has dissolved and the nuclear ring has become elliptical, resulting in the "twin peaked" morphology in the CO maps. NGC 5728 is nearly completely finished with its double bar phase and the molecular gas has lost its nuclear barred appearance, while the stars have not yet responded to the change in gravitational potential. A more detailed analysis of the star formation histories of these double barred galaxies will help clarify this picture of galaxy evolution among double barred galaxies.

4.4.3 Comparisons with Nuclear Activity and Main Bar Strength

The double barred model of Shlosman. Frank. & Begelman (1989) suggests that nuclear bars may be responsible for the feeding of both AGN and starburst activity. The factor that will determine whether an AGN or a starburst occurs is whether or not star formation occurs in the molecular gas as it flows into the nucleus through the nested set of bars. In order to test this hypothesis. we compare the CO line ratios with the nuclear activity.

We see no correlation between the ^{12}CO $J=3-2/J=2-1$ line ratio and nuclear activity. This suggests that the mechanisms responsible for determining if a galaxy becomes a Seyfert. LINER. or starburst are determined on size scales smaller than we can currently resolve the molecular gas. This is not surprising since our beam is $21''$ and the typical AGN is believed to be contained in a region smaller than 100 pc (Blandford et al. 1990). Conversely. this result also suggests that AGN and starburst activity have little effect on the molecular gas in the nuclear regions of galaxies. Unfortunately. with only one starburst galaxy in our sample. it is unlikely that we could see any convincing trends if they existed. We do note that the existence of star formation *and* Seyfert activity in galaxies with double bars (such as NGC 6951) tends to weaken the hypothesis of Shlosman. Frank. & Begelman (1989) that starbursts can prevent the formation of AGN in double barred galaxies. regardless of variations in molecular gas properties. It is possible that the star formation in the ring of NGC 6951 is not vigorous enough to prevent the molecular gas from flowing into the nucleus. where it can fuel the Seyfert 2 nucleus. The star formation rate in the ring of NGC 6951 is not high enough to be classified as a "starburst".

Even though all of the galaxies discussed here contain nuclear bars. our sample also includes a variety of morphological types. namely large scale bars of different strengths. For example. NGC 4736 is classified as an SA spiral galaxy in RC3 (de

Vaucouleurs et al. 1991), but recently has been found to contain a lenticular (or weak barred) appearance in the NIR images of Shaw et al. (1993). NGC 1097 and NGC 2273 on the other hand, contain very strong bar distortions and are classified as SB galaxies in RC3 (see Table 4.1 for the rest). Models and observations suggest that *large scale bars* alone are an excellent method of transporting molecular gas into the nuclei of galaxies. Observations suggests that there is an increase gas fraction in the nuclei of galaxies containing strong large scale bars (Sakamoto et al. 1999). Models suggest that stronger large scale bars create stronger galactic shocks and higher rates of inflow (Athanassoula 1992). This increase in inflow in strongly barred galaxies may manifest itself as an increased gas density in the nuclei of (strongly barred) SB galaxies compared to (weakly barred) SAB galaxies. An increased gas density could be reflected in a higher ^{12}CO $J=3-2/J=2-1$ line ratio. We see no correlation between CO $J=3-2/J=2-1$ line ratio and RC3 classification, suggesting that (at least on large scales) the large scale bar strength does not increase the density of the molecular gas in galaxies with stronger bars. We point out that bar classifications are taken from the RC3 catalogue (de Vaucouleurs et al. 1991) and may vary from wavelength to wavelength depending on the amount of dust obscuration in the nuclear regions and bars and are difficult to determine accurately. All of our galaxies appear barred or lenticular in the NIR images of Shaw et al. (1993), Mulchaey, Regan, & Kundu (1997), and Wozniak et al. (1995), which are less likely to be prone to extinction.

4.5 Molecular Gas Physical Conditions

All of these galaxies were chosen because the NIR images suggested the presence of a nuclear bar. The similarities in the NIR images suggest that the gravitational potentials are similar in these galaxies. The correlation between the ^{12}CO

$J=3-2/J=2-1$ line ratio and the CO morphology in the inner 21″ suggests that the molecular gas may have different physical conditions that allow different gas responses to similar gravitational potentials. In this section we will model the CO line ratios in an attempt to determine the true physical conditions of the molecular gas, such as excitation temperature, kinetic temperature, density, and column density.

Determining the physical conditions of molecular clouds in other galaxies can be very difficult. For single dish observations, the beam size is usually larger than the angular diameter of typical molecular clouds, and so the line strengths are beam-diluted. In addition, molecular clouds are known to be very clumpy (e.g. Stutzki & Güsten 1990) and the high resolution ^{12}CO $J=1-0$ maps of the galaxies in our sample show a variety of distributions within the inner 21″ (Kenney et al. 1992; Petitpas & Wilson 2001; Sakamoto et al. 1999), so the average emission likely originates in a mixture of high and low density material with different beam filling factors. In order to reduce the effects of beam dilution, we create beam matched integrated intensity line ratios which (assuming similar regions of the galaxy are responsible for the emission in both transitions) will help eliminate the unknown filling factor from the analysis.

In §4.5.1 we will analyze the line ratios under the Local Thermodynamic Equilibrium approximation. In this model (in addition to the unknown filling factor, f_ν), assumptions have to made about the optical depth of the emission lines. In §4.5.2 we will analyze the line ratios under the Large Velocity Gradient (LVG) assumption which is more complicated, but does not require any assumption regarding optical depths.

Calibration differences between different telescopes can introduce (often large) uncertainties in spectral line ratios (see discussion in Tilanus et al. 1991, for example). To prevent the introduction of such uncertainties, we will limit our analysis

in §4.5.1 to the interpretation of only those CO line ratios taken with the JCMT.
namely $^{13}CO/^{12}CO$ $J=2-1$ and ^{12}CO $J=3-2/J=2-1$. In the LVG approxima-
tion, we will need more than two CO line ratios to place strong constraints on the
molecular gas conditions, so in §4.5.2 we will use all of the line ratios listed in Table
4.3.

4.5.1 LTE Analysis

In the Local Thermodynamic Equilibrium (LTE) approximation, we assume
that the gas is collisionally dominated and hence the relative populations between
molecular energy levels are a function of a single temperature. The definition of LTE
is that the kinetic temperature (T_K) of the gas is equal to the excitation temperature
(T_{ex}). In this approximation, the brightness of an object at a given temperature
$(T = T_{ex} = T_K)$ and frequency (ν) is given by Planck's law, namely

$$B_\nu(T) = \frac{2h\nu^3}{c^2} \frac{1}{e^{h\nu/kT} - 1} \equiv \frac{2\nu^2 k}{c^2} J_\nu(T)$$ (4.2)

where c, h, and k are the speed of light, Planck and Boltzmann's constants, respec-
tively. The effective source radiation temperature (T_R) is defined as the temperature
that would be observed with a radio telescope having a perfect surface (no losses),
above the atmosphere, with an infinitesimally small beam (Kutner & Ulich 1981).
The radiation temperature can be written as follows

$$T_R = f_\nu \left[J_\nu(T_{ex}) - J_\nu(T_{bg})\right](1 - e^{-\tau})$$ (4.3)

where T_{bg} is the 2.7 K background temperature, f_ν is the unknown filling factor of
the emitting region within the beam as discussed above, and τ is the optical depth
of the emitting region.

There are generally three basic limits with which we are concerned: both lines are optically thick ($\tau \gg 1$): both lines are optically thin ($\tau \ll 1$): and the case where one line is optically thick and the other is optically thin. In the first case. the integrated intensity line ratio (e.g. ^{12}CO $J=3-2/J=2-1$) can be written

$$R^{\text{thick}}_{32/21} = \frac{[J_\nu(T_{32}) - J_\nu(T_{\text{bg}})]}{[J_\nu(T_{21}) - J_\nu(T_{\text{bg}})]} \tag{4.4}$$

which in LTE ($T_{32} = T_{21} = T_{\text{K}} = T_{\text{ex}} = T$) is just a weak function of frequency (contained in the definition of $J_\nu(T)$ and gives $R^{\text{thick}}_{32/21} \approx 1$ for $T > 30$K (see Figure 4.16). Note that we have assumed $f_{32} = f_{21}$. For the second case ($\tau \ll 1$) the integrated intensity line ratio can be expressed

$$R^{\text{thin}}_{32/21} = \frac{[J_\nu(T_{32}) - J_\nu(T_{\text{bg}})]\tau_{32}}{[J_\nu(T_{21}) - J_\nu(T_{\text{bg}})]\tau_{21}}. \tag{4.5}$$

which in LTE depends on frequency (as above) and τ_ν. The ratio of τ's can be expressed as a function of J. ν. CO-specific constants. and the Boltzmann equation (see for example Scheffler & Elsaesser 1987). In the third case. we compare integrated intensity line ratios for different isotopomers of CO in the same J transition (e.g. ^{13}CO/^{12}CO $J=2-1$). If we assume $T^{13\text{CO}}_{ex} = T^{12\text{CO}}_{ex}$ and that ^{12}CO $J=2-1$ is optically thick and ^{13}CO $J=2-1$ is optically thin. we have

$$R_{12/13} \approx \frac{X}{\tau(^{12}\text{CO})} \tag{4.6}$$

where X is the ^{12}CO/^{13}CO abundance ratio (which is measured to be 43-62 in the Milky Way: Hawkins & Jura 1987: Langer & Penzias 1993).

Plots of integrated intensity line ratio as a function of excitation temperature for the optically thick and thin cases are given in Figure 4.16. The excitation temperatures derived from the ^{12}CO $J=3-2/J=2-1$ line ratio are summarized in Table 4.5. We have also included the dust temperature derived from the IRAS 60

Table 4.5: LTE Parameters and Dust Temperatures

Galaxy	$T_{ex}^{J=3-2}$ (thin)	$T_{ex}^{J=3-2}$ (thick)	τ_{21}	f_{60}/f_{100}	T_{dust} ($\beta = 2.1$)	Refs.
NGC 0470	15 K	38 K	3.9	0.51	30. 37 K	1
NGC 1097	16 K	66 K	5.6	0.52	30. 36 K	1
NGC 2273	12 K	11 K	4.7	0.60	31. 38 K	1
NGC 3081	18 K	> 150 K	...	...	...	
NGC 4736	11 K	8 K	4.2	0.57	31. 37 K	2
NGC 5728	23 K	...	< 3.9	0.60	31. 38 K	2
NGC 6951	24 K	...	5.6	0.35	26. 31 K	1

For the optically thick columns. we assumed the -1σ limit for line ratios that were consistent with 1. The missing entries indicated that the line ratios were not consistent with optically thick emission within the uncertainties. For τ we assume a $^{12}CO/^{13}CO$ abundance ratio of 43 (Hawkins & Jura 1987). For T_{dust} the two values represent a dust emissivity (β) of 2 or 1 respectively.

(1) Moshir (1990): (2) Soifer et al. (1989)

μm and 100 μm fluxes assuming different dust emissivities. The f_{60}/f_{100} ratio as a function of dust temperature is shown in Figure 4.17.

The $^{12}CO/^{13}CO$ $J=2-1$ line ratio is uniform at the 2σ level over all galaxies and has an average value of 0.11. Assuming optically thick ^{12}CO. optically thin ^{13}CO. and the molecular gas in LTE. the $^{13}CO/^{12}CO$ $J=2-1$ line ratio suggests that the ^{12}CO optical depth in all six galaxies is consistent with $\tau \approx 5$. This suggests that the molecular gas is on the border between optically thin and optically thick (but marginally optically thick) in all of our galaxies. This is confirmed by the ^{12}CO $J=3-2/J=2-1$ ratios which (for the most part) are near 1 within the uncertainties.

The ^{12}CO $J=3-2/J=2-1$ line ratio suggests typical excitation temperatures that range from 11 to 24 K for optically thin emission (or 8 to 66 K if the emission is optically thick). There is no obvious correlation between excitation temperatures and dust temperature. suggesting that the gas and dust can exist at different temperatures (see §4.4.1 for further discussion without LTE assumptions). Also, there
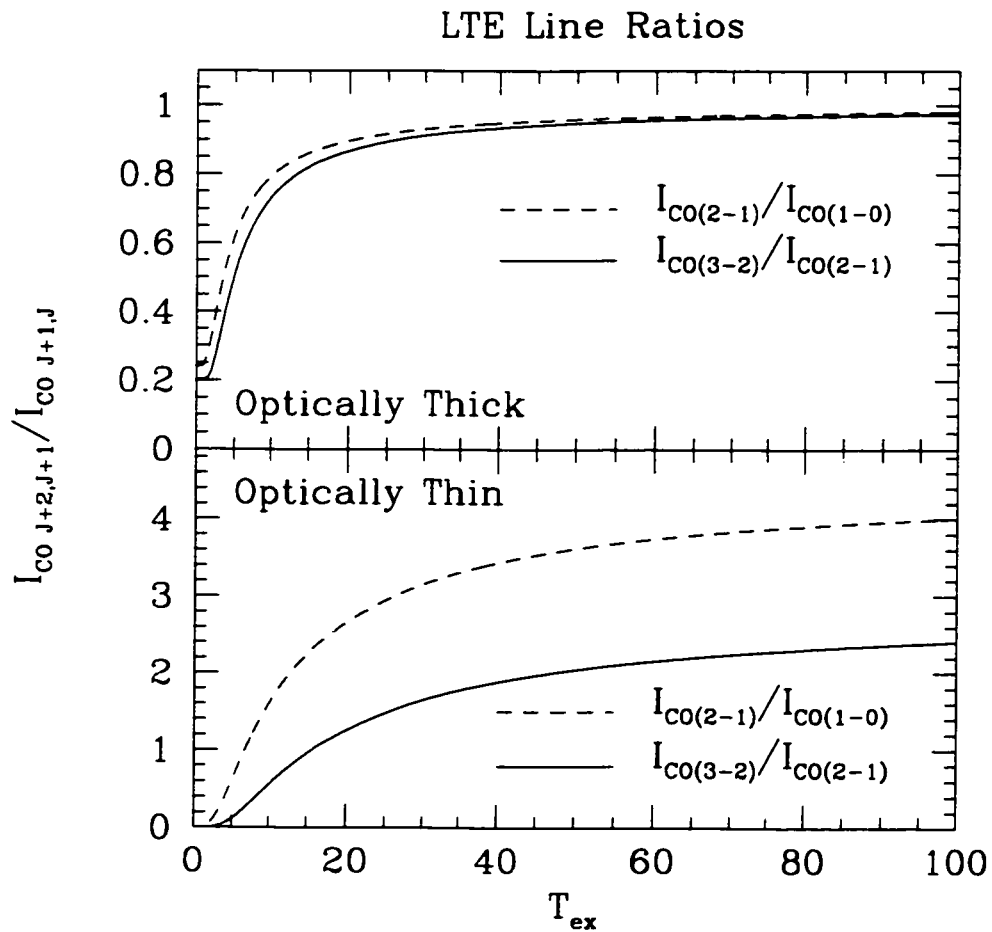
Figure 4.16: ^{12}CO $J=3-2/J=2-1$ CO Line Ratios in LTE Approximation
Plots of ^{12}CO integrated intensity line ratio as a function of excitation temperature
in the LTE approximation.

IRAS Flux Ratios
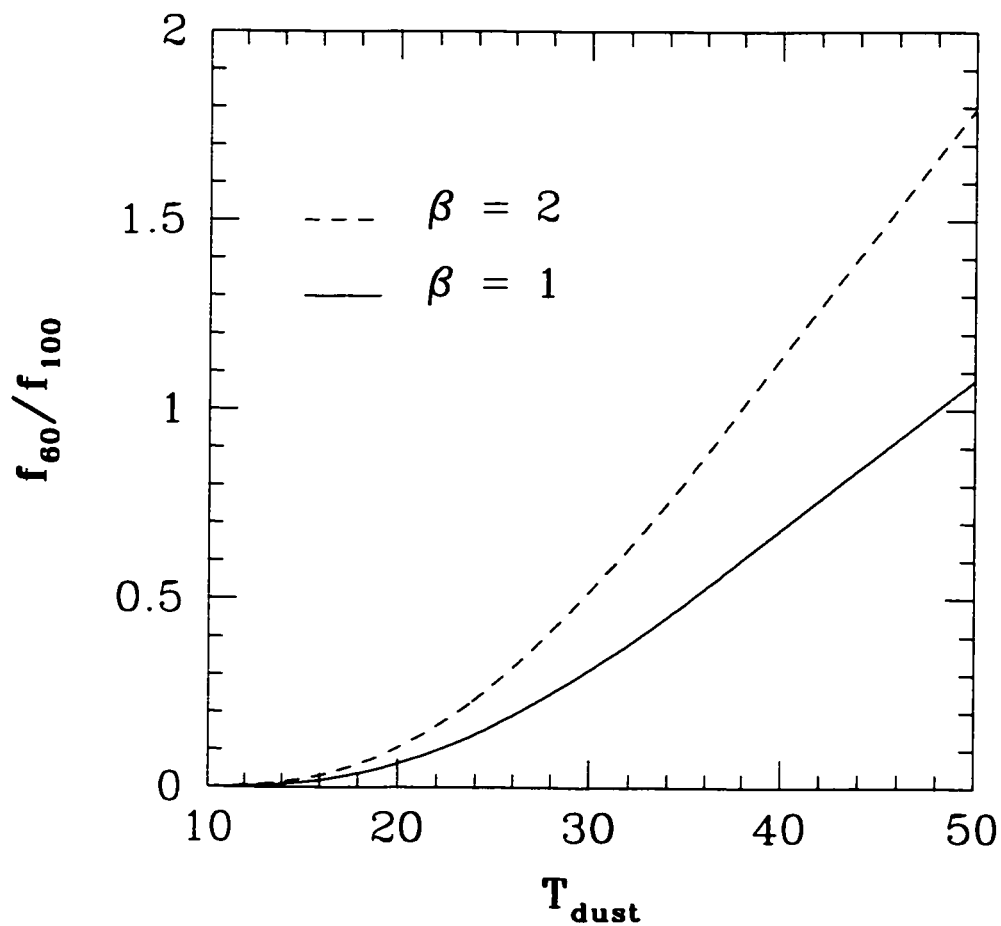
Figure 4.17: IRAS Flux Ratio as a Function of Dust Temperature

The IRAS 60 μm and 100 μm flux ratio as a function of dust temperature for a dust emissivity (β) of 1 and 2.

are no correlations between excitation temperatures and nuclear activity or nuclear CO morphology, as discussed in §4.4.2.

Comparing Tables 4.3 and 4.5 we can see that there are no correlations between dust temperatures and nuclear activity or CO morphology. One obvious reason for this is the similarities in the f_{60}/f_{100} ratios of the galaxies in our sample. It is surprisingly uniform within our sample with a mean value of 0.53 ± 0.04. which allows for a temperature range of only 5 to 7 K (depending on β). This f_{60}/f_{100} ratio for our sample of galaxies is higher than the average of the barred galaxies sample in Braine & Combes (1992). They find that the average f_{60}/f_{100} ratio for barred galaxies (SB) is 0.39 ± 0.04. and the average for intermediate barred galaxies (SAB) is 0.37 ± 0.03. Regardless of how you classify the galaxies. we find that on average the double barred galaxies in our sample have higher dust temperatures than those of the CO survey of Braine & Combes 1992 as discussed in §4.4.1.

4.5.2 LVG Analysis

The basic simplifying assumption in the Large Velocity Gradient (LVG) approximation is that there are velocity gradients in the gas that Doppler shift the emission so that it is the wrong frequency to be re-absorbed locally by the nearby gas in the molecular clouds. Thus. rather than solving the equations of radiative transfer over an entire molecular cloud (or cloud ensemble). you are only solving the equations locally. This makes the radiative transfer equations more tractable. but for observations of different isotopomers of CO such as (^{13}CO or $C^{18}O$) you still need to make assumptions regarding the abundance ratios of these molecules relative to ^{12}CO. Another free parameter is the velocity gradient. but this can be estimated from the line width of the CO emission lines. This leaves a 3D parameter space with axes of CO column density. molecular hydrogen density. and kinetic temperature to be ex-

plored. Naturally, the more spectral lines you observe, the stronger the constraints you can place of the temperature and density of the gas. The interested reader is referred to more complete descriptions by Goldreich & Kwan (1974) and Scoville & Solomon (1974).

We have performed a LVG analysis using a code written by Lee Mundy and implemented as part of the MIRIAD data reduction package. A sample of the output from the models is shown in Figure 4.18. The integrated intensity line ratios are shown as bands that indicate the $\pm 30\%$ upper and lower limits of the line ratios. We adopt 30% to account for the uncertainties involved in spectral line calibration and baseline removal as well as, in the case of the ^{12}CO $J=2-1/J=1-0$ ratio, the uncertainties involved in combining spectral lines from different telescopes. Solutions are indicated by the locations where the regions of the different ratio boundaries overlap. In many cases, the ^{12}CO $J=3-2/J=2-1$ line ratio only one of the contours are visible on the plot, so arrows indicate the allowed regions. A grayscale representation of the ^{12}CO $J=3-2/J=2-1$ is included to aid interpretation of this figure. A single component model provided an adequate fit to the observed line ratios.

There are four main variables in the LVG models: CO column density per unit velocity ($N(CO)/dv$), molecular hydrogen density ($n(H_2)$), kinetic temperature (T_{kin}), and the $^{12}CO/^{13}CO$ abundance ratio ($[^{12}CO]/[^{13}CO]$). With only three line ratios, we cannot place very strong constraints on the molecular gas physical conditions. We have performed a study of parameter space ranging from $15 <$ log $N(CO)/dv$ (cm^{-2}/km s^{-1}) < 21. $1 <$ log $n(H_2)$ (cm^{-3}) < 6. $30 < [^{12}CO]/[^{13}CO]$ < 70. and 30 K $< T_{kin} < 100$ K. In general, solutions were found for all temperatures and abundance ratios. Variations in the $[^{12}CO]/[^{13}CO]$ ratio made negligible changes to the solution compared to kinetic temperature. For this reason, we adopt

Table 4.6: LVG Solutions for a Kinetic Temperature of 30 K

Galaxy	log N(CO)/dv	log n(H_2)	τ_{10}	τ_{21}	τ_{32}
NGC 0470	16.8 ± 0.3	> 3.7	< 1.6	< 5.4	< 7.4
NGC 1097	17.0 ± 0.1	> 4.5	< 2.3	< 7.2	< 10
NGC 2273	18.0 ± 1.1	unbounded	< 64	< 190	< 190
NGC 4736	17.0 ± 0.1	3.1 ± 0.3	4.9	14	19
NGC 5728	< 16.7	> 3.7	< 1.7	< 5.4	< 7.4
NGC 6951	18.0 ± 0.2	2.0 ± 0.3	47	164	190

[^{12}CO]/[^{13}CO] = 50. consistent with the value obtained for the Milky Way (Hawkins & Jura 1987; Langer & Penzias 1993). The derived values from the LVG analysis are summarized in Table 4.6. For the purpose of clarity. we show results for only $T_{kin} = 30$ K.

In many cases we can only determine lower limits to the molecular hydrogen density. and thus we have upper limits on the optical depth. It is interesting that all galaxies except NGC 6951 have rather similar column densities of CO per unit velocity (within the uncertainty). They are generally all $\sim 10^{17}$ cm^{-2}(km s^{-1})$^{-1}$. If we wish to convert this to a true column density of CO. we must multiply by the velocity width of a typical molecular cloud in each galaxy. Unfortunately. the large beam of the JCMT covers many individual clouds in these distant galaxies in a single pointing. so the line width of individual clouds is difficult to determine. In the nearest galaxy in our sample (NGC 4736) our single dish CO spectra shows emission features (e.g. $V_{LSR} = 225$ km s^{-1}: Figure 4.5) with line widths of ~ 50 km s^{-1}. High resolution ^{12}CO J=1–0 maps of these galaxies indicate line widths of $\sim$30-50 km s^{-1}(Kohno. Kawabe. & Vila-Vilaró 1999). Even these are still prone to the effects of galaxy rotation. For consistency. we will assume that individual clouds in all galaxies have similar CO line widths of 10 km s^{-1}. similar to the Milky Way.
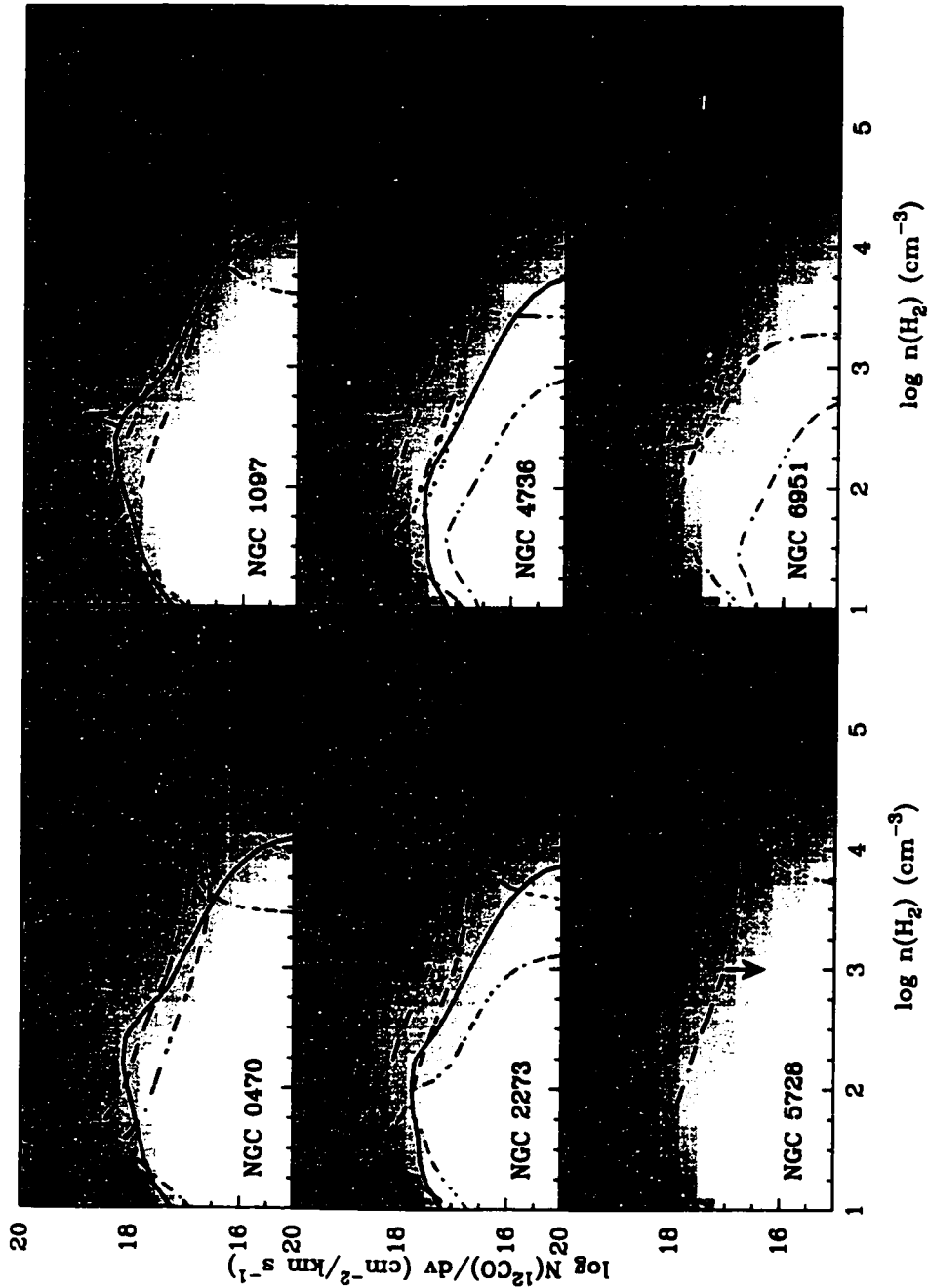
Figure 4.18: LVG Plots for Kinetic Temperature of 30 K

Plots of CO column density (per unit velocity) versus H_2 density for a kinetic temperature of 50 K and a $^{12}CO/^{13}CO$ abundance ratio of 50. The contours represent the $\pm$ 30% contours for the CO line ratios given in Table 4.3 and are indicated in the lower left panel. For NGC 4736 we have included the $^{12}CO/^{13}CO$ $J=1-0$ ratio of Sage & Isbell (1991). Solutions appear as regions where all line ratios overlap.

Adopting a line width of 10 km s^{-1}gives CO column densities of 10^{18} cm^{-3} for most of the galaxies in our sample. In order for star formation to occur, it is believed that the molecular gas must have exceed some critical column density. This value is believed to be on the order of 10^{22} cm^{-3} (Solomon et al. 1987; Elmegreen 1989). Assuming a number density ratio of $n(CO)/n(H_2) = 10^{-4}$ (Genzel 1992) we find a column density of molecular hydrogen of 10^{22} cm^{-3}. The molecular hydrogen column densities for the galaxies in our sample suggests that the molecular gas in these double barred galaxies may be on the verge of collapse. It is possible that this is the reason why we see such a high level of nuclear activity.

Only NGC 6951 has CO column densities per unit velocity that are higher than 10^{17} cm^{-3}(km s^{-1})$^{-1}$ within the uncertainties. Assuming similar line widths, we obtain hydrogen column densities of 10^{23} cm^{-3}, which is higher than the critical value proposed by Solomon, Rivolo, Barrett, & Yahil (1987) and Elmegreen (1989). NGC 6951 has regions of circumnuclear star formation in close proximity to the twin peaks of CO seen in the maps of Kohno, Kawabe, & Vila-Vilaró (1999). The high density of molecular gas may be the result of gas compression caused by the nearby star forming regions.

The similarity in CO column densities results in a similarity of optical depths in the LVG analysis. The model suggests optical depths of $\sim$ 2 to 10 (excluding NGC 2273 which is poorly constrained and NGC 6951 which is unusually high). These optical depths are in excellent agreement with the LTE models discussed in §4.5.1. This shows that the molecular gas in these galaxies is marginally optically thick in ^{12}CO emission.

4.6 Summary

We have taken ^{12}CO J=3–2, ^{13}CO J=3–2, and ^{12}CO J=3–2 spectra of the inner 21″ of a sample of galaxies that show a double barred nucleus in the near infrared. We find that that ^{12}CO/^{13}CO J=2−1 integrated intensity line ratio is uniform at the 2σ level while the ^{12}CO J=3−2/J=2−1 line ratio varies dramatically from galaxy to galaxy.

We find that the CO J=3−2/J=2−1 line ratio is higher in galaxies with non-centralized CO distributions and lower in galaxies that contain nuclear molecular bars and central peaks. Assuming the molecular gas is thermalized, this result suggests that the molecular gas is cooler in galaxies that contain molecular bars, which may enable them to clump more efficiently and form the more centrally concentrated condensations.

Under the Local Thermodynamic Equilibrium approximation, the uniform ^{12}CO/^{13}CO J=2−1 line ratios suggest that the molecular gas is marginally optically thick, with $\tau \sim 5$ in all galaxies. With the similarity in optical depths, the variation in the ^{12}CO J=3−2/J=2−1 line ratio suggests that the molecular gas is warmer in galaxies without nuclear bars.

Under the Large Velocity Gradient approximation, modeling the CO line ratios suggests that all galaxies (except NGC 6951) have similar CO column densities per unit velocity of $\sim 10^{17}$ cm^{-2}/km s^{-1}. This similarity in column density translates again into a similarity in optical depth of $\sim$2-10, confirming the results of the LTE analysis. NGC 6951 shows much higher column densities per unit velocity than the other galaxies ($\sim 10^{18}$ cm^{-2}/km s^{-1}) and may be the cause of the star formation that is occurring in the nuclear ring where we detect the strongest CO emission.

We find no correlation between molecular gas properties and nuclear activity (e.g. Seyfert, starburst, LINER) which suggests that the processes that determine which form of activity a galaxy nuclei takes on is determined on size scales smaller than we can resolve with a 21″ beam. We also find no correlations between molecular gas temperatures and dust temperatures, in agreement with the findings of Mauersberger et al. (1999).

Bibliography

Aalto. S.. Booth. R. S.. Black. J. H.. & Johansson. L. E. B.. 1995. *A&A* **300**. 369.

Aalto. S.. Johansson. L. E. B.. Booth. R. S.. & Black. J. H.. 1991. *A&A* **249**. 323.

Athanassoula. E.. 1992. *MNRAS* **259**. 345.

Barth. A. J.. Ho. L. C.. Filippenko. A. V.. & Sargent. W. L.. 1995. *AJ* **110**. 1009.

Blandford. R. D.. Netzer. H.. Woltjer. L.. Courvoisier. T.. & Mayor. M.. 1990. *Active galactic nuclei*. Berlin : New York : Springer-Verlag. c1990.

Braine. J. & Combes. F.. 1992. *A&A* **264**. 433.

Casoli. F.. Dupraz. C.. & Combes. F.. 1992. *A&A* **264**. 55.

Combes. F.. 1994. Nuclear gas flows in barred galaxies. In *Mass Transfer Induced Activity in Galaxies*. pp. 170. ed. I. Shlosman. Cambridge Univ. Press.

Combes. F. & Gerin. M.. 1985. *A&A* **150**. 327.

de Vaucouleurs. G.. de Vaucouleurs. A.. Corwin. H. G.. Buta. R. J.. Paturel. G.. & Fouque. P.. 1991. *Third Reference Catalogue of Bright Galaxies*. Volume 1-3. XII. 2069 pp. 7 figs.. Springer-Verlag Berlin Heidelberg New York.

Elmegreen. B. G.. 1989. *ApJ* **338**. 178.

Encrenaz. P. J.. Stark. A. A.. Combes. F.. & Wilson. R. W.. 1979. *A&A* **78**. L1.

Friedli. D. & Martinet. L.. 1993. *A&A* **277**. 27.

Genzel. R.. 1992. The galactic interstellar medium. In W. B. Burton. B. G. Elmegreen. & R. Genzel (Eds.). *The galactic interstellar medium Springer-Verlag. 412 p.*

Gerin. M.. Casoli. F.. & Combes. F.. 1991. *A&A* **251**. 32.

Gerin. M.. Combes. F.. & Nakai. N.. 1988. *A&A* **203**. 44.

Goldreich. P. & Kwan. J.. 1974. *ApJ* **189**. 441.

Hawkins. I. & Jura. M.. 1987. *ApJ* **317**. 926.

Jogee. S.. 1998. *Molecular Gas and Starbursts in the Circumnuclear Regions of Spiral Galaxies.* Ph.D. Thesis. Yale University.

Kenney. J. D. P.. Wilson. C. D.. Scoville. N. Z.. Devereux. N. A.. & Young. J. S.. 1992. *ApJL* **395**. L7.

Kinney. A. L.. Bohlin. R. C.. Calzetti. D.. Panagia. N.. & Wyse. R. F. G.. 1993. *ApJSS* **86**. 5.

Kohno. K.. Kawabe. R.. & Vila-Vilaró. B.. 1999. *ApJ* **511**. 157.

Kraus. J. D.. 1986. *Radio astronomy.* Powell. Ohio: Cygnus-Quasar Books. 1986.

Kruegel. E.. Chini. R.. & Steppe. H.. 1990. *A&A* **229**. 17.

Kutner. M. L. & Ulich. B. L.. 1981. *ApJ* **250**. 341.

Langer. W. D. & Penzias. A. A.. 1993. *ApJ* **408**. 539.

Mauersberger. R.. Henkel. C.. Walsh. W.. & Schulz. A.. 1999. *A&A* **341**. 256.

Moshir. M. E. A.. 1990. Iras faint source catalogue. version 2.0. In *IRAS Faint Source Catalogue. version 2.0 (1990).*

Mulchaey. J. S.. Regan. M. W.. & Kundu. A.. 1997. *ApJSS* **110**. 299.

Ondrechen. M. P.. van der Hulst. J. M.. & Hummel. E.. 1989. *ApJ* **342**. 39.

Petitpas. G. R. & Wilson. C. D.. 2001. *ApJ submitted.* .

Phillips. M. M.. Charles. P. A.. & Baldwin. J. A.. 1983. *ApJ* **266**. 485.

Sage. L. J. & Isbell. D. W.. 1991. *A&A* **247**. 320.

Sakamoto. K.. Okumura. S. K.. Ishizuki. S.. & Scoville. N. Z.. 1999. *ApJ* **525**. 691.

Sakamoto. S.. 1996. *ApJ* **462**. 215.

Scheffler. H. & Elsaesser. H.. 1987. *Physics of the galaxy and interstellar matter.* Berlin and New York. Springer-Verlag. 1987. 503 p. Translation.

Scoville. N. Z. & Sanders. D. B.. 1987. H2 in the galaxy. In *ASSL Vol. 134: Interstellar Processes.* pp. 21.

Scoville. N. Z. & Solomon. P. M.. 1974. *ApJ* **187**. L67.

Shaw. M. A.. Combes. F.. Axon. D. J.. & Wright. G. S.. 1993. *A&A* **273**. 31.

Shlosman. I.. Frank. J.. & Begelman. M. C.. 1989. *Nature* **338**. 45.

Sofue. Y.. Wakamatsu. K.. Taniguchi. Y.. & Nakai. N.. 1993. *PASJ* **45**. 43.

Soifer. B. T.. Boehmer. L.. Neugebauer. G.. & Sanders. D. B.. 1989. *AJ* **98**. 766.

Solomon. P. M.. Rivolo. A. R.. Barrett. J.. & Yahil. A.. 1987. *ApJ* **319**. 730.

Strong. A. W.. Bloemen. J. B. G. M.. Dame. T. M.. Grenier. I. A.. Hermsen. W.. Lebrun. F.. Nyman. L. .. Pollock. A. M. T.. & Thaddeus. P.. 1988. *A&A* **207**. 1.

Stutzki. J. & Güsten. R.. 1990. *ApJ* **356**. 513.

Tilanus. R. P. J.. Tacconi. L. J.. Sutton. E. C.. Zhou. S.. Sanders. D. B.. Wynn-Williams. C. G.. Lo. K. Y.. & Stephens. S. A.. 1991. *ApJ* **376**. 500.

Vila-Vilaró. B.. Taniguchi. Y.. & Nakai. N.. 1998. *AJ* **116**. 1553.

Wilson. C. D.. 1995. *ApJL* **448**. L97.

Wilson. C. D. & Scoville. N.. 1990. *ApJ* **363**. 435.

Wong. T. & Blitz. L.. 2000. *ApJ* **540**. 771.

Wozniak. H.. Friedli. D.. Martinet. L.. Martin. P.. & Bratschi. P.. 1995.
A&AS **111**. 115.

Yankulova. I. M.. 1999. *A&A* **344**. 36.

Young. J. S. & Sanders. D. B.. 1986. *ApJ* **302**. 680.

Chapter 5

Molecular Gas in Double Barred Galaxies III. A Lack of CO Emission?

Draft of a paper that will be submitted to the Astrophysical Journal

Abstract

Nuclear bars in barred galaxies have been proposed as a mechanism for transporting molecular gas interior to Inner Linblad Resonances where it may fuel a variety of nuclear activity. Models of these galaxies suggest that the molecular gas component is crucial for maintaining long-lived nuclear bars, and the resulting gas morphology can reveal important information regarding properties such as main bar pattern speed and the location of resonances that are not directly observable. We have undertaken a CO survey in an attempt to locate double barred galaxies that have strong CO emission that could be candidates for high resolution mapping. We observed ten galaxies in CO $J=2-1$ and $J=3-2$ and do not detect any new galaxies that have not already been detected in previous CO surveys. We preferentially detect emission from galaxies containing some form of nuclear activity. Simulations of these galaxies require that they contain 2 to 10% gas by mass in order to maintain long-lived nuclear bars. The fluxes for the galaxies for which we have detections suggest that the gas mass fraction is in agreement with these models requirements. The lack of emission in the other galaxies suggests that they contain as little as a few $\times 10^6$ $M_\odot$ of molecular material which corresponds to at least $\sim 0.1\%$ gas by

mass. This result suggests that the models may be underestimating the dissipative properties of the molecular gas.

keywords: Galaxies: starburst – galaxies: active

5.1 Introduction

Recent near infrared (NIR) surveys reveal isophote twists in the central regions of barred galaxies which are thought to be the signature of a bar within a bar (e.g. Mulchaey. Regan. & Kundu 1997). Recent models of double barred galaxies have had success in reproducing relatively long lived nuclear features that can explain these isophote twists. Shaw et al. (1993) model galaxies as collisionless stars and dissipative gas clouds and find that the NIR isophote twists are caused by viscous and gravitational torques that drag the nuclear regions of the main bar out of alignment with the rest of the bar. Friedli & Martinet (1993) suggest that the NIR isophote twists are the result of a kinematically distinct nuclear bar that can rotate with up to six times the pattern speed of the large scale bar. The one thing these two models have in common is the need for dissipation: both groups must include substantial amounts of molecular gas for the models to be able to reproduce the observed features. To date. the best observational test of how accurately these models are taking into account the gaseous component is the assumed gas mass to total mass ratio (usually adopted as 5 to 10%. in agreement with observations of regular disk galaxies: Young & Devereux 1991). The models of barred galaxies containing a gaseous component by Combes & Gerin (1985). Shaw et al. (1993). and Friedli & Martinet (1993) produce nuclear morphologies very different than the purely stellar models. In fact. Combes (1994) find the simulations exhibit different results by simply changing only the *viscosity* of the gas. Thus. detailed observations

of the molecular gas morphologies and physical conditions will make an excellent probe of the accuracy of these models.

In Paper I (Petitpas & Wilson 2001a) we used high resolution CO observations to search for the molecular gas components of these galaxies that the models of Friedli & Martinet (1993) and Shaw et al. (1993) require to be present. We found that in NGC 2273 the molecular gas emission takes the form of a nuclear bar that is aligned with the NIR isophote twists. In NGC 5728. we observed a rather disorderly molecular gas morphology that did not align with the NIR morphology. nor did it align with any features seen at other wavelengths in the nuclei of this galaxy. When comparing the CO maps of NGC 2273. NGC 5728 and other double barred galaxies with their star formation activity. we found evidence that the galaxies with nuclear CO bars may represent younger stages of barred galaxy evolution. The central concentrations of molecular gas may be exhausted and/or dispersed by vigorous star formation in the nuclei of the older double barred galaxies. which results in their more disordered appearance.

The similarity in the NIR images of these galaxies suggests that the galactic potentials may be similar. The variety of molecular gas morphologies suggests that the molecular gas may have different properties in each galaxy allowing it to respond differently to these similar potentials. In Paper II (Petitpas & Wilson 2001b). we performed a multi-transition CO survey of the nuclei of double barred galaxies for which high resolution CO maps exist. We found that the molecular gas was cooler in galaxies with more centrally concentrated gas distributions (i.e. nuclear molecular bars) and warmer in galaxies where the CO was scattered about the nucleus. When comparing this result with the evolutionary hypothesis of Paper I. we believe that the molecular gas has been heated by the past star formation. perhaps reducing its viscosity and resulting in a highly dispersed morphology.

The seven galaxies discussed in Papers I and II represent a small fraction of the total number of galaxies known to have nuclear bars (as indicated by NIR isophote twists). In order to strengthen the hypotheses of those papers, we need to study a larger sample of galaxies. Of the 93 galaxies studied by Jarvis et al. (1988). Shaw et al. (1993). Wozniak et al. (1995). Elmegreen et al. (1996). Mulchaey. Regan. & Kundu (1997). only 23 contain isophote twists on scales large enough to be resolved by the Caltech Millimeter and BIMA Arrays. Since the larger NIR surveys mentioned above were performed using southern observatories (i.e. La Silla. Chile). most of the candidates are located in the southern hemisphere. Of those 23 galaxies with resolvable bars. only 13 are at a declination > −30°. Six of these (NGC 470. NGC 2273. NGC 4736. NGC 5850. NGC 5728. and NGC 6951) have high resolution CO maps published or soon to be published (Jogee 1998: Petitpas & Wilson 2001a: Wong & Blitz 2000: Leon. Combes. & Friedli 2000: Kohno. Kawabe. & Vila-Vilaró 1999).

We have performed a CO survey of the nuclei of 10 galaxies known to have strong NIR isophote twists in an attempt to find CO-bright double barred galaxies that would make good candidates for high resolution CO mapping. Five of these galaxies (NGC 2273. NGC 3081. NGC 4736. NGC 5728. and NGC 6951) are discussed in detail in papers I and II. In §5.2 we discuss the observations and data reduction techniques. In §5.3 we discuss our detections (and non-detections) in more detail, and compare our observations to previous studies of these galaxies. We also determine the molecular gas masses, and discuss the implications of these masses to the double barred galaxy models. This work is summarized in §5.4.

5.2 Observations and Data Reduction

5.2.1 NRAO Spectra

The nuclei of nine double barred galaxies were observed in ^{12}CO $J=2-1$ using the National Radio Astronomy Observatory (NRAO)[1] 12-m Telescope. Observations were taken in remote observing mode over a 14 hour period on 15 February, 2000. The half-power beamwidth of the NRAO 12-m was $29''$ at 230 GHz (^{12}CO $J=2-1$). All observations were taken in 2IF mode with the Millimeter AutoCorrelator (MAC). The pointing was found to be accurate to $6''$ for the first half of the evening when we observed our galaxies with NGC < 4736. This is poorer than the normal value for the NRAO 12-m, likely due to the high winds. In the second half of the evening the winds diminished, and the pointing improved to the more normal value of $5''$ for observations of galaxies with NGC ≥ 4736. The calibration was also monitored by observing spectral line calibrators and planets and the spectral line calibrators agreed with the published values. Thus, we adopt the normal main beam efficiency from the NRAO Users Guide of 0.29 at 230 GHz.

5.2.2 JCMT Spectra

Previous CO studies of double barred galaxies show CO $J=3-2/J=2-1$ line ratios $\gtrsim 1$ (Petitpas & Wilson 2001b) so for galaxies that were not detected with the NRAO, we obtained higher resolution ^{12}CO $J=2-1$ and ^{12}CO $J=3-2$ spectra using the James Clerk Maxwell Telescope (JCMT)[2]. These observations were taken over

---

[1] The National Radio Astronomy Observatory (NRAO) is a facility of the National Science Foundation operated under cooperative agreement by Associated Universities, Inc.

[2] The JCMT is operated by the Joint Astronomy Centre in Hilo, Hawaii on behalf of the parent organizations Particle Physics and Astronomy Research Council in the United

Table 5.1: Observing Parameters

Galaxy	α (2000)	δ (2000)	V_{lsr} (km s^{-1})	Line (^{12}CO)	Tele.	$t_{int.}$ (h:m)	T_{sys} (K)	r.m.s. (mK)
NGC 2273	6:50:09.8	60:50:48.9	1870	J=2$-$1	NRAO	1:46	516	5
NGC 2859	9:24:19.5	34:30:42.5	1687	J=2$-$1	NRAO	1:58	467	4
NGC 2859	...	...	1687	J=3$-$2	JCMT	2:20	630	4
NGC 2950	9:42:35.1	58:51:05.0	1337	J=2$-$1	JCMT	0:30	254	4
NGC 3081	9:59:30.6	-22:49:40.7	2385	J=2$-$1	NRAO	2:09	1012	8
NGC 4340	12:23:35.8	16:43:16.4	950	J=2$-$1	NRAO	1:58	199	4
NGC 4340	...	...	950	J=3$-$2	JCMT	2:00	485	3
NGC 4371	12:24:55.5	11:42:10.0	943	J=2$-$1	NRAO	1:58	511	4
NGC 4371	...	...	943	J=3$-$2	JCMT	2:00	503	3
NGC 4736	12:50:53.4	41:07:02.1	308	J=2$-$1	NRAO	0:35	468	7
NGC 5728	14:42:23.8	-17:15:02.6	2788	J=2$-$1	NRAO	1:58	605	5
NGC 5850	15:07:07.5	1:32:42.7	2556	J=2$-$1	NRAO	1:58	453	4
NGC 6951	20:37:11.6	66:06:11.6	1424	J=2$-$1	NRAO	3:20	424	3

The beam size for the NRAO 12-m at CO J=2$-$1 is 29″. The beam size for the JCMT is 21″ at CO J=2$-$1 and 14″ at J=3$-$2.

the period of 1999 - 2000, mostly as part of bad weather backup projects. The half-power beamwidth of the JCMT is 21″ at 230 GHz (^{12}CO J=2$-$1) and 14″ at 345 GHz (^{12}CO J=3$-$2). All observations were obtained using the Digital Autocorrelation Spectrometer. The calibration was monitored by frequently observing spectral line calibrators. The spectral line calibrators showed very little scatter from the published values with individual measurements differing by typically $< 15\%$ from standard spectra. Thus, we adopt the normal main beam efficiencies from the JCMT Users Guide of 0.69 at 230/220 GHz and 0.63 at 345 GHz. A detailed observing summary for the JCMT and NRAO observations is given in Table 5.1.

5.2.3 Reduction

Similar data sets were averaged together using the software package SPECX for the JCMT data and the Bell Labs data reduction package COMB for the NRAO data. The data were binned to 10 km s^{-1} resolution (13.0 and 8.7 MHz at 230 and 345 GHz respectively) and zeroth (horizontal) or first order (linear sloped) baselines were removed. The emitting regions we detected were quite wide (> 300 km s^{-1}) but the spectrometer bandwidth was 800, 800, and 1200 km s^{-1} for the NRAO and JCMT $J=3-2$ and $J=2-1$, respectively, which allowed for accurate baseline determination. For the galaxies where we have no detections, the baseline levels were set using the region of the spectrometer outside a 400 km s^{-1} range centered on the rest velocity of the galaxies (i.e. $V_{lsr} \pm 200$ km s^{-1}) in order to maximize our changes of detecting any weak signal. The NRAO spectra for each galaxy are shown in Figure 5.1 and the JCMT spectra are shown in Figure 5.2. The spectral line intensities are summarized in Table 5.2.

Using the T_R^* temperature scale would ensure that our observed line strengths are as close to the true radiation temperatures as possible (Kutner & Ulich 1981). However, conversion to T_R^* from T_A^* requires knowledge of the forward scattering and spillover (η_{FSS}), which is difficult to measure and was not attempted during the JCMT observing runs. On the other hand, we do have good values for the main beam efficiencies and so an accurate conversion to main beam temperature ($T_{MB} = T_A^*/\eta_{MB}$) is possible. Therefore, we will display our spectra using the main beam temperature scale. For ease of calculations, we report our fluxes in Table 5.2 in T_A^*.
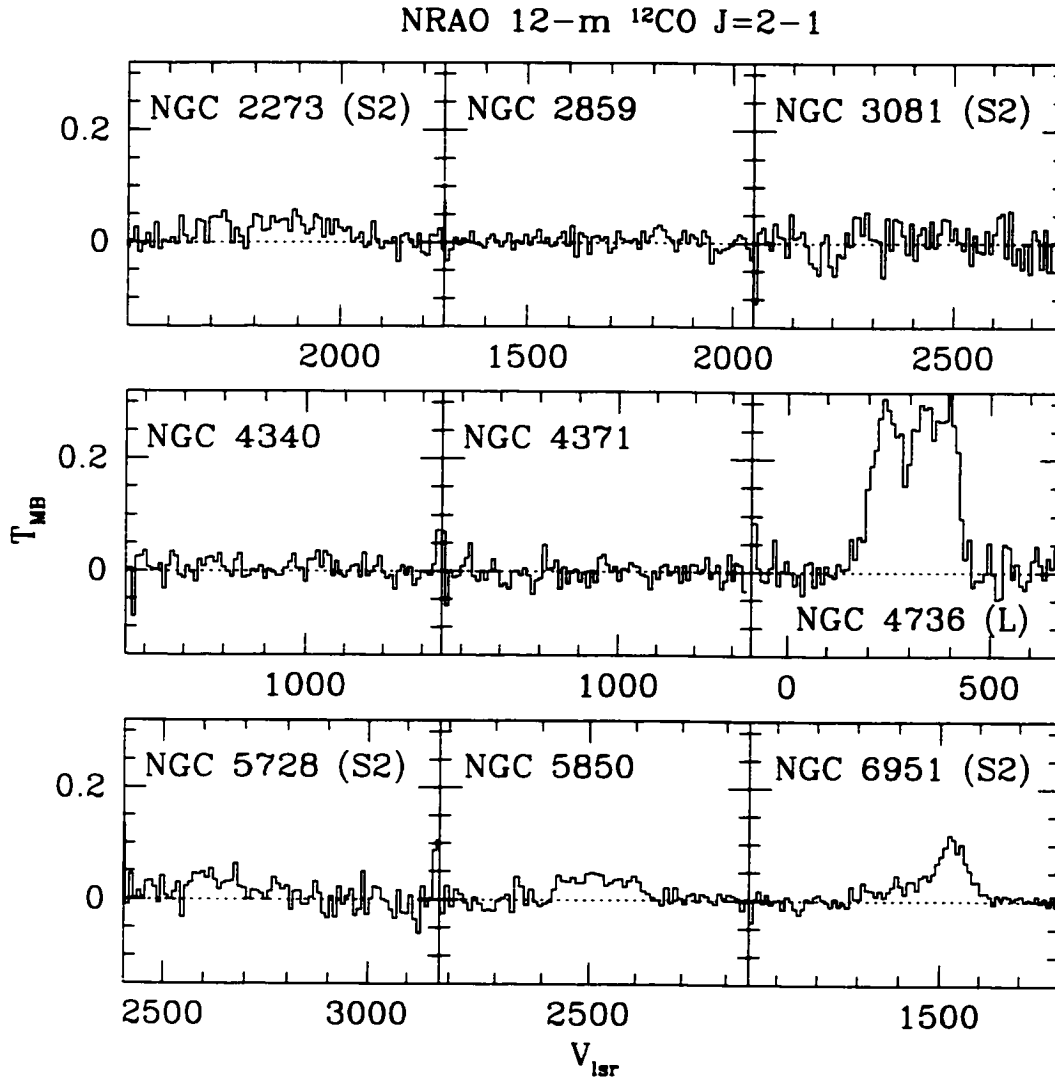
Figure 5.1: NRAO 12-m Spectra of Double Barred Galaxy Nuclei
^{12}CO J=2−1 spectra taken at the NRAO 12-m of a sample of galaxies thought to contain double bars. The spectra cover the inner 29″ of the galaxy nuclei, which is predicted to be gas rich by the models of Shaw et al. (1993) and Friedli & Martinet (1993). The type of nuclear activity exhibited is shown after the galaxy name (S2 = Seyfert 2; L = LINER). Note that we detect CO emission mostly from galaxies with some form of nuclear activity. The large tickmarks on the velocity axis correspond to 500 km s^{-1} intervals, while the smaller tickmarks are every 100 km s^{-1}. Higher recession velocities are to the right.
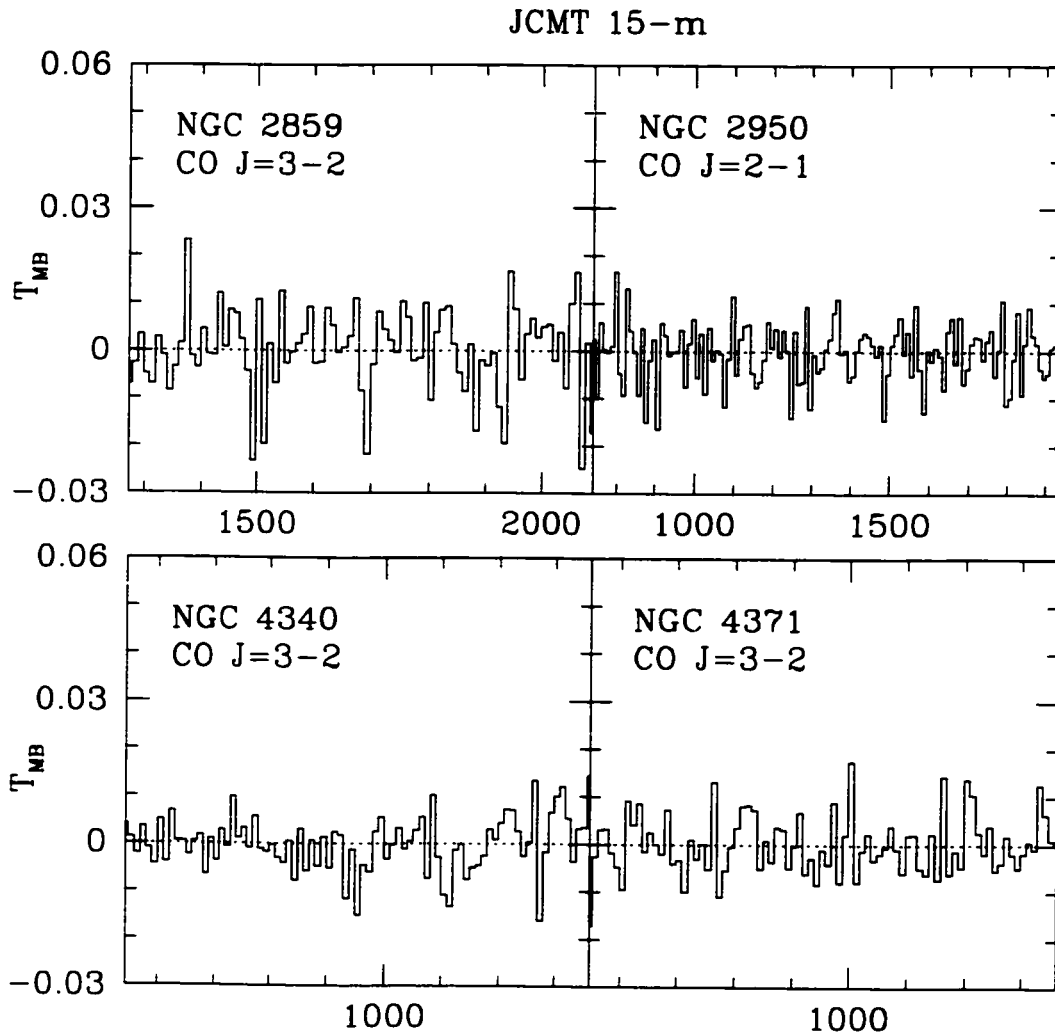
Figure 5.2: JCMT Spectra of Double Barred Galaxy Nuclei
^{12}CO $J=2-1$ and ^{12}CO $J=3-2$ spectra taken at the JCMT of a sample of galaxies thought to contain double bars. The $J=2-1$ spectra cover the inner $21''$ while the $J=3-2$ spectra cover $14''$. Note that despite the rather low noise, we still do not detect any emission from these galaxies.

5.3 Discussion

Figure 5.1 shows the spectra taken at the NRAO 12-m in ^{12}CO $J=2-1$. At first glance it appears that we have only detected three of the galaxies: NGC 4736. NGC 5850. and NGC 6951. These galaxies were all previously detected and detailed studies are published in Petitpas & Wilson (2001b). Sakamoto et al. (1999). Leon. Combes. & Friedli (2000). and Kohno. Kawabe. & Vila-Vilaró (1999). Observations of these galaxies were taken primarily for cross-calibration. The line profiles and peak strength for NGC 4736 agree well with those published in Petitpas & Wilson (2001b). The line profile of NGC 6951 is single peaked which is noticeably different than the JCMT ^{12}CO $J=2-1$ spectra for this galaxy (see Paper II). The profile of the NRAO spectrum more closely resembles the CO $J=3-2$ spectra taken with the JCMT at an offset of $(0''.-7'')$ as part of our 5-point mapping procedure discussed in Petitpas & Wilson (2001b). In addition to this. the peak line strength in the NRAO spectrum is much lower than the JCMT ^{12}CO $J=2-1$ spectrum. suggesting that pointing inaccuracies may have resulted in pointing the telescope too far south. missing the strongest emission in the northern part of the nucleus (Kohno. Kawabe. & Vila-Vilaró 1999) with the most sensitive part of the beam. There are no published single dish CO spectra for NGC 5850. but interferometric maps are published in Leon. Combes. & Friedli (2000).

For NGC 2273. we have JCMT $J=2-1$ spectra with a strong detection (Petitpas & Wilson 2001b). so despite the weak emission in the NRAO spectrum for this region we expect to see emission over the velocity range from 1600 to 2000 km s^{-1}. While there are no clear emission peaks visible in the NGC 2273 spectrum of Figure 5.1. we do see an increase in the baseline that can likely be attributed to the faint spectral line. The emission in NGC 5728 is known to cover a wide range of velocities from less than 2600 km s^{-1} to greater than 3050 km s^{-1} and is very clumpy (Petitpas

& Wilson 2001a: Schommer et al. 1988). The line would nearly cover the entire
spectrometer which makes it difficult to determine the baseline for the spectra of
NGC 5728 shown in Figure 5.1. We have used the very ends of the spectrometer
to determine the baseline level. and the result is a lumpy spectra with no strong
noticeable peaks. but a general tendency for the noise to remain slightly greater
than zero. We have JCMT CO $J=2-1$ spectra for NGC 3081 that show emission
over a region from 2200 to 2500 km s^{-1}. while in the NRAO spectrum. we see no
detectable line. The significance of these marginal detections is discussed in more
detail in §5.3.1.

Despite our rather high sensitivity (T_{MB}(rms) $\approx$ 14 mK) we have failed to detect
CO $J=2-1$ lines in NGC 2859. NGC 4340. or NGC 4371. In addition. Figure 5.2
shows that we do not detect the CO $J=3-2$ emission line in NGC 2859. NGC 4340.
or NGC 4371. despite higher sensitivity (T_{MB}(rms) $\approx$ 6 mK). For the single $J=2-1$
spectra taken at the JCMT. we do not detect emission in NGC 2950 despite reaching
the 5 mK rms limit. In short. we do not detect any galaxies that have not been
previously detected in the CO surveys of Braine & Combes (1992). Mauersberger
et al. (1999). and Young et al. (1995).

Beside the galaxy names in Figures 5.1 and 5.2 are codes (in parentheses) that
indicate the types of nuclear activity found in these galaxies. Seyfert 2s are marked
as "S2" and LINERs are flagged with "L". Galaxies without any detected nuclear
activity are not flagged and show no signs of Seyfert. LINER. or starburst activity.
If we neglect the higher sensitivity spectra published in Petitpas & Wilson 2001b
for now and use only Figures 5.1 and 5.2. we would see convincing detections in
NGC 2273 (Seyfert 2). NGC 4736 (LINER) and NGC 5850 (quiescent) and NGC
6951 (Seyfert 2). We would see no detections for NGC 2859 (quiescent). NGC 2950
(quiescent). NGC 3081 (Seyfert 2). NGC 4340 (quiescent). NGC 4371 (quiescent),

and NGC 5728 (Seyfert 2). Thus three out of four (75%) of our detected galaxies show signs of some form of nuclear activity. Four out of six (67%) of our undetected galaxies show no signs of activity. These rather small number statistics are enhanced when we include the CO detections published in Petitpas & Wilson (2001b). Inclusion of these data moves the Seyfert 2 galaxies NGC 3081 and NGC 5728 into the 'detected' bin. Now, five of the six galaxies (83%) that we have detected show signs of nuclear activity. Of the four galaxies that we have not detected CO emission, none of them show any signs of nuclear activity.

We note that in performing a literature search, the galaxies that we have not detected are quite a bit less studied than NGC 4736 and NGC 6951, for example, and may harbor yet undetected nuclear activity, which could change our small number statistics noticeably.

5.3.1 Molecular Gas Mass

The double barred galaxy models of Friedli & Martinet (1993) and Shaw, Combes, Axon, & Wright (1993) suggest that there needs to be substantial amounts of molecular gas in double barred galaxies. In fact, the molecular gas inflow in these double barred galaxies may accumulate enough mass so that the nuclear bar can become kinematically distinct (Friedli & Martinet 1993; Pfenniger & Norman 1990). Thus, we may expect to see high molecular gas masses in the centers of these double barred galaxies.

The intensity of the CO emission can be related to the molecular mass using the equation

$$M_{mol} = 1.61 \times 10^4 \left(\frac{\alpha}{\alpha_{Gal}} \right) \left(\frac{115 \text{ GHz}}{\nu} \right)^2 d^2_{Mpc} \frac{S_{CO}}{R} M_\odot \qquad (5.1)$$

(Wilson & Scoville 1990: Wilson 1995) where S_{CO} is the ^{12}CO $J=2-1$ flux in Jy km s^{-1}. R is the ^{12}CO $J=2-1/J=1-0$ line ratio. ν is the frequency of the emission (230 GHz for the $J=2-1$ transition). d_{Mpc} is the distance to the galaxy in Mpc. α is the CO-to-H$_2$ conversion factor for that galaxy. and α_{Gal} is the Galactic value $(3 \pm 1 \times 10^{20}$ cm^{-2}(K km s^{-1})$^{-1}$. Strong et al. 1988: Scoville & Sanders 1987). We use 24.7 Jy K^{-1}. 27.8 Jy K^{-1} ($\eta_{ap}=$ 0.63. 0.56) and 70.6 Jy K^{-1} to convert our JCMT ($J=2-1.J=3-2$) and NRAO $J=2-1$ data (respectively) from Kelvins (T_A^*) to Janskys (Kraus 1986: JCMT Users Guide: NRAO 12-m Users Manual). We assume a coupling efficiency (η_c) of 0.7 to correct our observed fluxes to true fluxes. The CO-to-H$_2$ conversion factor (α) is a globally averaged property of the galaxy and hence there are uncertainties involved in its use in one specific region of the galaxy and it is only accurate to within ~ 30%. Our fluxes are typically accurate to about 10%. The distances for these relatively nearby galaxies is likely uncertain by at least 30%. We therefore adopt a total uncertainty of 50% in our mass estimates.

For the galaxies where we have CO detections with other telescopes or at other frequencies. we integrate over the velocity range where the emission line was seen. For galaxies with no previous detections. we integrate over a 400 km s^{-1} range centered on the rest velocity of the galaxy (this region was excluded from the baseline subtraction). In the cases where the integrated intensity is greater than the rms noise. we give both the integrated intensity and the noise regardless of how insignificant. We are not claiming these as detections. but are simply using these as a more realistic value for the detection cut-off limit. If the integrated intensity is less than or equal to the rms noise the noise value is given as an upper limit. The results are summarized in Table 5.2.

Table 5.2 shows that there is a wide variety of molecular gas masses in the inner regions of these galaxies. For the galaxies in our sample that have been detected

Table 5.2: CO Fluxes and Molecular Gas Masses

Galaxy	Transition (^{12}CO)	V limits (km s^{-1})	Flux (K km s^{-1} T_A^*)	Distance (Mpc)	Gas Mass (M$_\odot$)
NGC 2273	$J=2-1$	1600-2020	2.83 ± 0.30	25	8.2×10^8
NGC 2859	$J=2-1$	1490-1890	(0.76 ± 0.25)	22	2.0×10^8
NGC 2859	$J=3-2$	1490-1890	< 0.25	22	$< 2.9 \times 10^7$
NGC 2950	$J=2-1$	1140-1540	< 0.23	18	$< 1.8 \times 10^7$
NGC 3081	$J=2-1$	2200-2550	(1.05 ± 0.52)	32	6.2×10^8
NGC 4340	$J=2-1$	750-1150	(0.83 ± 0.24)	13	8.1×10^7
NGC 4340	$J=3-2$	750-1150	< 0.20	13	$< 8.2 \times 10^6$
NGC 4371	$J=2-1$	740-1140	< 0.28	13	$< 2.7 \times 10^7$
NGC 4371	$J=3-2$	740-1140	< 0.18	13	$< 7.3 \times 10^6$
NGC 4736	$J=2-1$	100-450	17.9 ± 0.4	4	1.7×10^8
NGC 5728	$J=2-1$	2500-3050	2.16 ± 0.37	37	1.3×10^8
NGC 5850	$J=2-1$	2400-2650	1.99 ± 0.19	34	1.3×10^9
NGC 6951	$J=2-1$	1250-1620	3.90 ± 0.18	19	2.9×10^8

All distances are taken from the NASA-IPAC Extragalactic Database (NED) and assume a Hubble Constant of 75 km s^{-1} (Mpc)$^{-1}$. For calculating gas masses for NGC 2273. NGC 5728. NGC 6951 we adopt CO $J=2-1/J=1-0$ ratios of 0.88. 0.7. and 1.96 respectively (Petitpas & Wilson 2001b). For the other galaxies we have assumed a ^{12}CO $J=2-1/J=1-0$ ratio of 0.7 and (where necessary) a $J=3-2/J=2-1$ line ratio of 1 similar to the values found for other double barred galaxies (Petitpas & Wilson 2001b). The flux values for the questionable detections are enclosed in parentheses.

with the JCMT, we find that the masses determined here are typically lower than the masses determined with CO $J=2-1$ data in Petitpas & Wilson (2001b) by less than a factor of two. The exception is NGC 6951 which is lower here by more than a factor three. This discrepancy can likely be attributed to the pointing offset discussed in §5.3. It is interesting that the masses derived here for NGC 2273 and NGC 5728 using NRAO fluxes agree more closely (within 25-70%) with the masses derived using CO $J=1-0$ interferometric fluxes which are known to miss large scale emission (Petitpas & Wilson 2001a). This may reflect the differences in pointing accuracy between the JCMT and NRAO. Since the emission in these galaxies is confined to a small region of the nucleus, the larger pointing errors of the NRAO may have resulting in the most sensitive part of the main beam missing the emission peak. It may also reflect the higher dish surface precision of the JCMT. In any case, the similarities between the masses obtained with the weaker NRAO 12-m spectra (even in the cases where no obvious lines are visible such as NGC 3081 and NGC 5728) and the masses obtained with the JCMT $J=2-1$ spectra gives us confidence that our mass estimates and upper limits are accurate to at least a factor of two.

Of particular interest is the galaxy NGC 5850, whose spectrum indicates that there is more than 10^9 M. of molecular gas in the inner 29″. This comparable to the amount of gas in the entire Milky Way, but now contained in its inner 2.5 kpc radius. The optical size of this galaxy is 4′3×3′7 ($D_{25} \times d_{25}$), which corresponds to 43×37 kpc at its distance of 34 Mpc (NED). This clearly makes it the largest galaxy in our sample (the second runner up is NGC 5728 at 33×19 kpc). Given its rather strong bar, it is possible that the large quantity of gas in the inner regions of this galaxy may have been transported inward by the inflow mechanisms known to be associated with bar perturbations. The high resolution CO maps of this galaxy (Leon, Combes, & Friedli 2000) detect only 6.7×10^7 M$_\odot$ of molecular gas, mostly

concentrated in a small off-center peak of emission approximately 8″ north of the galactic center. On the other hand, their single dish IRAM 30-m CO $J=1-0$ maps of the entire primary bar detects 3.4×10^9 M$_\odot$. Leon, Combes, & Friedli (2000) point out that this galaxy is surprisingly quiescent given the large amounts of molecular gas, and propose that the reason for this is that the molecular gas is below the critical surface density for gravitational instabilities (Kennicutt 1989).

The large size of NGC 5850 and the fact that it is the only quiescent galaxy with a strong detection lead us to wonder if we are detecting emission lines in predominantly the largest galaxies (with possibly the largest molecular gas reservoirs). All the other galaxies are in the 15 to 20 kpc (major axis) size range with the exception of NGC 2859, NGC 5728, and NGC 5850 who have major axes of 28, 33, and 43 kpc respectively. The strongest line occurs in the closest galaxy, NGC 4736, which is incidentally one of the smallest in our sample with major axis of $\sim$14 kpc. So it seems that we are not detecting CO emission preferentially in larger galaxies. Since NGC 5850 is the second most distant galaxy in our sample, it also appears that we are not preferentially detecting emission from the closest galaxies.

Since we are searching for emission with the CO $J=2-1$ line, our lack of success in finding bright candidates may not be the result of a lack of molecular gas, but that the gas in these galaxies is very cool and possibly at a low density. Is it possible that all of the molecular emission is dominated by $J=1-0$ emission and it is not excited into the $J=2-1$ levels enough to be detected? In our mass calculation, we assume a $J=2-1/J=1-0$ line ratio of 0.7. In the Local Thermodynamic Equilibrium approximation, in order to achieve this line ratio, the gas must be at a temperature of only 7 K. This temperature is low enough that it can be maintained by cosmic ray heating (Goldsmith & Langer 1978). Higher values of the $J=2-1/J=1-0$ line ratio

will act to decrease our molecular gas mass, meaning that the mass values quoted here are likely upper limits.

Another possible explanation for the low molecular gas mass may be that the gas is just not located in the inner 29″. There are observations of other galaxies that contain large molecular rings that seem to have prevented any of the molecular gas from reaching the nucleus (e.g. NGC 7331: Sheth et al. 2000). We will need spectra covering a wider field of view to verify if this is happening in any of these galaxies.

5.3.2 Implications to Double Barred Galaxy Models

Recall that all of the galaxies in this survey were chosen because they are known to contain the NIR isophote twists believed to be the signature of a double barred galaxy. As mentioned in §5.1, the models of double barred galaxies by Shaw et al. (1993) and Friedli & Martinet (1993) require large amounts of molecular gas in the nuclear regions of these galaxies in order to sustain long-lived double bars. The gas requirements vary from 4 to 6% globally (Shaw et al. 1993: Friedli & Martinet 1993) to as little as 2% molecular gas in the nucleus (Friedli & Martinet 1993). This gas is required to provide the dissipation needed to prevent the stellar component from dynamically heating so much that the nuclear bar is destroyed. We point out that we are studying the molecular gas properties in *only the nuclear region* so we expect to see gas mass fractions on the order of 2% or more.

The molecular gas content of the galaxies for which we have detections are in agreement with the model requirements and are discussed elsewhere (Leon et al. 2000: Petitpas & Wilson 2001a: Sakamoto et al. 1999). We will focus our attention here on the galaxies where we have failed to detect a strong molecular gas com-

ponent. These are the galaxies that are difficult to explain in light of the current models of double barred galaxies.

As mentioned in §5.3. the galaxies where we have not detected any CO emission are in general less well studied. As such. we are not able to find direct measurements of the masses of all the galaxies in our sample in the literature. We have estimated the mass for these galaxies from their blue magnitude (extrapolated to infinity: $m_{B(T)}$ in de Vaucouleurs et al. 1991). Table 5.3 shows the apparent blue magnitudes for our sample of galaxies. the absolute magnitude. and the luminosity in solar luminosities. We have assumed the absolute blue magnitude of the sun to be +5.43 (Allen 1964) and note that variations in magnitude of ∼0.3 result in variations in luminosity of a factor of ∼2. Table 5.3 shows that all of these galaxies (except NGC 5850) have masses of approximately a few $\times 10^{10}$ $M_\odot$. Independent measurements for the masses of some galaxies in our sample exists in the literature. Rubin (1980) determined the dynamical mass of the disk (the dominant source of the blue light) of NGC 5728 to be ∼ 8×10^{10} $M_\odot$: Marquez & Moles (1993) find the mass of NGC 6951 to be 1.3×10^{11} $M_\odot$: Smith et al. (1991) determine the mass of NGC 4736 to be 4×10^{10} $M_\odot$. These masses are in acceptable agreement with our estimates considering the uncertainties associated with our technique. It seems though. that our method is underestimating the galaxy mass by a factor of 2 to 4. whichs is likely the result of the blue light missing much of the older. redder stellar population of stars in these galaxies. Our estimate therefore provides a lower limit to the true galaxy mass. and thus. an upper limit to the gas mass fraction.

The limits on the molecular gas masses for the undetected galaxies in our sample range from as high as 2×10^8 $M_\odot$ (for NGC 2859) down to 8×10^6 $M_\odot$ for NGC 4371. Using the galaxy masses shown in Table 5.3. this corresponds to a molecular gas mass fraction of 0.08% and 0.05% for NGC 2859 and NGC 4371. respectively. Recall

Table 5.3: Galaxy Masses Estimated from Blue Light

Galaxy	$m_{B(T)}$ (app.)	M_B (abs.)	L_B $(L_\odot)$	Mass $(M_\odot)$
NGC 2273	12.55	-19.44	8.7×10^9	2.6×10^{10}
NGC 2859	11.83	-19.87	13×10^9	3.9×10^{10}
NGC 2950	11.84	-19.87	13×10^9	3.9×10^{10}
NGC 3081	12.85	-19.68	11×10^9	3.3×10^{10}
NGC 4340	12.10	-18.47	3.6×10^9	1.1×10^{10}
NGC 4371	11.79	-18.78	4.7×10^9	1.4×10^{10}
NGC 4736	8.99	-19.18	6.9×10^9	2.1×10^{10}
NGC 5728	12.57	-20.27	19×10^9	5.7×10^{10}
NGC 5850	11.54	-21.18	43×10^9	13×10^{10}
NGC 6951	11.64	-19.75	12×10^9	3.6×10^{10}

$m_{B(T)}$ is the apparent blue magnitude of the galaxy extrapolated to infinite radius (RC3). We adopt $+5.41$ for the suns absolute blue magnitude (Allen 1964) and note that variations of ~ 0.3 in either the galactic or solar magnitude result in a factor of ~ 2 variation in the luminosity. The last column assumes a mass to light ratio of 3, which is typical for barred spiral galaxies (Forbes 1992).

that the models of Shaw et al. (1993) and Friedli & Martinet (1993) require 4% to 10% gas mass fractions to maintain long lived nuclear bars. Friedli & Martinet (1993) state that the molecular gas requirements for the inner kpc of these galaxies can be as low as 2%. The gas mass fractions obtained here suggest that some of these galaxies do not contain enough molecular gas to be able to support nuclear bars.

There are four possible explanations that can bypass this perceived problem. The first possibility is that the gas in our galaxies is not in molecular form. The gaseous components of the models are basically a dissipation mechanism that acts to prevent the stellar components from being dynamically heated. Models of these galaxies generally treat this gas as being primarily molecular, contained in regions of high density and low filling factor (e.g. Combes & Gerin 1985). Molecular gas also has a higher cooling capacity, since it contains many more emission lines available

to it compared to atomic gas. It would take much more HI gas to dissipate as much energy as molecular gas. There are currently no HI maps of NGC 4340 in the literature, but Burstein, Krumm, & Salpeter (1987) have detected very weak HI emission in NGC 2859 using Arecibo, so it is unlikely that the HI gas contributes greatly to the galactic cooling.

Another possibility is that the molecular gas is not confined to the nuclei of these galaxies. A circumnuclear CO morphology is seen in other galaxies (e.g. NGC 7331; Sheth et al. 2000), so it is possible that the molecular gas is outside of the inner 29"covered by the NRAO beam for the seemingly gas deficient galaxies in our sample. We will need CO observations over a larger area in order to determine if this is the case, but the models of Friedli & Martinet 1993 still require that the inner kpc contain at least 2% gas. If we assume similar disk and bulge profiles for NGC 2859 as those adopted for NGC 5738 by Rubin (1980), we estimate that roughly one tenth of the stellar mass (bulge + disk) is contained in the inner 29" of NGC 2859. This translates into a gas to mass ratio of *0.8% for the inner 3 kpc* of NGC 2859, so the lack of CO in this galaxy is still a problem for the Friedli & Martinet (1993) model. Even if the gas is located in a large circumnuclear ring, it will not have much of an impact on the cooling of the nuclear regions.

The third possibility is that the NIR isophote twists are not correlated with the gas properties at all. It is possible that the NIR isophote twists are caused by a triaxial stellar bulge, as originally proposed by Kormendy (1979). In this scenario, the lack of molecular gas is not a problem, because there is not much molecular gas in the bulges of galaxies anyway. Evidence against the triaxial bulge model is discussed in Petitpas & Wilson (2001a) where the existence of a nuclear molecular bar that aligns with the isophote twists confirms the existence of a true nuclear bar in the disk of NGC 2273. It has also been proposed that the NIR isophote twists

are the result of the stars following the stable x_2 orbits that exist inside the inner Lindblad resonance of barred galaxies (e.g. Maciejewski & Sparke 2000). Again. in this scenario. the molecular gas is not required. so the weak CO emission is not a problem. It is difficult to get the x_2 orbits (which tend to be perpendicular to the x_1 orbits that dominate the main galactic bar) to become misaligned from the large-scale bar as is seen in many galaxies (see discussion in Shaw. Combes. Axon. & Wright 1993. for example).

It is possible that different mechanisms are at work in different galaxies. and they need to be studied on a case by case basis to determine if the isophote twists are the result of a nuclear bar or a triaxial stellar bulge. In either case. we will need either more sensitive arrays or a sub-millimeter interferometer in the southern hemisphere in order to obtain high resolution CO maps for a larger number of these galaxies.

The final possibility is that the models are underestimating the dissipative properties of the molecular gas. Since the molecular gas basically acts as an energy dissipation agent. if the dissipation in the models were increased. it should take less gas to sustain the long-lived nuclear bars. This counters the findings of Paper I. which propose that the dissipation properties of the molecular gas may be overestimated. In any case. it is clear that the study of the dissipative properties of molecular gas will greatly increase the accuracy of these galaxy models.

5.4 Summary

In an attempt to find double barred galaxies that are bright in CO emission, we have obtained ^{12}CO $J=2-1$ spectra for nine galaxies with the NRAO 12-m Telescope. We detect emission in four (perhaps five) of these galaxies. Three of the

four galaxies detected exhibit some form of nuclear activity. while of the galaxies that were not detected. four out of six are quiescent. showing no signs of any nuclear activity. Thus. within our small sample. the CO emission seems to be detected predominantly in galaxies that harbor some form of nuclear activity (e.g. Seyfert. LINER). If we include CO detections from a previous study (Petitpas & Wilson 2001b). this result becomes slightly more convincing. We note that the quiescent galaxies are less well studied than the active galaxies in our sample. so it may be that they harbor some form of nuclear activity that has yet to be discovered.

Models of double barred galaxies suggest that they should be gas rich in order provide a means of dissipating energy that would otherwise heat the stellar population and subsequently destroy the nuclear bars. We use the CO fluxes to estimate the amount of molecular gas in the centers of these galaxies and we find gas masses that range from less than a few $\times 10^6$ $M_\odot$ to more than $\sim 10^9$ $M_\odot$. The one quiescent galaxy that was detected with the NRAO 12-m (NGC 5850) contains a very large amount of molecular gas: 10^9 $M_\odot$. This is equivalent to all the molecular gas in the Milky Way being contained within a radius of 2.5 kpc. Leon. Combes. & Friedli (2000) find that the gas in this galaxy is below the critical surface density required for star formation to occur. which would explain the absence of activity despite the very large fuel reservoir.

In the cases where no emission was found with the NRAO 12-m. we obtained higher resolution ^{12}CO $J=3-2$ and $J=2-1$ spectra with the James Clerk Maxwell Telescope. There are no detections in the JCMT spectra of these galaxies despite reaching sensitivities of 4 mK (T_A^*). The lack of detections in these galaxies places very strict limits on the amounts of molecular gas in these galaxies. For some galaxies. there must be less than a few $\times 10^6$ $M_\odot$ of molecular gas. which (assuming these galaxies are typical disk galaxies) corresponds to 0.05 to 0.08% of the total

mass of the galaxy. This is a lower mass fraction than required by the models of double barred galaxies to create long lived nuclear bars. This result suggests that either the NIR isophote twists are the result of a triaxial stellar bulge in these CO weak galaxies, or the dissipative properties of the molecular gas in the simulations have been underestimated.

Bibliography

Allen. C. W.. 1964. *Astrophysical Quantities*. Astrophysical Quantities. London: Athlone Press (2nd edition). 1964.

Braine. J. & Combes. F.. 1992. *A&A* **264**. 433.

Burstein. D.. Krumm. N.. & Salpeter. E. E.. 1987. *AJ* **94**. 883.

Combes. F.. 1994. Nuclear gas flows in barred galaxies. In *Mass Transfer Induced Activity in Galaxies*. pp. 170. ed. I. Shlosman. Cambridge Univ. Press.

Combes. F. & Gerin. M.. 1985. *A&A* **150**. 327.

de Vaucouleurs. G.. de Vaucouleurs. A.. Corwin. H. G.. Buta. R. J.. Paturel. G.. & Fouque. P.. 1991. *Third Reference Catalogue of Bright Galaxies*. Volume 1-3. XII. 2069 pp. 7 figs.. Springer-Verlag Berlin Heidelberg New York.

Elmegreen. D. M.. Elmegreen. B. G.. Chromey. F. R.. Hasselbacher. D. A.. & Bissell. B. A.. 1996. *AJ* **111**. 1880.

Forbes. D. A.. 1992. *A&AS* **92**. 583.

Friedli. D. & Martinet. L.. 1993. *A&A* **277**. 27.

Goldsmith. P. F. & Langer. W. D.. 1978. *ApJ* **222**. 881.

Jarvis. B. J.. Dubath. P.. Martinet. L.. & Bacon. R.. 1988. *A&AS* **74**. 513.

Jogee. S.. 1998. *Molecular Gas and Starbursts in the Circumnuclear Regions of Spiral Galaxies*. Ph.D. Thesis. Yale University.

Kennicutt. R. C.. 1989. *ApJ* **344**. 685.

Kohno. K.. Kawabe. R.. & Vila-Vilaró. B.. 1999. *ApJ* **511**. 157.

Kormendy. J.. 1979. *ApJ* **227**. 714.

Kraus. J. D.. 1986. *Radio astronomy*. Powell. Ohio: Cygnus-Quasar Books. 1986.

Kutner. M. L. & Ulich. B. L.. 1981. *ApJ* **250**. 341.

Leon. S.. Combes. F.. & Friedli. D.. 2000. Single co peak in the double bar galaxy
ngc 5850. In *ASP Conf. Ser. 197: Dynamics of Galaxies: from the Early
Universe to the Present*. pp. 61.

Maciejewski. W. & Sparke. L. S.. 2000. *MNRAS* **313**. 745.

Marquez. I. & Moles. M.. 1993. *AJ* **105**. 2090.

Mauersberger. R.. Henkel. C.. Walsh. W.. & Schulz. A.. 1999. *A&A* **341**. 256.

Mulchaey. J. S.. Regan. M. W.. & Kundu. A.. 1997. *ApJSS* **110**. 299.

Petitpas. G. R. & Wilson. C. D.. 2001a. *ApJ submitted*.

Petitpas. G. R. & Wilson. C. D.. 2001b. *ApJ to be submitted*.

Pfenniger. D. & Norman. C.. 1990. *ApJ* **363**. 391.

Rubin. V. C.. 1980. *ApJ* **238**. 808.

Sakamoto. K.. Okumura. S. K.. Ishizuki. S.. & Scoville. N. Z.. 1999. *ApJ* **525**.
691.

Schommer. R. A.. Caldwell. N.. Wilson. A. S.. Baldwin. J. A.. Phillips. M. M..
Williams. T. B.. & Turtle. A. J.. 1988. *ApJ* **324**. 154.

Scoville. N. Z. & Sanders. D. B.. 1987. H2 in the galaxy. In *ASSL Vol. 134:
Interstellar Processes*. pp. 21.

Shaw. M. A.. Combes. F.. Axon. D. J.. & Wright. G. S.. 1993. *A&A* **273**. 31.

Sheth. K.. Regan. M. W.. Vogel. S. N.. & Teuben. P. J.. 2000. *ApJ* **532**. 221.

Smith. B. J.. Lester. D. F.. Harvey. P. M.. & Pogge. R. W.. 1991. *ApJ* **373**. 66.

Strong. A. W.. Bloemen. J. B. G. M.. Dame. T. M.. Grenier. I. A.. Hermsen. W.. Lebrun. F.. Nyman. L. .. Pollock. A. M. T.. & Thaddeus. P.. 1988. *A&A* **207**. 1.

Wilson. C. D.. 1995. *ApJL* **448**. L97.

Wilson. C. D. & Scoville. N.. 1990. *ApJ* **363**. 435.

Wong. T. & Blitz. L.. 2000. *ApJ* **540**. 771.

Wozniak. H.. Friedli. D.. Martinet. L.. Martin. P.. & Bratschi. P.. 1995. *A&AS* **111**. 115.

Young. J. S. & Devereux. N. A.. 1991. *ApJ* **373**. 414.

Young. J. S.. Xie. S.. Tacconi. L.. Knezek. P.. Viscuso. P.. Tacconi-Garman. L.. Scoville. N.. Schneider. S.. Schloerb. F. P.. Lord. S.. Lesser. A.. Kenney. J.. Huang. Y.. Devereux. N.. Claussen. M.. Case. J.. Carpenter. J.. Berry. M.. & Allen. L.. 1995. *ApJSS* **98**. 219.

Chapter 6

Temperature and Density Gradients

Across the Nucleus of M82

Abstract

This paper presents ^{12}CO $J=3-2$. ^{13}CO $J=3-2$. $C^{18}O$ $J=3-2$. and ^{13}CO $J=2-1$ spectra of the irregular starburst galaxy M82 taken with the 15 m James Clerk Maxwell Telescope. All maps exhibit a double peaked morphology. despite evidence that the higher J transitions are optically thick. This morphology suggests that the double peaked structure is not the result of an edge-on torus of molecular gas as is commonly assumed. We observe line ratio gradients that can best be explained by a temperature gradient increasing from NE to SW in conjunction with a density gradient that increases in the opposite sense. These gradients may have been caused by the interaction with M81. resulting in increased star formation that both heats and depletes the molecular gas in the SW lobe of M82.

Galaxies: irregular — galaxies: individual (M82) — galaxies: ISM — ISM: molecules — Local Group

6.1 Introduction

M82 (NGC 3034, Arp 337) is considered the prototypical starburst galaxy. Its close proximity (D=3.25 Mpc, Tammann & Sandage 1968) and strong CO lines (Rickard et al. 1975) make it an excellent location to study the effects of a burst of star formation on molecular gas properties. Its edge-on orientation make essential the use of optically thin molecular gas tracers for probing the physical conditions in the interstellar medium. Interferometric maps (e.g. Shen & Lo 1995; Neininger et al. 1998) show that M82 contains three bright lobes: two main lobes on the outer edges, which are thought to be a torus of molecular gas seen edge-on (e.g. Tilanus et al. 1991), and a central peak which may be housing an AGN (Muxlow et al. 1994; Seaquist et al. 1997). Early CO studies showed that M82 had an unusually large ^{12}CO J=2−1/J=1−0 line ratio ($\gtrsim$2, Knapp et al. 1980; Sutton et al. 1983), which suggested that the ^{12}CO gas in M82 is optically thin. As calibration techniques and telescope surface quality improved, the value for the ^{12}CO J=2−1/J=1−0 line ratio has decreased to ~1 (Tilanus et al. 1991; Wild et al. 1992), which suggests that ^{12}CO is likely optically thick. A high optical depth leads to some problems in the interpretation of the double lobes as a molecular torus. Neininger et al. (1998) point out that if the gas were optically thin, a torus seen from the edge would have a double peaked appearance, while if the torus were optically thick, we should see a elongated, bar-like structure.

Mapping a galaxy in many transitions will help our understanding of the molecular gas dynamics since different transitions and molecules do not necessarily trace the same gas (Petitpas & Wilson 1998b; Kohno, Kawabe, & Vila-Vilaró 1999). While M82 has been painstakingly mapped and studied by many authors in the lower-J transitions of CO and its isotopomers (see references above), improvements in receiver sensitivity and telescope surface quality have made fully sampled maps of the

higher-J transitions of rarer CO isotopes more tractable. This paper presents first

results from ^{12}CO. ^{13}CO. C^{18}O $J=3-2$ and ^{13}CO $J=2-1$ maps of M82. In §6.2 we

describe the observations and discuss the appearance of the spectra in comparison

to each other and previously published data. In §6.3 we use integrated intensity line

ratios to derive the physical conditions inside the nucleus of M82 and discuss the

results and possible causes for the observed gradients.

6.2 Observations and Data Reduction

One of the difficulties in the interpretation of line ratios is that the different lines

are often measured with different telescopes. This method introduces calibration

uncertainties (see for example. Figure 6 of Wild et al. 1992) that can be reduced if

all the data are taken with the same telescope (which is often impossible. given the

large variation in frequency between some transitions).

A variety of CO $J=3-2$ observations of M82 were taken using the James Clerk

Maxwell Telescope (JCMT) over the period of 1996 April 5 - 10. The ^{12}CO $J=3-2$

map covers an area of $120'' \times 100''$. the ^{13}CO $J=3-2$ map covers $56'' \times 35''$. and the

C^{18}O $J=3-2$ map covers a $34''$ strip along the bar major axis. We also include ^{12}CO

and ^{13}CO $J=2-1$ data taken during CANSERV at the JCMT over 1993 April 22 -

25. The data were reduced using the data reduction package SPECX. The raw data

had a linear baseline removed and then the $J=3-2$ data were binned to 12.5 MHz

(10.8 km s^{-1}) and the $J=2-1$ data to 5 MHz (6.7 km s^{-1}). Since the CO $J=2-1$

data have a different beam size and grid spacing than the CO $J=3-2$ data. it was

necessary to interpolate and convolve the spectra before measuring the integrated

intensity line ratios. The data were exported to the data reduction package COMB.

and the CO $J=3-2$ data were convolved to the same beam size and interpolated to

the same location as the nearest CO $J=2-1$ spectra.

The calibration was monitored by frequently observing both planets and spectral line calibrators. The spectral line calibrators for the CO data had intensities that were within $\sim$15% of the published values. We therefore adopt the published values for η_{MB} of 0.58 for the CO J=3-2 data and 0.67 for the ^{12}CO J=2-1 data. Pointing was checked frequently and was determined to be accurate to within 2" r.m.s.

The individual ^{12}CO J=3-2, ^{13}CO J=3-2, C^{18}O J=3-2, ^{12}CO J=2-1, and ^{13}CO J=2-1 spectra for the three bright regions of M82 are shown in Figure 6.1. The individual spectra for M82 appear asymmetric on either side of the center, indicating rotation. The line profiles appear similar for each transition which indicates that, at least on large scales, the emission is coming from co-moving material. There are indications of double peaked line profiles at the (0,0) position in the J=2-1 spectra. Since we do not see this structure as strongly in the J=3-2 spectra, it is likely the result of the larger beam overlapping both the NE and SW peaks simultaneously.

6.3 Physical Conditions from Line Ratios

It is well known that the filling factor of molecular clouds in a galaxy is often low. Thus, integrated intensities are generally not a good measure of the physical conditions of individual molecular clouds because the signal is diluted by the large radio telescope beams, which also cover much empty space. We must therefore use integrated intensity line ratios to determine the physical conditions of individual clouds. Using the ratio of two integrated intensities will help cancel out the effects of beam dilution, assuming that similar regions of space are responsible for the emission at both frequencies. The physical conditions recovered from the analysis of line ratios are the average conditions for all clouds within the beam.

Individual Spectra for Regions in M82
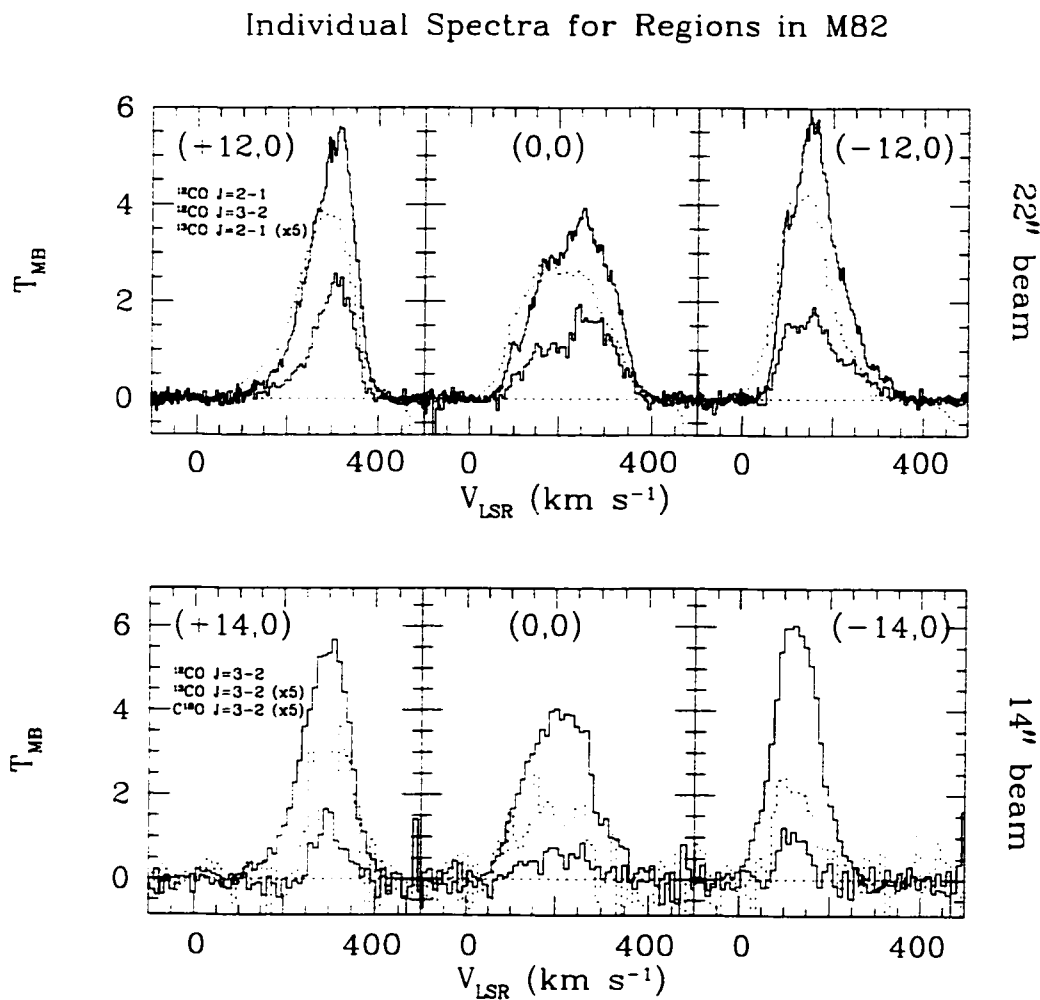
Figure 6.1: Individual spectra for the starburst galaxy M82.
The transitions are labeled in the same vertical order as they appear in the plots. The (0,0) position is centered on α = $09^\circ51'43.''00$, δ = $069^h55^m00.^s00$ (B1950.0). The orientation is such that north corresponds to an angle of 70° from the positive x-axis. and the bar runs horizontally. The temperature scale is main-beam temperature. The upper panel shows the spectra taken with (or convolved to) a $22''$ beam. while the lower panel shows data taken with a $14''$ beam.

The differing morphology in the ^{13}CO and ^{12}CO $J=3-2$ lines results in a gradient of the ^{12}CO/^{13}CO $J=3-2$ line ratios, increasing from east to west (Figure 6.2). If both lines are optically thin, this observation indicates a ^{13}CO/^{12}CO abundance gradient across the disk of M82. This same 'abundance'-type gradient is not visible in the lower J transitions (see ^{12}CO/^{13}CO $J=1-0$ and $J=2-1$ ratios: Neininger et al. 1998; Loiseau et al. 1990), which suggests that the ^{12}CO emission is not optically thin and the gradient may be the result of a variation in optical depth. Since optical depth is a function of density and temperature, we have performed a Large Velocity Gradient (LVG) analysis using a code written by Lee Mundy and implemented as part of the Miriad data reduction package. A single component model provided a very nice fit to the observed line ratios. We kept the C^{18}O abundance as a free parameter, so a survey of parameter space was performed using $T_{kin} = 50 \pm 20$ K (Wild et al. 1992), [^{12}CO]/[^{13}CO] = 50 ± 20 (Tilanus, Tacconi, Sutton, Zhou, Sanders, Wynn-Williams, Lo, & Stephens 1991), n(H$_2$) from 10 to 10^6 cm^{-3}, and N(CO)/dv from 10^{15} to 10^{20} cm^{-2}/km s^{-1}(see (Petitpas & Wilson 1998a) for more details). The $\pm 1\sigma$ error bars for the line ratios shown in Figure 6.2 were entered into the program and the solutions are shown in Table 6.1. The ^{12}CO $J=2-1/J=1-0$ ratios from Tilanus et al. (1991) also overlap our solutions.

In the simplest scenario, the observed line ratio gradients can be explained by varying either temperature or density across the galaxy while holding the other variable constant. Our analysis suggests that either the density varies from 1.6×10^4 to 0.6×10^4 cm^{-2} (for $T_{kin} = 50$ K), or the temperature varies from 70 to 30 K (for n(H$_2$) $= 10^4$ cm^{-2}) from east to west. Of course, the gradients can also be produced by a combination of varying T and n, which suggests we need to include observations at other frequencies to constrain the models.
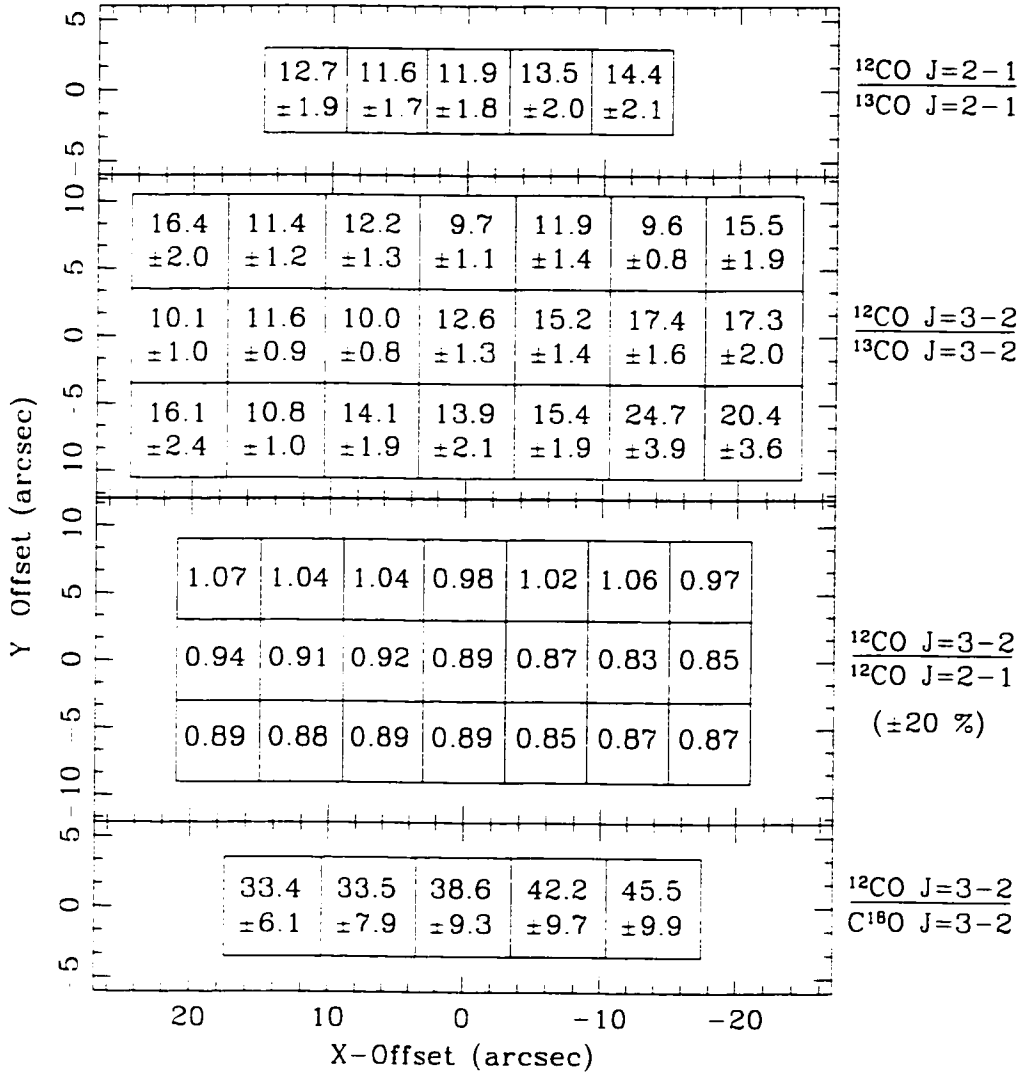
Figure 6.2: CO line ratios for M82

Integrated intensity line ratios for $^{12}CO/^{13}CO$ $J=2-1$, $^{12}CO/^{13}CO$ $J=3-2$, ^{12}CO $J=3-2/J=2-1$, and $^{12}CO/C^{18}O$ $J=3-2$(from top to bottom respectively). The ratios are in main beam temperature scale (T_{MB}). The uncertainties are based on the rms noise in the data, except for the ^{12}CO $J=3-2/J=2-1$ ratio, which is given as 20% to reflect the calibration uncertainties. The $J=3-2$ line ratios use data taken with a 14″ beam size; the $J=2-1$ line ratio uses 22″ resolution data. The ^{12}CO $J=3-2$ data were convolved to a 22″ beam to create the ^{12}CO $J=3-2/J=2-1$ line ratios.

A similar line ratio gradient was seen in HCO$^+$ J=4−3/J=1−0 by Seaquist, Frayer, & Bell (1998), but since their data combined single dish and interferometry data, they dismissed the gradient, attributing it to an abundance of diffuse emission on the eastern side of M82, which would cause the HCO$^+$ emission to be underestimated. However, our model fits show a higher density and/or temperature in the NE lobe, which could produce an increased HCO$^+$ J=4−3/J=1−0 ratio. Previous ^{12}CO and ^{13}CO J=1−0 interferometric studies by Kikumoto et al. (1998) find ^{12}CO/^{13}CO J=1−0 ratios that increase across M82, but in the opposite direction from our J=3−2 ratios. This result helps rule out the possibility that the observed gradients are the result of a ^{13}CO and C^{18}O abundance gradient across M82. The J=1−0 line ratio gradients are likely the result of the higher temperatures and/or densities in the NE lobe of M82, which bump the CO into the higher J transitions, leaving the lower J levels less populated.

We can use the 850 μm continuum maps of M82 (Alton, Davies, & Bianchi 1999) to remove the degeneracy between density and temperature in our models. Since the SW lobe is brighter in the 850 μm continuum maps, which trace the product of the temperature and the column density, we can conclude that either the column density and/or temperature is higher in the SW lobe. In this scenario, the HCO$^+$ maps of Seaquist, Frayer, & Bell (1998) would require that density be higher in the NE. The pair of LVG solutions which best satisfy the combined CO, HCO$^+$, and continuum data are flagged with check marks in Table 6.1. Utilizing these additional data sets, we therefore conclude that the observed line ratios are the result of a temperature gradient that increases from NE to SW in conjunction with a density gradient that increases from SW to NE.

One possible reason for this density and temperature gradient may be interaction with the nearby galaxy M81. Gravitational interaction may be triggering vigorous

Table 6.1: MS2 LVG Solutions

T_{kin}	^{13}X	^{18}X	log N(CO)/dr	log n(H$_2$)	$\tau_{J=1-0}$	$\tau_{J=3-2}$	preferred solution
			NE Lobe (+12.0)				
30	30	100	16.5	4.4	0.5	3	✓
30	50	100	16.6	4.4	1.1	5	✓
30	70	200	17.0	4.5	3.5	15	✓
50	30	100	16.8	4.2	0.4	4	
50	50	150	17.0	4.2	1.0	7	
50	70	200	17.2	4.2	2.1	12	
70	30	100	16.7	4.0	0.1	3	
70	50	150-200	17.0	4.0	0.5	5	
70	70	200-250	17.4	4.0	1.2	9	
			SW Lobe (−12.0)				
30	30	75	16.3	4.0	0.6	3	
30	50	100-150	16.6	4.1	1.3	6	
30	70	200	16.7	4.1	1.2	6	
50	30	75	16.4	3.7	0.2	3	
50	50	150	16.8	3.8	0.6	5	
50	70	200	17.0	3.8	1.2	8	
70	30	75	16.4	3.6	0.1	3	✓
70	50	100-150	16.8	3.7	0.4	5	✓
70	70	200	17.0	3.7	0.9	8	✓

This table shows all the possible solutions for the JCMT line ratios for $T_{kin} = 50 \pm 20$ and [^{12}CO]/[^{13}CO] $= 50 \pm 20$. The first column is the kinetic temperature, the second column is the ^{12}CO/^{13}CO abundance ratio, and the third column is the fit to the ^{12}CO/C^{18}O abundance ratio. The fourth and fifth columns are the CO column density (per km s^{-1}) and H$_2$ density required to produce the observed line ratios, while the sixth and seventh columns are the optical depth for the ^{12}CO $J=1-0$ and ^{12}CO $J=3-2$ transitions respectively. The last column flags the solutions that are preferred when considering data at other frequencies (see text).

star formation in the SW lobe, which could be heating the gas (increasing T) at the same time that it is being consumed (decreasing the average density by turning the densest regions into stars). While previous galaxy interaction simulations do not show any indication of density gradients across the smaller galaxy, it is unlikely that the current simulations would be able to detect a factor of three difference in the mean density of molecular clouds across the galaxy.

There is some dispute over the nature of the double peaked structure seen in M82. Most studies suggest that it is the result of a molecular torus seen edge-on. This would only be the case if the molecular gas in the clouds were optically thin (Neininger et al. 1998), or there were not enough molecular clouds in the telescope beam to 'shadow' the more distant clouds. Our LVG analysis indicates that ^{12}CO $J=1-0$ transition is on the border between optically thin and optically thick $(\tau_{J=1-0} \sim 0.1 - 3.5)$. However, the $J=2-1$ and $J=3-2$ maps also indicate a double peaked structure even though these transitions are likely optically thick (Table 6.1). This result can only be consistent with the torus model if the filling factor of the optically thick clouds within the beam is low enough that shadowing of one cloud by another is not a problem. We can estimate the filling factor by comparing the predicted and observed line temperatures. The LVG models predict temperatures of 19 K for ^{12}CO $J=2-1$ while our data show temperatures of $\sim$ 6 K. In addition, the high resolution CO maps of Neininger et al. (1998) suggest that M82 is only $\sim$ 10" thick and thus the filling factor of the CO emission is $\sim$ 60% of the 22" JCMT beam. This filling factor is high enough that cloud shadowing may be important in this region. If cloud shadowing plays a large role, the double peaked structure in M82 could not be explained as the result of an edge-on torus of molecular gas. Instead, it could be produced by the accumulation of molecular gas at the Inner Lindblad Resonance radius as it flows inward along the bar (e.g.

Kenney et al. 1992). There is evidence for these double peaks (on similar size scales) in nearly face-on barred galaxies (Kenney et al. 1992: Petitpas & Wilson 1998b). where we would not expect them to be caused by torus of gas. since the torus would have to be out of the plane of the galaxy.

Bibliography

Alton. P. B.. Davies. J. I.. & Bianchi. S.. 1999. *A&A* **343**. 51.

Kenney. J. D. P.. Wilson. C. D.. Scoville. N. Z.. Devereux. N. A.. & Young. J. S.. 1992. *ApJL* **395**. L7.

Kikumoto. T.. Taniguchi. Y.. Nakai. N.. Ishizuki. S.. Matsushita. S.. & Kawabe. R.. 1998. *PASJ* **50**. 309.

Knapp. G. R.. Leighton. R. B.. Wannier. P. G.. Phillips. T. G.. & Huggins. P. J.. 1980. *ApJ* **240**. 60.

Kohno. K.. Kawabe. R.. & Vila-Vilaró. B.. 1999. *ApJ* **511**. 157.

Loiseau. N.. Nakai. N.. Sofue. Y.. Wielebinski. R.. Reuter. H. .. & Klein. U.. 1990. *A&A* **228**. 331.

Muxlow. T. W. B.. Pedlar. A.. Wilkinson. P. N.. Axon. D. J.. Sanders. E. M.. & de Bruyn. A. G.. 1994. *MNRAS* **266**. 455.

Neininger. N.. Guelin. M.. Klein. U.. Garcia-Burillo. S.. & Wielebinski. R.. 1998. *A&A* **339**. 737.

Petitpas. G. R. & Wilson. C. D.. 1998a. *ApJ* **496**. 226.

Petitpas. G. R. & Wilson. C. D.. 1998b. *ApJ* **503**. 219.

Rickard. L. J.. Palmer. P.. Morris. M.. Turner. B. E.. & Zuckerman. B.. 1975. *ApJ* **199**. L75.

Seaquist. E. R.. Frayer. D. T.. & Bell. M. B.. 1998. *ApJ* **507**. 745.

Seaquist. E. R.. Frayer. D. T.. & Frail. D. A.. 1997. *ApJ* **487**. L131.

Shen. J. & Lo. K. Y.. 1995. *ApJ* **445**. L99.

Sutton. E. C.. Phillips. T. G.. & Masson. C. R.. 1983. *ApJ* **275**. L49.

Tammann. G. A. & Sandage. A.. 1968. *ApJ* **151**. 825.

Tilanus. R. P. J.. Tacconi. L. J.. Sutton. E. C.. Zhou. S.. Sanders. D. B.. Wynn-Williams. C. G.. Lo. K. Y.. & Stephens. S. A.. 1991. *ApJ* **376**. 500.

Wild. W.. Harris. A. I.. Eckart. A.. Genzel. R.. Graf. U. U.. Jackson. J. M.. Russell. A. P. G.. & Stutzki. J.. 1992. *A&A* **265**. 447.

Chapter 7

Summary and Future Work

7.1 Summary of Results from this Thesis

Active galactic nuclei in the form of starbursts or Seyfert galaxies are believed to be converting molecular material into stars or accreting this material onto the surfaces of black holes. Observations of the nuclei of active galaxies have shown that they are so luminous, they should exhaust all the molecular gas in the nucleus in a relatively short time. Statistical studies of the occurrence of starburst and Seyfert galaxies compared to regular (quiescent) galaxies suggests that there must be some form of refueling mechanism that enables them to live longer than they would otherwise (Beckman 1994).

According to theory and observations, barred galaxies should be an excellent means of transporting molecular gas inwards from the disk of a galaxy towards the nuclei. Models and observations also predict that gas may be halted at an inner Lindblad resonance, preventing it from reaching the nucleus (Athanassoula 1992; Kenney et al. 1992). To overcome this, Shlosman, Frank, & Begelman (1989) proposed that the gas at the ILR may become unstable and collapse into a secondary bar that can sweep material interior to the resonance, thus feeding the AGN or starburst activity.

Observations of barred galaxies have revealed the existence of isophote twists in the nuclear regions of early type barred galaxies, which may be the signature of a

nuclear bar. The three competing models explaining these isophote twists predict different gas dynamics and morphologies (see Chapter 1). In an effort to test these models, I have undertaken a series of studies of the molecular gas properties of these galaxies.

In **Chapter 3**, I present high resolution ^{12}CO J=1–0 maps of the nuclei of two barred galaxies known to contain NIR isophote twists (NGC 2273 and NGC 5728). Despite the similarities in the NIR images, the CO maps of these galaxies look very different. NGC 2273 shows a nuclear molecular bar that aligns with the NIR isophote twists observed by Shaw et al. (1993), while the CO map of NGC 5728 exhibits a disordered appearance that does not coincide with any nuclear features seen at other wavelengths.

The CO map of NGC 2273 clearly proves the existence of a double bar in this galaxy. In theory, one can determine if this nuclear bar is kinematically distinct (as proposed by Friedli & Martinet 1993) by comparing the rotation curve of the nuclear bar with the rotation curve of the rest of the galaxy. Unfortunately, there are no rotation curves published for inner 1′ of this galaxy, so this comparison is not yet possible.

The CO map of NGC 5728 shows an arc of CO clumps that peaks to the south-west of the dynamical centre of the galaxy and follows the southern-most dust lane. There is no convincing evidence for a nuclear bar in the CO maps, so it is possible that the isophote twists seen in the NIR images of this galaxy are caused by a triaxial stellar bulge.

The differences in the CO maps of these galaxies suggest that perhaps we are seeing them in different evolutionary stages. Galaxy models predict that after black holes are created in the centres of double barred galaxies, the gravitational potential gradually grows more spherically symmetric (Pfenniger & Norman 1990). This

symmetry acts to disrupt first the nuclear bar, then the large scale bar, resulting in an unbarred galaxy with a triaxial bulge.

The lack of a nuclear bar in the CO maps of NGC 5728 suggests that it may be in a later stage of evolution. The central black hole has begun to sphericalize the gravitational potential, and the molecular gas has responded first. The stars, which can not dissipate orbital energy as efficiently as molecular gas, are still in the double barred phase, and will respond to the changing potential more slowly.

Despite the similarity of the NIR images of NGC 2273 and NGC 5728, the molecular gas distributions are very different. This suggests that there may be differences in the properties of the molecular gas (i.e. temperature and density) that allow it to respond differently in similar gravitational potentials. In **Chapter 4**, I present multi-transition observations of a sample of galaxies containing NIR isophote twists for which high resolution CO maps exist.

I have observed the ^{12}CO $J=3-2$, ^{12}CO $J=2-1$, and ^{13}CO $J=2-1$ emission lines in in inner $21''$ of seven galaxies with NIR isophote twists. By analyzing the integrated intensity line ratios, I was able to determine the physical conditions of the molecular gas in these galaxies. The $^{12}CO/^{13}CO$ $J=2-1$ line ratios are similar in all galaxies, suggesting that the optical depths of the gas in each galaxy are similar. This result indicates that variations in the ^{12}CO $J=3-2/J=2-1$ line ratio directly reflects changes in the molecular gas temperatures and densities. It is clear that variations in the line ratio may simply be tracing variations in the opacity of CO emission in different galaxies.

I find that the ^{12}CO $J=3-2/J=2-1$ line ratio is lower in galaxies that contain nuclear bars and central concentrations of molecular gas, and higher in galaxies that exhibit a dispersed molecular morphology. The elevated line ratios suggest that the molecular gas is warmer in galaxies with twin peaks and circumnuclear rings, and

cooler in the galaxies with centrally concentrated CO emission. It is possible that the cooler gas is more viscous. which enhances its ability to dissipate energy. coalesce into clumps. and flow into the nucleus.

Analysis of the star formation activity and histories of these galaxies suggests that the variation in CO morphology and physical conditions in these galaxies may be the result of evolution through the double barred phase. The galaxies with more dispersed CO distributions (e.g. NGC 6951 and NGC 5728) represent an old population of galaxies that have already undergone nuclear staburst activity (perhaps the result of the earlier stages of the double barred phase). This starburst activity has exhausted. heated. and/or dispersed the nuclear molecular gas. leaving the observed circumnuclear distribution of warmer gas. The galaxies with nuclear molecular bars (such as NGC 470 and NGC 2273) are at an earlier stage of evolution. and the star formation has not yet disrupted the nuclear bar.

Of course. with only six galaxies in this sample. it is difficult to make very convincing arguments regarding the evolution of a class of galaxies. In **Chapter 5.** I present the results of a search for molecular gas in the nuclei of double barred galaxy candidates. The original goal was to find galaxies with bright emission that would make good candidates on which to perform analysis similar to that of Chapters 3 and 4. I did not find any significant new detections in either ^{12}CO $J=2-1$ or $J=3-2$. despite achieving rather high sensitivity.

The lack of CO emission in these galaxies indicates that they contain less than $0.7 - 3.0 \times 10^{7}$ $M_{\odot}$ of molecular gas. This corresponds to less than 0.08% molecular gas (by mass) which is much less than is required by the models of Shaw et al. (1993) and Friedli & Martinet (1993). Thus. either the NIR isophote twists in these gas-poor galaxies are the result of triaxial stellar bulges. or the models have underestimated the dissipation in the molecular gas.

In **Chapter 6**. I present CO spectra for the nuclear region interior to the inner Lindblad resonance of the nearby starburst galaxy M82. We find density and temperature gradients across the nuclear region interior to the ILR radius. Note that all of the structure and gradients observed in M82 would be unresolvable with the James Clerk Maxwell Telescope if it were as far away as the galaxies in Chapter 4. Thus, it is a cautionary example of how the molecular gas properties can vary dramatically in the nuclear regions of galaxies. In Chapter 4 we are actually measuring the *average* molecular gas properties over the entire nuclei of these galaxies. We will need a larger, more sensitive millimetre-wave telescope (such as the Atacama Large Millimeter Array) before we are able to analyze the molecular gas properties of our double barred galaxies in as much detail as we can in M82. It is important to learn all we can about the nearby galaxies with our current generation of telescopes since, in terms of spatial resolution, the more distant galaxies will appear to ALMA as M82 does to the JCMT.

7.2 Closing Remarks: The Big Picture

I have shown that nuclear bars appear in molecular gas observations in 2 (perhaps 3) out of the 6 galaxies studied. This result suggests that nuclear bars are real, but are not necessarily the cause of all the isophote twists seen in barred galaxies.

I have proposed a scenario in which galaxies with molecular nuclear bars represent an earlier stage of galaxy evolution, while the galaxies with NIR isophote twists, but no molecular nuclear bars, represent a more evolved stage. This theory is supported by the star formation activity of these galaxies. In the galaxies containing nuclear bars and central concentrations in the CO maps, the star formation is relatively new, suggesting an earlier evolution state. In the galaxies without nu-

clear bars. we see evidence of past star formation and the molecular gas is dispersed around the nucleus.

The physical conditions of the molecular gas are also in agreement with this evolutionary picture. In galaxies with molecular bars and new star formation. the molecular gas is cooler. possibly because it has not yet been heated. exhausted. or dispersed by the newly formed stars. In galaxies with no nuclear molecular bars and older star formation. the molecular gas is warmer. as if it has already been heated by the previous rounds of star formation.

The NIR isophote twists seen in the centres of galaxies without molecular nuclear bars could be the result of two separate mechanisms: either a) the bars' dissolution has just begun. and the molecular gas is responding to the changing gravitational potential faster than the stellar populations. or b) bar dissolution is complete. and the NIR isophote twists are the result of the triaxial stellar bulge as originally proposed by Kormendy (1979) and modeled by Pfenniger & Norman (1990).

Clearly a larger sample of double barred galaxies will need to by mapped in CO before these hypotheses can be confirmed.

7.3 Future Directions

The BIMA SONG and OVRO-NRO surveys have shown that the molecular gas distribution does not often resemble the stellar light distribution. This suggests that the dynamics of the molecular gas (and likely the ISM in general) is rather different from the stellar dynamics. Nearly all of the current and past computer simulations are able to successfully reproduce the steady-state. surface features of galaxies. Since these models (or at least the computers that run them) do not have the capacity to include all the details we currently know about the ISM, we need to find alternate

methods to test them against observations. For example. Regan. Sheth. & Vogel (1999) studied the molecular gas dynamics and showed that the molecular gas is better represented by hydrodynamic models than by ballistic particle models. and found streaming motions associated with inflow along a bar. This suggests that by studying the dynamics of the molecular gas we may be able to determine galaxy parameters such as galactic potentials. bar strengths. resonance radii. and other parameters that are predicted by (and used as input for) simulations of galaxies.

7.3.1 Dynamics of Strong Bars, Weak Bars, and Spirals   Molecular gas is extremely susceptible to torques and other external driving forces. Thus the molecular gas dynamics may be a better tracer of the underlying galactic potential than stellar light distributions (which are prone to reddening). Since computer simulations predict different dynamical signatures for strong bars. weak bars. and spiral arms. I plan to compare the molecular gas dynamics of spiral and barred galaxies with the dynamics predicted by the model used in Piner. Stone. & Teuben (1995) in an attempt to determine the underlying galactic potential. After a large enough sample of galaxies have been analyzed. this technique may be applied to heavily obscured galactic nuclei such as those seen in mergers and edge on galaxies. where large scale structure may not be apparent in optical maps.

7.3.2 Inflow in Bars and Spiral Arms   Bars and open spiral arms have long been believed to be a good way to transport gas into the nuclei of galaxies. This inflow is generally thought to be responsible for the feeding of starburst and active galactic nuclei. bar dissolution. and bulge growth (Combes & Gerin 1985; Pfenniger & Norman 1990). There is indirect evidence for inflow in barred galaxies. One example is the shallower metallicity gradients in barred galaxies which suggests

a mixing effect (Vila-Costas & Edmunds 1992). Another is Hα luminousities that seem to be higher in barred galaxies than in unbarred galaxies, indicating more vigorous star formation (Ho, Filippenko, & Sargent 1997). Until recently there have been very few direct measurements of the rate of inflow in barred galaxies. Inflow velocities have been used to estimate inflow rates (Quillen, Frogel, Kenney, Pogge, & Depoy 1995; Benedict, Smith, & Kenney 1996) but measurements of inflow flux require observations at many wavelengths and comparison with models. Regan, Vogel, & Teuben (1997) estimate the gas inflow rate for NGC 1530, but the large number of assumptions that had to be made (mass-to-luminosity ratio, pattern speed, etc.) suggest that more measurements of this sort are needed to obtain more precise inflow rates for barred galaxies. I plan to use BIMA data in conjunction with Hα Fabry-Perot and optical data to perform similar analysis to Regan et al. (1997) on other barred galaxies and spiral arms in order to obtain inflow rate statistics and determine if the inflow rates in these galaxies are correlated with nuclear Hα and NIR luminousities.

7.3.3 Warm Gas at Higher Resolution

There is evidence that ^{12}CO $J=1-0$ may not be a good tracer of molecular gas in the centers of active or starburst nuclei (Petitpas & Wilson 1998b; Kohno, Kawabe, & Vila-Vilaró 1999). It is possible that the CO may be heated such that the CO molecules are excited to higher J transitions leaving the lower J rotational levels depopulated (Petitpas & Wilson 2000). I hope to use BIMA to map ^{12}CO $J=2-1$ in the nuclei of the brightest of the BIMA SONG galaxies to study warmer molecular gas in nuclei. This will allow me to study the morphology and dynamics of the gas at much higher resolution. Regan, Sheth, & Vogel (1999) discuss spectral features that may be the result of the larger beam overlapping the other side of the galaxy. The higher resolution data will

allow a more precise study of the dynamics that will not be as prone to the beam smearing, providing higher confidence when comparing with the model predictions. In addition to the benefits of higher resolution, the $J=2-1$ data can be combined with the $J=1-0$ data to create line ratios that can combined with the full multiline study of the BIMA SONG nuclei discussed below.

7.3.4 The Interstellar Medium in Starburst and Active Galactic Nuclei: A Complete Set of Molecular Gas Properties

Recent high resolution ^{12}CO $J=1-0$ surveys of nearby galaxies have shown that the nuclear molecular gas distribution seems to bear little resemblance to the parent galaxy's stellar distribution. This suggests that there may be differences in the molecular gas properties that allow it to respond differently to similar gravitational potentials. I am in the process of performing a survey of molecular gas properties for a sample of Seyfert, starburst, and non-active galaxies to search for differences in the molecular gas properties, which may explain the wide range of nuclear activity and CO morphologies.

7.3.4.1 Molecular gas properties compared to nuclear CO morphology The nuclei of galaxies are often the setting for extraordinary events such as starbursts, molecular rings, inflow, and Seyfert activity. Recently, a variety of groups have been undertaking high resolution ^{12}CO $J=1-0$ surveys of nearby galaxies (e.g. NRO-OVRO ^{12}CO $J=1-0$ Survey, Sakamoto, Okumura, Ishizuki, & Scoville 1999; BIMA SONG, Helfer, Thornley, Regan, Wong, Blitz, Bock, Sheth, Vogel, & Harris 1999). Early results suggest that there is a wide variety of observed CO distributions, even within samples of the same Hubble Classification (Kartik Sheth, *private communica-*

tion: Sakamoto. Okumura. Ishizuki. & Scoville 1999). This suggests that there may be differences in the molecular gas properties that allow it to respond differently to similar gravitational potentials. There is evidence for this in Chapter 4. where in a sample of galaxies containing large scale barred structure we found that warmer gas tends to form nuclear bars. while cooler gas forms nuclear rings and spirals. These results need to be confirmed using a much larger sample of galaxies. The existing high resolution ^{12}CO $J=1-0$ interferometry data allow us to determine the morphology and dynamics of the molecular gas in these galaxies. but in order to measure properties such as temperature and density. we need observations of many different lines of CO and its isotopomers (see Petitpas & Wilson 1998a for example).

I will use the Caltech Submillimeter Observatory and the James Clerk Maxwell Telescope to map the inner regions of a variety of normal and active galactic nuclei which have already been observed in the high resolution ^{12}CO $J=1-0$ surveys mentioned above. We will map the brightest and largest of the BIMA/OVRO/NRO galaxies in ^{12}CO $J=1-0$. $J=2-1$. $J=3-2$. $J=4-3$ and $J=6-5$ and. where feasible. attempt to detect ^{13}CO $J=2-1$ and $J=3-2$. The smaller beam of JCMT will provide higher resolution for the lower J transitions of CO than possible with the CSO. These CSO/JCMT and OVRO/BIMA observations will be used in conjunction with radiative transfer models to provide the the physical conditions and column densities of the molecular gas in these galaxies. providing a *complete set of molecular gas data for a sample of quiescent. starburst and AGN galaxies*. Using these data. I will search for relationships between temperature. density and nuclear CO morphology. to see if the physical conditions in the molecular gas determine whether the nucleus forms molecular spirals. rings. bars. or central peaks.

7.3.4.2 Molecular gas properties compared to computer simulations   The need to understand the mechanisms driving the phenomena described above has inspired a great number of computer simulations. Models suggest that bars and spiral arms in galaxies can drive molecular gas into the nucleus where it can fuel the vigorous star formation or Seyfert activity that would otherwise exhaust the molecular gas content on very short timescales (e.g. Combes 1994; Shlosman, Frank, & Begelman 1989). The ^{12}CO J=1−0 surveys show that molecular gas can take on many shapes as it flows inward towards the galactic nucleus. Rings, 'twin peaks', and double bars are common in galactic nuclei and have been successfully modeled by many authors (e.g. Combes & Gerin 1985; Piner, Stone, & Teuben 1995; Friedli & Martinet 1993; Shaw, Combes, Axon, & Wright 1993). One trait common to all models is the need to include a gaseous component. Purely stellar simulations cannot maintain the features discussed above for acceptably long timescales. Unfortunately, there are currently no detailed studies of the gas properties of these galaxies in the literature.

Previous galaxy simulations (e.g. Combes 1994; Friedli & Martinet 1993) produce very different results simply by changing the gas properties. Due to a lack of detailed molecular gas data, the current best observational test of how accurately a model takes into account the gaseous component is the assumed gas mass to total mass ratio (usually adopted as 5 to 10%, in agreement with most observations). With a variety of other options available, such as observed density, temperature, and column density, theorists would have a much stronger set of constraints to place on the gaseous components of the simulations.

7.3.4.3 Molecular gas properties compared to nuclear activity   One question that remains to be answered is what determines whether a galaxy exhibits starburst or Seyfert activity. Shlosman, Frank, & Begelman (1989) suggest that it depends on

whether or not star formation occurs in the gas as it is transported inwards towards the galactic center. If star formation occurs. inflow is halted and a starburst galaxy is born. If star formation does not occur. the inflow can continue to the center and accrete onto a central massive object and fuel an AGN. The projects described above will allow a direct comparison of the physical conditions and distribution of the gas in the Seyfert galaxies and the starburst galaxies will provide valuable insight into what determines if a galaxy transporting material into the nucleus forms a Seyfert or a starburst galaxy.

Bibliography

Athanassoula. E.. 1992. *MNRAS* **259**. 345.

Beckman. J.. 1994. Molecular inflow towards galactic nuclei. In *Mass Transfer Induced Activity in Galaxies*. pp. 160. ed. I. Shlosman. Cambridge Univ. Press.

Benedict. G. F.. Smith. B. J.. & Kenney. J. D. P.. 1996. *AJ* **112**. 1318.

Combes. F.. 1994. Nuclear gas flows in barred galaxies. In *Mass Transfer Induced Activity in Galaxies*. pp. 170. ed. I. Shlosman. Cambridge Univ. Press.

Combes. F. & Gerin. M.. 1985. *A&A* **150**. 327.

Friedli. D. & Martinet. L.. 1993. *A&A* **277**. 27.

Helfer. T. T.. Thornley. M. D.. Regan. M. W.. Wong. T.. Blitz. L.. Bock. D. C. .. Sheth. K.. Vogel. S. N.. & Harris. A.. 1999. Imaging and large-scale structure with the bima survey of co in nearby spiral galaxies (bima song). In *American Astronomical Society Meeting*. Volume 194. pp. 0703.

Ho. L. C.. Filippenko. A. V.. & Sargent. W. L. W.. 1997. *ApJ* **487**. 591.

Kenney. J. D. P.. Wilson. C. D.. Scoville. N. Z.. Devereux. N. A.. & Young. J. S.. 1992. *ApJL* **395**. L7.

Kohno. K.. Kawabe. R.. & Vila-Vilaró. B.. 1999. *ApJ* **511**. 157.

Kormendy. J.. 1979. *ApJ* **227**. 714.

Petitpas. G. R. & Wilson. C. D.. 1998a. *ApJ* **496**. 226.

Petitpas. G. R. & Wilson. C. D.. 1998b. *ApJ* **503**. 219.

Petitpas. G. R. & Wilson. C. D.. 2000. *ApJL* **538**. L117.

Pfenniger. D. & Norman. C.. 1990. *ApJ* **363**. 391.

Piner. B. G.. Stone. J. M.. & Teuben. P. J.. 1995. *ApJ* **449**. 508.

Quillen. A. C.. Frogel. J. A.. Kenney. J. D. P.. Pogge. R. W.. & Depoy. D. L.. 1995. *ApJ* **441**. 549.

Regan. M. W.. Sheth. K.. & Vogel. S. N.. 1999. *ApJ* **526**. 97.

Regan. M. W.. Vogel. S. N.. & Teuben. P. J.. 1997. *ApJ* **482**. L143.

Sakamoto. K.. Okumura. S. K.. Ishizuki. S.. & Scoville. N. Z.. 1999. *ApJ* **525**. 691.

Shaw. M. A.. Combes. F.. Axon. D. J.. & Wright. G. S.. 1993. *A&A* **273**. 31.

Shlosman. I.. Frank. J.. & Begelman. M. C.. 1989. *Nature* **338**. 45.

Vila-Costas. M. B. & Edmunds. M. G.. 1992. *MNRAS* **259**. 121.

Appendix A

Glossary of Terms

Beam: The effective field of view of a radio telescope.

Beam matched line ratios: A ratio of integrated intensities or fluxes that compare two values measured over the same field of view (or beam).

CLEAN: A computer algorithm that breaks the interferometric data down into a series of point sources. then convolves these points with the synthesized beam of the interferometer to reconstruct a map that has a much higher signal to noise ratio that the original map.

f_{60}/f_{100}: The ratio of the flux at 60 μm and 100 μm as measured by the IRAS satellite. Higher values of f_{60}/f_{100} indicate higher dust temperatures.

ILR: The Inner Lindblad Resonance is a resonance that occurs in barred galaxies at radii of a few kiloparsecs. It is strong enough to trap molecular gas at this radius. often resulting in rings encircling the nucleus. See §2.6 for more details.

Isophote: Contour lines on an image that mark constant brightness or luminosity.

Isotopomer: Similar to isotopes in atoms. but for molecules. e.g.. ^{13}CO and $C^{18}O$ are isotopomers of the more abundant ^{12}CO.

Lenticular: Slightly lense shaped. In barred galaxies. lenticular shapes are indicative of weak bars.

LVG: Radiative transfer models that assume there are Large Velocity Gradients across a molecular cloud that Doppler shift the emission from one region so that it cannot be reabsorbed by another part of the same cloud. Thus, the equations of radiative transfer are much easier to solve.

LTE: Radiative transfer models that assume the gas is collisionally dominated. and thus can be represented by a single temperature and that the level populations are simply given by the Boltzmann distribution.

Nucleus: In this work. we refer to the nucleus of a galaxy as the region interior to the Inner Lindblad Resonance (see §2.6). It is typically a few kiloparsecs across.

Parsec: A unit of measure that is derived from the trigonometric parallax observed in stars caused by the Earths orbit around the Sun. A parsec is defined such that a star that is 1 parsec away will be observed to undergo a parallax shift of 1 arcsecond in the sky once a year. 1 parsec $= 3.3$ light years $= 3.1 \times 10^{16}$ metres.

Pattern speed: The angular speed at which the large scale bar perturbation of a barred galaxy appears to rotate. Since the bar is comprised of stars and gas that move in distinct orbits within the bar. the Doppler shift of the stellar or gaseous emission lines do not allow us to measure this value directly.

Track: Optical and single dish radio telescopes measure the length of an observation by integrations time: the time the telescope was pointing at the source. Interferometers require that the Earth rotate sufficiently that the geometry of the interferometer (as seen from space) changes noticeably. The longer the source is tracked through the sky. the more the Earth has rotated. The more the Earth has rotated. the better the resulting image will be. Thus, interferometric observations are measured in 'tracks' rather than integration times.

T_A^*: The power (P) that is received at a radio telescope is converted to antenna temperature using $P \equiv kT_A$. The chopper wheel calibration actually allows is to measure T_A^* which is as close as we can get to T_A.

T_{MB}: The main beam temperature is T_A^*/η_{MB} which is the antenna temperature (T_A^*) corrected for the main beam of the telescope. It is the appropriate temperature scale to use for sources that are comparable in size to the main beam of the radio telescope.

T_R^*: This temperature is as close to the true source temperature that we can measure. It is T_A^*/η_{fss}.

η_{fss}: The front scattering and spillover efficiency is a factor that corrects antenna temperature for reflection from the ground and support arms of a telescope. It is difficult to measure.

η_{MB}: The main beam efficiency is a factor that corrects the antenna temperature to the main beam strength.